Phase relations of Al-bearing dense hydrous phases up to the uppermost lower mantle and sound velocities of Al-bearing phase D

by

Chaowen Xu (徐超文)

Submitted for Partial Fulfillment of the Requirements for the Degree

of

Doctor of Science

From

Geodynamics Research Center

Graduate School of Science and Engineering

Ehime University

Japan

June 2019

Phase relations of Al-bearing dense hydrous phases up to the uppermost lower mantle and sound velocities of Al-bearing phase D

Dissertation Submitted to Geodynamics Research Center, Graduate School of Science and Engineering, Ehime University for Partial Fulfillment of the Degree of **Doctor of Science** in **High Pressure Earth Science**.

by

Chaowen Xu (徐超文)

Supervisor: Professor Toru Inoue (井上 徹)

Geodynamics Research Center

Ehime University, Matsuyama 790-8577, Japan

CERTIFICATE

This is to certify that the work in this thesis entitled "**Phase relations of Al-bearing dense hydrous phases up to the uppermost lower mantle and sound velocities of Al-bearing phase D**", is carried out by **Chaowen Xu** at **Geodynamics Research Center** (GRC), Ehime University, Japan, under supervisions of Professor **Toru Inoue**, GRC, Ehime University, Matsuyama, Japan for partial fulfillment of the degree of **Doctor of Science in High Pressure Earth Science**. The thesis is prepared in accordance to the rules and regulations of the **Graduate School of Science and Engineering, Ehime University**. **No part** of **this dissertation** has been submitted anywhere for award of any degree or otherwise to the best of my knowledge.

Professor & Director: Yuji Sogabe
Graduate School of Science and Engineering
***Ehime University*, Japan 790-8577**

(Official Seal)

Graduate School of Science and Engineering
***Ehime University*, Matsuyama, Japan 790-8577**

Abstract

Water as one of the most important volatile components plays an important role on Earth's interior. It influences the physical and chemical properties of minerals and melts, which further effects the evolution of the Earth. Water can be transported into the deep Earth as form of hydrous phases in subducting slabs,espeically those of dense hydrous magnesium silicate phases (DHMSs), such as phase A (PhA), phase E (PhE), superhydrous phase B (SUB), phase D (PhD) phase H (PhH), which have been suggested as potential water carriers to transition zone and even to the lower mantle under the conditions presented in the cold subducting slabs (Kanzaki, 1991; Kawamoto et al., 1996; Ulmer and Trommsdorff, 1999; Irifune et al., 1998; Litasov and Ohtani, 2002; Ohtani et al., 2001; Ohtani et al., 2004; Komabayashi et al., 2005, Komabayashi and Omori, 2006; Nishi, 2015). Among the DHMSs, phase H was reported to exist even up to the deepest part of the lower mantle (Nishi et al., 2014). These DHMSs contain 3-18wt% H_2O are also regarded as important storage sites for water in Earth's interior.

Therefore, it is of great importance to illustrate the stability of DHMSs. Recent studies have shown that Al hugely increases the stability region of DHMSs (Ghosh and Schmidt, 2014; Pamato et al., 2015; Kakizawa et al., 2018). To systematically ascertain the effect of Al on stability of DHMSs from various aspects, we have conducted several high pressure and high temperature experiments and found that

1. Al-bearing PhE, SUB and PhD were observed with P-T increasing in serpentine+Al_2O_3 system. Following the P-T path of cold subduction, the phase assemblage PhE + PhD was stable at 14-23 GPa, and even a trace of PhE was identified at 900 ℃ and 25 GPa coexisting with PhD. The phase SUB was stable between 16 and 22 GPa coexisting with PhE + PhD. Following the P-T path of hot subduction, the phase assemblage PhE + Gt was observed at 14-18 GPa coexisting with melt. The phase assemblage SUB + PhD was stable at 18-25 GPa, which was expected to survive at higher P-T condition. Some amount of SUB was even stable at normal mantle geotherm at transition zone pressure. It was obvious that Al enhanced the stabilities of these DHMSs, and the water content drastically increased. Our results may indicate that the wide stabilities of Al-bearing DHMSs increase the chance of obtaining water after antigorite (serpentine) decomposes at the shallow region of the subduction zone and transporting water to the deep lower mantle even in hydrous peridotite and MORB composition.

2. Al-rich PhD has a very wide stability region from 900 ℃ and 14 GPa to at least 1500 ℃ and 25 GPa. With pressure increasing, Al-rich PhD decomposes to phase Egg and then to δ at above hot subduction at transition zone in MgO-Al_2O_3-SiO_2-H_2O (MASH) system between14 and 25 GPa at 900-1500 ℃. The wide stability region determined in this study makes Al-bearing PhD an important storage site for water in transition zone, suggesting that it can deliver a certain amount of water into the lower mantle along hot subduction and even the normal mantle geotherm P-T condition.

3. Fe slightly decreased the stability region of PhD in FeOOH-PhD system, however, Although Fe decreases the stability region of PhD, Al, Fe-bearing PhD drastically shift to

higher temperatures in both MORB and pyrolite type compositions compared to pure Mg-PhD. Therefore, Al, Fe-bearing PhD could act as long water reservoir along subduction to the deep lower mantle.

4. PhE coexisting with wadsleyite or ringwoodite is at least stable at 15-16.5 GPa and below 1050 ℃. PhD coexisting with ringwoodite at pressure higher than 16.5 GPa and temperature below 1100 ℃ in Fe-rich MgO-Al_2O_3-FeO-SiO_2-H_2O (MAFSH) system between 15 and 21 GPa at 900-1500 ℃. We also noticed that transition pressure of the loop in wadsleyite-ringwoodite boundary shifted towards lower pressure in iron-rich system compared with hydrous pyrolite model on Earth

5. Al is strongly partitioned into PhD than coexisting Brg, and partition coefficient of Al (KD) between PhD and Brg slightly decreases with increasing temperature. Al-bearing PhD totally decomposes around 28 GPa and 1350 ℃, in which Brg is found to be coexisting with a large amount of melt. At 31 GPa and 1350 ℃, Brg coexists with trace amount of melt and Al-rich phase H, which means some amount of water might be transported into the lower mantle.

6. A binary eutectic diagram is formed without dehydration or melting below 1200 ℃ at 20 GPa in AlOOH and FeOOH system. We also observe that maximum solubilities of Al and Fe in the solid solutions were more strongly influenced by temperature than by pressure. Our results suggest that $CaCl_2$-type hydroxides subducted in to the deep mantle form a solid solution over a wide composition ranges. As AlOOH and FeOOH are present in hydrous crust, these phases may be subducted into the deep interior, transporting a significant amount of hydrogen to deeper regions. Therefore, a greater understanding of this binary system may

help to elucidate the model geodynamic processes associated with the deep water cycles of the Earth.

7. Modeled velocities of Al-bearing PhD in hydrous pyrolite along normal mantle geotherm shows that Al-bearing PhD generates high velocity anomalies compared with dry pyrolite in mantle transition zone, however, it is seismically invisible due to the small anisotropy. Once Al-bearing PhD is transported to the uppermost lower mantle, it shows a lower signature than dry pyrolite or higher velocities within the slab region. Thus the observed velocity anomalies at the uppermost lower mantle may be considered as the presence of water in subduction zone. Due to its high thermal stability region, Al-bearing PhD is expected to transport water to the Earth's lower mantle, elucidating model geodynamic processes associated with the deep water cycles.

Abstract ..... **I**

Chapter 1 ..... **1**

Introduction **1**

1. Background 2

2.Related researches and limits 3

3. Purpose of this study 7

Chapter 2 ..... **10**

Effect of Al on stabilities of DHMSs up to the uppermost lower mantle: Implication for water transports into the deep mantle **10**

Abstract 11

1. Introduction 11

2. Experimental procedures 14

3. Results and Discussion 15

3.1. Phase assemblages 15

3.2. Mineral composition 20

3.3. Melt composition 21

3.4. The effect of temperature on Al content in DHMSs 22

3.5. The Al substitution mechanism in DHMSs 23

3.6. The stabilit of Al-bearing DHMSs in the Earth's interior 24

3.7. Water distribution in the mantle 25

4. Implication 27

Chapter 3 ..... **45**

Melting of Al-rich phase D up to the uppermost lower mantle and transportation of H_2O to the deep Earth **45**

Abstract 46

1. Introduction 46
2. Experimental 49
3. Results and discussion 51
3.1 Lattice Parameters 51
3.2 Raman spectrum 52
3.3 Phase relations 54
4. Geophysical implications 57
Chapter 4 68
Melting phase relation of Fe-bearing PhD up to the uppermost lower mantle and transportation of H_2O to the deep Earth 68
Abstract 69
1. Introduction 70
2. Experimental procedures 72
3. Results and discussion 73
3.1 Phase relations 73
3.2 Mineral chemistry 76
3.3 Lattice parameters 77
3.4 The stability of Fe-bearing PhD in the mantle 78
3.5 Long water reservoir 80
Chapter 5 90
Phase relations in MAFSH system up to 21 GPa: Implications for water cycles in Martian interior 90
Abstract 91
1. Introduction 91
2. Experimental procedures 93

3. Results and discussion 94
3.1 Phase relations 94
3.2 Mineral chemistry in DHMSs, wadsleyite and ringwoodite 95
3.3 The stability and water content of hydrous phases in iron-rich Martian mantle 96
4. Implications 98
Chapter 6 106
Al partitioning between phase D and bridgmanite up to 31 GPa: Implications for high electrical conductivity, velocity anomalies and deep earthquakes occur between 670 and 850 km 106
Abstract 107
1.Introduction 108
2.Experimental procedures 109
3.Results and Discussions 110
4.Implications 112
Chapter 7 120
Solubility behavior of δ-AlOOH - ε-FeOOH at high pressures 120
Abstract 121
1.Introduction 121
2.Materials and Methods 123
3. Results and Discussion 124
4. Implications 127
Chapter 8 134
Sound velocities of Al-bearing phase D to 22 GPa and 1300 K 134
Abstract 135
1.Introduction 135

2.Materials and Methods 137
3. Results and Discussion 139
3.1 Compressibility of Al-phase D 139
3.2 Sound velocity measurements 141
4 Implications 142
Chapter 9 158
Discussion and conclusions 158
1. Stability of DHMSs in Al-bearing system 159
2. Stability of PhD in (Fe, Al)-bearing system 161
3. Al partitioning between phase D and bridgmanite up to 31 GPa 162
4. Elastic property of Al-bearing PhD 162
5. Futher work 163
References 165
Acknowledgements 181

Chapter 1

Introduction

1. Background

Hydrogen is the most abundant element in our solar system (90%). Athough bulk water content on earth is uncertain, it makes the Earth unique amiong planets in our solar system. Water as one of the most important volatile components plays an important role on Earth's interior. It influences the physical and chemical properties of minerals and melts, which further effects the evolution of the Earth. Therefore, it is important to estimate the water abundance and water circulation in the Earth.

The ocean holds much of the earth's water. Hydrous minerals will form during the high pressure metamorphism when the ocean crust reacting with the overlying seawater. These hydrous minerals will be transpoeted to the deep earth by cold subducting slabs. Most of the hydrous minerals would dehydrate along subduction due to the low thermal stability region. The dehydration of these hydrous minerals may cause partial melting. However, high pressure experimental studies have inducated that many hydrous phases may be stable at mantle conditions.

Since the high pressure hydrous magnesium silicates was first reported by Ringwood and Major (1967), more and more people investigated the stability region of various DHMSs in MgO-SiO_2-H_2O (MSH) system. It is reported that a series of DHMSs such as PhA, PhE, superhydrous SUB, PhD and PhH act as potential water carriers to the deep Earth by subducting (Kawamoto et al., 1996; Ohtani et al., 2001a; Litasov and Ohtani, 2003; Komabayashi et al., 2005; Nishi et al., 2014). These DHMSs contain 3-18 wt% H2O are also regarded as important storage sites for water in Earth's interior. A plenty of high-pressure

experiments and thermodynamic calculations have been performed to clarify the phase relations of DHMSs in MgO-SiO_2-H_2O (MSH) system. According to these studies, PhA, PhE, SUB, PhD and PhH were observed with pressure increasing from lower part of upper mantle to middle part of lower mantle. However, these DHMSs seems to be stable in very cold subducting slabs only. (Kanzaki, 1991; Kawamoto et al., 1996; Ulmer and Trommsdorff, 1999; Irifune et al., 1998; Litasov and Ohtani, 2002; Ohtani et al., 2001; Ohtani et al., 2004; Komabayashi et al., 2005, Komabayashi and Omori, 2006; Nishi, 2015).

Recently, experimental results have shown that Al hugely increases the stability region of DHMSs (Ghosh and Schmidt, 2014; Pamato et al., 2015; Kakizawa et al., 2018), which even stablelise SUB and PhD up to 2000 ℃ at mantle transition zone pressure(Pamato et al., 2015; Kakizawa et al., 2018).

2. Related researches and limits

Although several experiments have shown Al can increase the stability of DHMSs however, there are still many questions that have not been clarified, for example:

1. It was reported that a new Al-rich form of phase D, containing up to 50 wt% Al_2O_3 was synthesized at 1300 ℃ and 25 GPa in mid-ocean ridge basalt bulk compositions (MORB) (Ballaran et al., 2010). It indicated that DHMSs may have the potential to incorporate large amount of Al_2O_3 in the structure. Currently, one experiment determining the melting phase relations of PhD up to lower mantle condition showed that stability field of Al-bearing PhD could remain stable up to 1600 ℃ at 24 GPa when only incorporating 1wt% Al_2O_3 (Ghosh and Schmidt, 2014). The other experiment reported that end member Al-rich PhD was stable

at temperatures up to 2000 ℃ at 26 GPa (Pamato et al., 2015). Both studies indicated Al increases stability regions of DHMSs. Unfortunately, no further experiments were conducted in the MgO-Al_2O_3-SiO_2-H_2O (MASH) system to clarify the phase relations in DHMSs at high pressures. Almost all of the previous studies conducted in MSH system do not necessarily yield the maximum thermal stability of DHMSs and the water content in DHMSs might be underestimated, since Al_2O_3 is one of abundant components in both pyrolite and MORB composition, has been shown to prefer to distribute in DHMSs than coexisting wadsleyite, ringwoodite and bridgmanite (Bolfan-Casanova et al., 2003; Litasov et al., 2005; Ghosh and Schmidt, 2014; Ohira et al., 2014).

2. PhD is the decomposed product of serpentine in subducting slabs at mantle transition zone, with ideal fomula $MgSi_2O_6H_2$. In the MSH system, it has been proposed that the maximum thermal stability of phase D is 1400 ℃ at 26 GPa (Frost and Fei, 1998), and could exist around 45 GPa along cold subduction (Frost and Fei, 1998; Shinmei et al., 2008; Tsuchiya, 2013; Nishi et al., 2014; Ohtani et al., 2014). Recently, there are two kinds of experiments performed on the stability of phase D in the MgO-Al_2O_3-SiO_2-H_2O (MASH) system at transition zone and lower mantle conditions. One is determining the melting phase relations of Al-bearing PhD at uppermost lower mantle condition (Ghosh and Schmidt, 2014). It was noticed that this type of Al-bearing PhD containing 1wt% Al_2O_3 was stable up to 1600 ℃ at 24 GPa according to their experimental results. The other reported that the synthesized end member Al-rich PhD was observed stable at temperatures up to 2000 ℃ at 26 GPa (Pamato et al., 2015). Both studies indicate that Al could increases stability regions of DHMSs. Unfortunately, the stability region was not further reported. So it is possible that the

maximum thermal stability of PhD is underestimated by previous studies due to the positive Clapeyron slope dP/dT of PhD and its ability to absorb large quantity of Al.

3. We have known that PhD is potential stabilizing phase in hydrous peridotite among DHMSs at upper part lower mantle, playing key role in transportation and reserving water, which further transforms to PhH at 50 GPa (Nishi et al., 2014) and Al increases the stability region of PhD. However, there remain discrepancy in effect of Fe on Phase D. Ghosh and Schmidt (2014) argued that PhD almost had same stability region in both FeO-MgO-Al_2O_3-SiO_2-H_2O (FMASH) and MSH system, but lower than that of MASH system between 22-24 GP, while Ganskow and Langenhorst (2014) found that Fe increased stability of PhD in FMASH system compared with MSH system between 18-23 GPa, which even stabilized up to 1450 ℃ at 20.5 GPa. We know that Fe is an abundant and important element in both pyrolite and MORB composition (Irifune and Ringwood, 1987), may greatly change stability and water solubility of PhD. On the other hand, stability of PhD contains Al and Fe content simultaneously closer to pyrolite or MORB composition is still unknown. Due to the limited data, we could not fully understand stability, water solubility and crystal chemistry of PhD.

4. The existence of water in Mars has long been controversial. According to the recent topographic features studies, for instance, northern plains, sedimentary deposits and valley networks (Cardenas et al., 2017; Chan et al., 2018; Ivanov et al., 2017), and to the finding of subsurface ice as well as various hydrous minerals in Lyot crater, suggesting existence of an ancient Martian ocean on surface (Byrne et al., 2009; Balme et al., 2015; Pan and Ehlmann, 2018). If there were tectonic activities on ancient Mars as proposed (Blasio and Martino, 2017; Dohm et al., 2018), some parts of the hydrated crust of Mars have been tectonically

embedded and subducted into the deep interior together with some hydrous materials (serpentinized composition) (Wade et al. 2017). Therefore, as an Earth-like planet, there may exist some hydrous minerals in the subducting plate on iron-rich Mars, and wadsleyite and ringwoodite may also hold huge amount of water in Martian interior, as is argued on Earth today. Several studies have identified phase relations in the MSH and MgO-Al_2O_3-SiO_2-H_2O (MASH) systems, and observed various hydrous minerals at *P*-*T* conditions related to the cold subduction slabs (Frost 1999; Litasov et al., 2005; Komabayashi and Omori, 2006; Ohira et al., 2014; Nishi et al., 2014; Pamato et al., 2015). However, few data available in hydrous iron-bearing system for the Earth, while data in iron-rich system like Mars is still remain unclear.

5. PhD is the dominant high pressure phase among DHMSs in hydrous pyrolite from the shallow parts of the lower mantle to at least middle region, has been shown to coexist with Brg (Bolfan-Casanova et al., 2003; Litasov et al., 2005; Ghosh and Schmidt, 2014; Ohira et al., 2014; Nishi et al., 2014), which is widely viewed as the most abundant mineral assemblage in the Earth's interior (Irifune, 1994; Tschauner et al., 2014). The experimental result indicated that Brg is the main host mineral for Al_2O_3 in the lower mantle (Liu et al., 2016). Therefore, partitioning of Al between PhD and Brg is particularly needed to constrain water distribution in the deep mantle, since a trace amount of water may greatly influence geodynamic process of the Earth's interior, especially because Al^{3+}+H^+ substitutes for Si^{4+} in PhD greatly enhances its water content, implying that water transported into the lower mantle along subducting may be underestimated by previously thought. However, direct experimental results are limited.

6. The existence of PhD in the uppermost lower mantle may explain the observed low-velocity layers due to its wide pressure-temperature region (Liu et al., 2016; Nishi et al., 2014). Although several studies have suggested that H_2O could reduce the sound velocities of nominally non-hydrous minerals (Inoue et al., 1998; Jacobsen et al., 2004; Mao et al., 2012) there is only few studies that addressed the sound velocity of hydrous minerals, especially for those DHMSs. Therefore, direct velocity-density data of PhD is particularly needed to illustrate the detected seismic anomaly at bottom of transition zone. However, the elasticity of PhD is to this day poorly investigated because ultrasonic measurement requires well sintered samples with high purity, which is difficult to achieve for PhD as substantial amount of pores, chemical heterogeneities or accessory phases appear as a consequence of the high water content and therefore such sample were not available. The few existing studies (e.g. PVT studies) showed that hydrous phases generally have lower densities than anhydrous mantle minerals and therefore could lower velocities compared to the surrounding dry mantle (Frost and Fei, 1998; Litasov et al., 2008; Hushur et al., 2011; Rosa et al., 2013). Presence of PhD at the lowermost part of the mantle transition region and in the uppermost part of the lower mantle could therefore be an alternative to partial melting or ancient basalts (Kaneshima 2009) to explain local seismic reflectors beneath 660 km depth.

3. Purpose of this study

To illustrate these questions, we conducted following experiments:

1. To systematically investigate the effect of Al on the stability region of DHMSs, we conducted high-temperature and high-pressure experiments using natural chlorite in FeO-

MgO-Al_2O_3-SiO_2-H_2O (FMASH) system, which is high pressure polymorphs of serpentine, is believed to be one of the main storage sites for water in subducting slabs (Cannatet al., 1995). In addition, a chemical mixture in MASH system was used to make comparison. We determined the stability region of chlorite up to the uppermost lower mantle pressure along the cold, hot subduction and normal mantle geotherm condition. Finally, we determined water distribution in deep earth.

2. We investigated the effect of Fe on the stability of PhD in FeOOH-PhD system at pressures between 18-25 GPa and temperatures between 1000-1600 ℃. This help us better understand a more Fe-rich condition, such as the hydrous minerals on Fe-rich Mars. We also determined the stability of PhD in a moderate Al and Fe content similar to pyrolite and MORB in AlOOH-FeOOH-PhD system whose composition is close to natural system .We can clarify the Mg and Si effect on phase relation of AlOOH-FeOOH binary system at transition zone condition simultaneously, which have been suggested that Mg and Si change symmetry of δ-AlOOH (Komatsu et al., 2011), might influence stability of AlOOH-FeOOH binary system.

3. We determined phase relations in MgO-Al_2O_3-FeO-SiO_2-H_2O (MAFSH) system may help to elucidate the geodynamic processes associated with the deep water cycles of Mars. Therefore, experiments were conducted to determine phase relations in iron-rich MAFSH system up to 21 GPa to estimate the possible water transportation into Martian interior by subducting processes.

4. We performed multi-anvil experiments in the MgO-Al_2O_3-SiO_2-H_2O composition up to 31 GPa and 1350 ℃. This allow us to investigate the partitioning of Al between PhD and

Brg simultaneously contribute to explain some important geophysical observations by analyzing phase relations.

5. Experiments were conducted to determine the solubility behavior of AlOOH-FeOOH binary system at 15–25 GPa and 700–1200 ℃.

6. We report the longitudinal (V_P) and shear (V_S) velocities, as well as the density of Al-bearing PhD up to 22 GPa and 1300 K by in situ synchrotron X-ray techniques combined with ultrasonic measurements of a polycrystalline sample in the multianvil apparatus at the BL04B1 beamline of SPring-8, Japan. Our results provide an understanding of the sound velocities of PhD under a wide pressure and temperature range in which elastic behavior of PhD can be modeled, therefore enhancing our knowledge of how water distribution in upper parts of lower mantle where melt generation may lead to be detected as local discontinuity and low-velocity zones in some typical region at top of the lower mantle.

Chapter 2

Effect of Al on stabilities of DHMSs up to the uppermost lower mantle:

Implication for water transports into the deep mantle

(Will submit to Contributions to Mineralogy and Petrology)

Abstract

We have investigated the stability of natural clinochlore containing about 16 wt% H_2O and about 14 wt% Al_2O_3 between14 and 25 GPa at 800-1600 ℃ by MA8-type apparatus. A chemical mixture similar to Fe-free clinochlore was also investigated for comparison. Following the *P-T* path of cold subduction, the phase assemblage Phase E + Phase D was stable at 14-25 GPa. The phase superhydrous phase B was observed between 16 and 22 GPa coexisting with Phase E + Phase D. Following the *P-T* path of hot subduction, the phase assemblage Phase E + Garnet was identified at 14-18 GPa coexisting with melt. The phase assemblage superhydrous phase B + Phase D was found at 18-25 GPa, which was expected to survive at higher *P-T* condition. DHMSs in chemical mixture approximately had the same phase assemblage as natural sample. We noticed that Al enhanced the stabilities of these DHMSs, and the water content drastically increased. Our results may indicate that the wide stabilities of Al-bearing DHMSs increase the chance of obtaining water after antigorite (serpentine) decomposes at the shallow region of the subduction zone and transporting water to the deep lower mantle even in hydrous peridotite and MORB composition. Dehydration of Al-bearing DHMSs may hugely change physical and chemical properties of surroundings.

1. Introduction

Water can be transported into the deep Earth via subducting slabs as form of hydrous minerals. Several hydrous phases in subducting slabs have been suggested, especially those dense hydrous magnesium silicate phases (DHMSs), such as phase A (PhA), phase E (PhE),

superhydrous phase B (SUB), phase D (PhD) phase H (PhH), which have been suggested as potential water carriers to transition zone and even to the lower mantle under the conditions presented in the cold subducting slabs (Kawamoto et al., 1996; Ohtani et al., 2001; Komabayashi and Omori, 2006; Nishi et al., 2014; Walter et al., 2015). Among the DHMSs, phase H was reported to exist even up to the deepest part of the lower mantle (Nishi et al., 2014; Walter et al., 2015). These DHMSs contain 3-18 wt% H_2O are also regarded as important storage sites for water in Earth's interior (Ohtani et al., 2004) and the dehydration of DHMSs may lead to partial melt and cause earthquakes in the subducting slabs (Omori et al., 2004).

Because of its importance, a plenty of high-pressure experiments and thermodynamic calculations have been performed to clarify the phase relations of DHMSs in MgO-SiO_2-H_2O (MSH) system. According to these studies, PhA, PhE, SUB, PhD and PhH were observed with pressure increasing from lower part of upper mantle to middle part of lower mantle. However, these DHMSs seems to be stable in very cold subducting slabs only. (Kanzaki, 1991; Kawamoto et al., 1996; Irifune et al., 1998; Litasov and Ohtani, 2002; Ohtani et al., 2001; Ohtani et al., 2004; Komabayashi et al., 2005, Komabayashi and Omori, 2006; Nishi, 2015).

It was reported that a new Al-rich form of PhD, containing up to 50 wt% Al_2O_3 was synthesized at 1300 ℃ and 25 GPa in mid-ocean ridge basalt bulk compositions (MORB) (Ballaran et al., 2010). It indicated that DHMSs may have the potential to incorporate large amount of Al_2O_3 in the structure. Currently, one experiment determining the melting phase relations of PhD up to lower mantle condition showed that stability field of Al-bearing PhD

could remain stable up to 1600 ℃ at 24 GPa when only incorporating 1wt% Al_2O_3 (Ghosh and Schmidt, 2014). Another experiment reported that Al-PhD end member was stable at temperatures up to 2000 ℃ at 26 GPa (Pamato et al., 2015). Both studies indicated Al increases stability regions of DHMSs. In addition, Liu et al. (2019) ascertained the stability field of Al-rich PhD in hydrous MORB bulk composition along a cold subducting condition, they found that Al-rich PhD could remain stable up to 23 GPa, which further transformed to Al-rich PhH. Unfortunately, no further experiments were conducted in the MgO-Al_2O_3-SiO_2-H_2O (MASH) system to clarify the phase relations in DHMSs. Almost all of the previous studies conducted in MSH system may do not necessarily yield the maximum thermal stability of DHMSs and the water content in DHMSs might be underestimated, since Al_2O_3 is one of abundant components in both pyrolite and MORB composition, has been shown to prefer to distribute in DHMSs than coexisting wadsleyite, ringwoodite and bridgmanite (Bolfan-Casanova et al., 2003; Litasov et al., 2005; Ghosh and Schmidt, 2014; Ohira et al., 2014).

To systematically investigate the effect of Al on the stability region of DHMSs, we conducted high-temperature and high-pressure experiments using natural clinochlore, which is high pressure phase of serpentine, is believed to be one of the main storage sites for water in subducting slabs (Cannat et al., 1995). Furthermore, a chemical mixture in Fe-free system was used to make comparison. We determined the stability region of clinochlore up to the uppermost lower mantle pressure along the cold, hot subduction and normal mantle geotherm condition. Finally, we estimated water distribution in deep earth.

2. Experimental procedures

Two starting materials were used in present study. One was natural clinochlore (ChN) found somewhere in Russia, with the composition close to $Mg_{4.8}Fe_{0.2}Al_2Si_3O_{18}H_8$, containing about 15 wt% H_2O, 14 wt% Al_2O_3 and 3 wt% FeO. The other was Fe-free chemical mixture (ChM) with the composition similar to clinochlore $Mg_5Al_2Si_3O_{18}H_8$. The compositions were listed in Table 1. Both sample were preserved in a drying oven at 110 ℃ for a few weeks.

We conducted high-temperature and high-pressure experiments by using a Kawai-type 2000 ton multi-anvil apparatus installed at Geodynamics Research Center (GRC), Ehime University. Pressures at room temperature were calibrated by the diagnostic changes in the electrical resistances of ZnTe (9.6 and 12.0 GPa), ZnS (15.5 GPa), GaAs (18.3 GPa) and GaP (23.0 GPa) induced by the semiconductor-metal phase transitions at high pressures. In some experiments, we put forsterite in the center of cell assemblage to calibrate the pressures at high temperature. The results shows the obtained pressure at high temperatures are almost consistent with the calibration at room temperature. Tungsten carbide cubes with a truncation edge length (TEL) of 4 mm in combination with Cr-doped MgO-octahedra of 10 mm edge length (10/4 assemblage). Preformed pyrophyllite gaskets were used between the cubes. Rhenium was used as the heater. Two double sample capsule were used in cell assemblage, and we weld both sides of the sample capsule (AuPd) to prevent water loss during the experiment. The temperature was monitored by using a $W_{97}Re_3$-$W_{75}Re_{25}$ the thermocouple emf was not corrected for the effect of pressure. The cell assemblage is shown in Figure 1. The sample compressed to the desired value first and then held constant, after that, the AC

power was supplied to the Re heater in the furnace assemblage. After heating at high pressure, the charge was quenched by shutting off the electric power supply. The samples were recovered after releasing pressure slowly in 720h. The recovered sun products were mounted in epoxy resin and polished to perform phase identification and composition analysis.

The phase assemblages were identified using a micro-focus X-ray diffractometer (MicroMax-007HF; Rigaku Corp.), which is equipped with a rotative anode (Cu Ka_1 radiation), a two-dimensional imaging plate detector and ø100 μm collimator. The operating conditions were 40 kV, 30 mA, and exposure time for XRD analyses was 600 s. The microtextures and compositions were obtained using a field emission scanning electron microscope (FESEM, JSM7000F; JEOL) combined with an energy dispersive X-ray spectrometer (EDS, X-MaxN; Oxford Instruments plc.) with working parameters of 15 kV, 1 nA and collection times of 30–50 s. The EDS data were processed by the software Aztec (version 2.4, Oxford Instruments Nanotechnology Tools Ltd) using the XPP method (put forward by Pouchou and Pichoir in 1989). More detailed information see Zhou et al. (2016).

3. Results and Discussion

3.1. Phase assemblages

The experiments were performed at conditions of 14-25 GPa and 800-1600 ℃ for both the ChN and ChM by using two sample capsules. The experiment conditions and results for ChN and ChM were summarized in Table 2.

Natural clinochlore (ChN)

Figure 2 showed some back-scattered images (BSEI) of the run products for ChN. BSEI clearly indicated the micro-textures of some typical samples with bulk compositions of $Mg_{4.8}Fe_{0.2}Al_2Si_3O_{18}H_8$. The quenched crystals were big enough to be precisely identified. In Fig. 2a, PhE was found coexisting with garnet and some amount of liquid or melt appeared at 14 GPa and 1200 ℃. It is hardly to identify the water dissolve in melt or melt dissolve in water due to the high water content. Litasov and Ohtani (2002) also met the same situation when they tried to distinguish fluid and melts at high temperatures. To simplify the results, the melt was used in both run products. At 21 GPa and 1300 ℃, an enlargement of the ChN sample was shown in Fig. 2b, indicating composed of elongated shape of SUB and fine crystals of PhD. Fig. 2c revealing SUB + PhD and a trace of PhE + brucite were observed at 23 GPa and 1100 ℃, which means brucite was also an important water carrier in subduction slabs. At 25 GPa and 1600 ℃ garnet + bridgmanite and large amount of liquid appeared as shown in Fig. 2d. Furthermore, we did not observe any enstatite, wadsleyite or ringwoodite in quenched samples, which was complete different from previous studies. It suggested that those Al-bearing DHMSs have very broad thermal stability region.

The phase diagram of ChN was shown in Figure 3. The Al-bearing hydrous PhE, SUB and PhD were observed with *P*-*T* increasing in present study. The tendency of phase relations in our results were basically consistent with those of the previous works for DHMSs in MSH system (Kanzaki, 1991; Irifune et al., 1998; Litasov and Ohtani, 2003) however, huge differences were observed in our results, for example, PhE was occurred at low pressure and could remain stable up to transition zone condition. SUB + PhD were stable at least up to

uppermost lower mantle condition after PhE decomposed. Obviously, the added Al_2O_3 has greatly stabilized stability of DHMSs. Following the *P-T* path of cold subduction, the phase assemblage PhE + PhD was stable between 14-23 GPa, and even a trace of PhE was detected at 1150 ℃ and 25 GPa coexisting with PhD. The phase SUB was stable between 16-22 GPa coexisting with PhE + PhD. Following the *P-T* path of hot subduction, the phase assemblage PhE + Gt was observed between 14-18 GPa coexisting with fluid. The phase assemblage SUB + PhD was stable between 18-25 GPa, which may extend to higher pressures and temperatures. Following the *P-T* path of normal mantle geotherm condition, SUB was identified even at 1500 ℃ and 25 GPa.

According to a preliminary study by kanzaki (1991), PhE was stable at 13-17 GPa and 1000 ℃, whose stability limit was much lower compared with this study. Ohtani et al. (2000) found that SUB appeared after PhE decomposed around 1300 ℃ at 20 GPa in $MgSiO_3$+15 wt% H_2O system. In Figure 3, we can see PhE could exist up to uppermost lower mantle at very lower temperatures. The following mineral assemblages were observed coexisting with PhE in the pressure range from 14 to 18 GPa: Gt + PhE + Melt transformed to Gt + PhE + PhD, from Gt + PhE + PhD to Gt + PhE + SUB + PhD, and then to Gt + SUB + Melt at 1200 ℃. Stability field of PhE at 14 GPa should be stable up to1400 ℃ determined according to phase assemblage. The negative Clapeyron slope dP/dT of the phase boundary at high temperature for PhE was consistent with previous study by Irifune et al. (1998). Kawamoto et al. (1995) reported highest temperature stability of PhE was 1400 ℃ and 15.5 GPa, containing 1.5 wt% Al_2O_3, which indicated a trace amount of Al_2O_3 hugely increased its stability region.

The stability field of SUB was given in the phase diagram of Fig. 3. Generally, the stability region of SUB increased with pressure and temperature increasing, range from 1000 ℃ to 1400 ℃ and 18-25 GPa together with PhD. Perhaps due to positive Clapeyron slope of the phase boundary, SUB could remain stable at greater depth before transform to PhD. Some amount of SUB was observed at 1500 ℃ and 18 GPa, which almost 300 ℃ higher than Al-free SUB determined by in situ X-ray diffraction measurements (Inoue et al., 2006) at same pressure. Phase assemblage SUB + PhD were found to be stable at conditions of 800-1200 ℃ and 18-25 GPa in Al-free serpentine composition, which means those DHMSs only stable in very cold subduction. By contrast, we observed assemblage of SUB + PhD were stable up to 1400 ℃ and 25 GPa in ChN composition.

The stability region of PhD was identified in the pressure range from 14 to 25 GPa and the temperature range from 800 to 1400 ℃. It was surprising that PhD had a much extensive stability region, which never been reported before. PhD was observed under the following conditions; from 14 to 25 GPa below 950 ℃ coexisting with PhE, and transformed to SUB + PhD at temperature and pressure higher than 1000 ℃ and 18 GPa, then transformed to Gt + Brg + L at temperature and pressure higher than 1400 ℃ and 22 GPa. Frost and Fei (1998) reported the stability limit of PhD coexisting with SUB up to 1400 ℃ at 24 GPa in Mg_2SiO_4+ 20.5 wt % H_2O system. While another melting experiment has shown that PhD was stable at 1600 ℃ and 24 GPa in MASH system with 1 wt% Al_2O_3 (Ghosh and Schmidt, 2014). Although maximum thermal stability of PhD in our results may around 1500 ℃ at 25 GPa, which almost similar to above-mentioned results, water content was drastically increasing when PhD dissolving large amount of Al in structure described later in this article. All in all,

it was obvious that Al enhanced the stability region of DHMSs. Those Al-bearing DHMS remained stable along hot subduction, and some of them even survived in normal mantle geotherm condition.

Chemical mixture clinochlore (ChN)

Figure 4 showed BSEIs of the run products for ChM with bulk compositions of $Mg_5Al_2Si_3O_{18}H_8$. Phase assemblage illustrated here were almost consistent with that showed in Fig. 2, except for Fig. 4a and Fig. 4d. In Fig. 4a, PhE was coexisting with garnet and some amount of SUB appeared. In Fig. 4d, only garnet and liquid were observed. It seems that Fe contributed to form bridgmanite at high *P-T* condition. The bridgmanite observed in Fig. 2d was shown to contain a certain amount Fe and Al based on EDS results. Also, a trace amount of H_2O was obtained based on deficit from EDS weight total. This may suggested that dissolved Al and Fe help to absorb H_2O in bridgmanite. We have known that bridgmanite has ability to dissolve a certain amount of Fe, even in the natural one found in shocked meteorite (Tschauner et al., 2014). Also, bridgmanite has been suggested as the dominant host mineral for Al_2O_3 in the in lower mantle (Liu et al., 2016). Thus, there might be a large water reservoir in deep lower mantle.

The phase diagram of chemical mixture clinochlore (ChM) was shown in Figure 5. Generally, the phase relation in ChM was similar to ChN. PhE + PhD occurred throughout the pressure range from 14 to 25 GPa along cold subduction. PhE transformed to SUB + PhD at high pressures along hot subduction. Gt + PhE + PhD were observed at 800 ℃ and 14 GPa, transformed to Gt + PhE + SUB + Melt between 1050 ℃ and 1250 ℃, and then to Gt + Melt at higher temperatures. The assemblage of Gt + PhE + SUB + PhD were observed at 1100 ℃

and 18 GPa. Although we did not determine the accurate stability field of assemblage Gt + PhE + SUB + PhD around 1100 ℃ and 18 GPa, SUB should be stable between 1000 ℃ and 1300 ℃, which further transformed to SUB + PhD at high pressures and transformed to Gt + Melt at high temperatures. SUB + PhD had a very wide stability region from 1100 ℃ and 18 GPa at least up to 1400 ℃ and 25 GPa due to the positive slope dP/dT of the phase boundary. Single PhD was observed at 1100 ℃ and 25 GPa.

3.2. Mineral composition

Table 3 summarized the compositions of the minerals observed in the experiments.

PhE: The Mg/Si ratio in PhE varied from 1.451 to 3.43 for ChN and from 1.406 to 3.12 for ChM. It seems that Mg/Si ratio increasing with increased temperature in both starting composition. In ChN, PhE incorporated 9.5 wt% Al_2O_3 and 3.3 wt% FeO on average. In ChM, PhE incorporated 12.3 wt% Al_2O_3 on average. The H_2O contents estimated from the deficits from the EDS weight totals varied from 12.2 to 26.8 wt% for ChN and 12.8 to 33.7 wt% for ChM, respectively. kanzaki (1991) reported Mg/Si ratio of PhE was about 1.8 in $Mg(OH)_2$-SiO_2 system at 13-17 GPa and 1000 ℃, and contained 11.4 wt% H_2O. Containing about 1.8 at 14-17 GPa and 1100 ℃, and 11.8 wt% H_2O in hydrous peridotite (13.6 wt% H_2O) composition (Kawamoto 1996). Although the water content may be overestimated in our results, it drastically increased by Al incorporation.

SUB: SUB always had larger stoichiometric Mg/Si ratio (i.e., 3.2) for both ChN and ChM, which was consistent with previous studies (Ohtani et al., 2000; Ohtani et al., 2001). ChN contained 3.4 wt% Al_2O_3 and 3.14 wt% FeO and ChM contained 9.5 wt.% Al_2O_3 on

average, respectively. Compared with PhE, Al content decreased in SUB. The water content in SUB was estimated about 8.8 wt% for ChN and 14.8 wt% for ChM, which was higher than previous reports for Al-free system in both Mg_2SiO_4+5 wt% H_2O, Mg_2SiO_4+11 wt% H_2O system (Ohtani et al., 2001) and ideal H_2O content of Mg-SUB of 5.8wt%.

PhD: The Mg/Si ratio in phase D varied from 0.78 to 1.06 and H_2O contents calculated from the deficit in weight totals was 16.3 wt% on average for ChN, and varied from 0.84 to 0.95 and H_2O contents was 15.9 wt% on average for ChN. The variation of Mg/Si ratio and H_2O contents were negligible between ChN and ChM. The Mg/Si ratio varies from 0.57 to 0.71 and H_2O contents was 15.0 wt% on average reported by Frost and Fei (1998) in Mg_2SiO_4+20.5 wt% H_2O system. In the FMASH bulk composition (Ghosh and Schmidt, 2014), Mg/Si ratio varied from 0.56 to 0.66, H_2O content was 12.1 wt% on average. The higher Mg/Si ration in our results were due to the substitution mechanism between Al and Si, and discussed later.

Garnet: As we know, the ideal formula of pyrope garnet is $Mg_3Al_2Si_3O_{12}$ with 25.3 wt%Al_2O_3. Garnet appeared in quenched run products contained 19.2 wt% Al_2O_3 in ChN and 21.0 wt% Al_2O_3 in ChM at 1100 ℃ and 18 GPa coexisting some of DHMSs, indicating DHMSs could absorb a large amount of Al even coexisting with garnet.

3.3. Melt composition

The temperature where liquid just began to appear in run products was higher than reported in H_2O-saturated KLB-1 peridotite (Kawamoto 1996) and hydrous CMAS (Litasov and Ohtani, 2003). Composition of partial melt was measured by EDS. Melt obtained here

had both low MgO (27.0-36.6 wt%) and SiO_2 (10.0-25.8 wt%) in ChN and MgO (29.1-38.2wt%) and SiO_2 (6.6-15.6wt%) in ChM relative to those study for hydrous CMAS-pyrolite (Litasov and Ohtani, 2003).

The relationship between pressure and melt composition shown in Figure 6, compared with results reported by Kawamoto (1996). It clear showed that the tendency of relationship for ChN and ChM was consistent with each other. With pressure and temperature increased, almost all the oxide contents increasing, except for FeO decreased around 25 GPa, because of the bridgmanite appeared in ChN. Compared with garnet, iron was more like to incorporate into bridgmanite. The MgO content increasd in both ChN and ChM, however, it decreased in H_2O-saturated KLB-1 peridotite (Kawamoto 1996). It was because that melt composition obtained in our result at temperatures higher than 1200 ℃ and even up to 1500 ℃. DHMSs became unstable in this temperature range, decomposing of DHMSs drastically increased MgO content. In Fig. 6, we found that only small amount of Al_2O_3 dissolved in melt, especially temperatures below the stability region of Al-bearing DHMSs, suggesting DHMSs could contain large amounts of Al.

3.4. The effect of temperature on Al content in DHMSs

Considering mentioned above, Al-bearing bulk composition has broadened the stability region of DHMSs and increased the water content. In order to identify the relationship between temperature and Al content, we determined the temperature dependence of Al at certain pressures was shown in Fig. 7. Fig. 7(a) showed temperature dependence of Al in SUB. It was obvious that with temperature increasing Al content also increased in both ChN

and ChM. PhD had the same tendency with SUB as shown in Fig. 7(b). Combine the pressure effects, we may infer that SUB and PhD become much stable with increased Al due to the positive Clapeyron slope of phase boundary for SUB + PhD up to uppermost lower mantle. On the contrary, Al content decreased in PhE as shown in Fig. 7(c), which indicated PhE become unstable at elevated pressure and temperature, probably due to the negative Clapeyron slope of phase boundary.

According to our results, Al greatly broadens the stability region of DHMSs. Since a small amount of Fe incorporated in ChN, we can hardly determine its effect. More work need to be done to clarify the effect of Fe on stability of DHMSs.

3.5. The Al substitution mechanism in DHMSs

The Al substitution mechanism in DHMSs were analyzed by using cell check method shown in Figure 8 based on chemical composition of SUB, PhE, and PhD.

In Fig. 8(a), a negative relationship between Mg and Al was observed for SUB, with Al content increased Mg content decreasing in both ChN and ChM. The trend of our result was consistent with those of previous studies with FMASH and CMAS-pyrolite composition. All the data were constrained by two reaction, $Si^{4+} = Al^{3+} + H^{+}$ in red color and $2Mg^{2+} = Al^{3+} + H^{+}$ in green color. Then, we can acquire the Al substitution for Mg in SUB by using cell check method, (Mg + Fe) : Al = (10.0-8.0) : (2.0-0.0) = 1 : 1. Fig. 8(b) showed relationship between Al and Si content in ChN and ChM for SUB. Although some data in ChN, ChM and those of previous studies were little higher than that of the fitting result as shown in pink line, substitution mechanism between Al and Si was identified with Si : Al = 1 : 2 by using cell

check method. Combining Mg + Fe and Si together, we can finally determine the Al substitution mechanism in SUB by reaction $2Mg^{2+}+ Si = 2Al^{3+} + 2H^{+}$. In the same way, Al substitution mechanism in PhD and PhE were determined by following reaction $Si = Al^{3+} + H^{+}$ and $2Mg^{2+} = Al^{3+} + H^{+}$ as shown in Fig. 8(c), (d), (e) and (f), respectively.

3.6. The stabilit of Al-bearing DHMSs in the Earth's interior

Phase relation of DHMSs have been investigated by several scientists (Kanzaki, 1991; Gasparik 1993; Kawamoto 1996; Ohtani et al., 2001; Litasov and Ohtani, 2002; Ohtani et al., 2004; Komabayashi and Omori, 2006; Nishi et al., 2014). Although different starting composition were used, they found that almost all DHMSs were only stable within cold subduction slab condition in MSH system, no matter whether in water-saturated condition or not. However, we found that the stability fields of Al-bearing DHMSs greatly shift to higher temperatures, much of them still remain stable above slabs geotherm, and even some of them stable up to geotherm at manle transition zone condition.

The water content estimated from weight total in PhE, SUB and PhD as a function of temperature were shown in Figure 8. Generally, the water content in Al-bearing DHMSs drastically increased compared with Al-free system due to the Al substitution mechanism in DHMSs as shown before. The dissolved Al in DHMSs also ensure them stable at relative high temperature and possess large amount of water simultaneously. Studies have indicated that Al prefer to distribute in DHMSs than coexisting phases (Bolfan-Casanova et al., 2003; Litasov et al., 2005; Ghosh and Schmidt, 2014; Ohira et al., 2014; Kakizawa et al., 2018). Ghosh and Schmidt (2014) reported that Al-bearing PhD could remain stable up to 1600 ℃

at 24 GPa when only incorporated 1% Al_2O_3. Pamato et al. (2015) found that Al-rich PhD was stable at temperatures up to 2000 ℃ at 26 GPa. We have known that there is about 5 wt% Al_2O_3 in peridotic model, and even much higher in MORB composition. Therefore, it is expected that Al-bearing DHMSs are act as important water storage sites in mantle transition zone and uppermost lower mantle.

Studies have suggested that large amount of water was possibly trapped in transition zone (Inoue 1994; Inoue et al., 1995; Pearson et al., 2014; Fei et al., 2016). Much of trapped water would be released when ringwoodite transforming to bridgmanite, since partitioning experiment has shown water solubility in bridgmanite was quite low (Ballaran et al., 2000). Although study has shown MORB would lost its water during subducting (Litasov and Ohtani, 2005), the trapped water in transition zone may react with Al-rich MORB composition to form Al-bearing DHMSs. In addition, fluid released from bottom of heated subducting slab may also react with overlying descending slab. Thus, these Al-bearing DHMSs may become important water storage sites in the pyrolitic mantle due to their broad thermal stabilities.

3.7. Water distribution in the mantle

Previous studies have concluded that DHMSs would lost much of their water along subduction at the chock point due to their limited stability, which only restricted to the cold slab geotherm (Litasov and Ohtani, 2003; Komabayashi and Soichi Omori, 2006). The bulk water content in subducting slab would decrease from 12.2 to 3.66 wt%, was controlled by $5Atg = 14phA + 142En + 113H_2O$ at depth around 200 Km. Only 3.66 wt% water was

transported into deep mantle in cold subducting slab (Komabayashi and Soichi Omori, 2006).

In the present study, we systematically determined stability region of Al-bearing DHMSs, confirming their stability limit shifted to higher temperatures and water content drastically increased by Al substitution in crystal structure. Water transportation into the Earth's mantle can't be merely discussed on the basis of water-bearing reactions in MSH system. Although we didn't conduct experiments to identify effect of Fe on stability of DHMSs, previous study reported thermal stability of SUB and PhD extended in Fe-rich hydrous FMAS system (Ganskow and Langenhorst, 2014). Thus, a certain amount of water would be trapped in Al, Fe-bearing system in relatively natural composition along subduction.

Studies have shown Al prefer to distribute in DHMSs than coexisting phases (Bolfan-Casanova et al., 2003; Litasov et al., 2005; Ghosh and Schmidt, 2014; Ohira et al., 2014). Because of bridgmanite is the main host for Al and PhD is the major DHMS in lower mantle condition (Liu et al., 2016; Nishi et al., 2014), therefore, Al-bearing PhD should have a large thermal stability region than previously thought due to its high Al content, which suggests much water can be transported into lower mantle in subducting slab. Since PhH high pressure polymorph of PhD was identified to form solid solution with δAlOOH and εFeOOH (Nishi et al., 2014; Ohira et al., 2014; Walter et al., 2015; Kawazoe et al., 2017; Nishi et al., 2017; Panero and Caracas, 2017), it is expected that δAlOOH-εFeOOH-phase H ternary system deliver a certain amount of water to deepest part of lower mantle. The released hydrogen may hugely influence physical and chemical properties of deep lower mantle locally or regionally.

4. Implication

The stability of Al-bearing DHMSs have been shown can remain stable above slabs geotherm. Much more than chock point water (3.66 wt%) could be transported into transition zone and lower mantle. Our result is likely to provide upper limit for maximum amount of water transported into deep earth. If descending slabs stagnate at transition zone, Al-poor DHMSs may become unstable as they are cooked by surroundings. The dehydration of these minerals may cause seismic discontinuity at transition zone, for example beneath China. Hydrous ringwoodite was found as inclusions in diamond suggested that transition zone was in hydrous condition, at least partially hydrated (Pearson et al., 2014). The released water from transition zone at elevated pressure and temperature probably react with Al-rich mafic crustal rocks as referred by Pamato et al. (2015) again to form Al-rich DHMSs. Due to their wide thermal stabilities and high water content, the dehydration of Al-bearing SUB and PhD are likely in charge of discontinuity at depths of 730-770 Km beneath North America and Japan slab and Western-Pacific Subduction Zones above 800 Km (Chen and Ai, 2009; Schmandt et al., 2014; Liu et al., 2016; Porritt and Yoshioka, 2016).

To illustrate the stability of subducted carbonates is the key to understanding global carbon cycle. Melting of carbonates has close ties with formation of diamonds, especially in C-H-O system (Li et al., 2016). Since stability of Al-bearing DHMSs seems to have overlapped stability region as overlying carbonates, it is expect that dehydration of Al-bearing DHMSs greatly change melting behavior of those carbonates. This may be one of possible reasons to explain formation mechanism of ultradeep diamonds. Because of released

water will influence the redox state and chemical reaction of carbonates. The high mobility of carbonatitic melt possibly upwells from transition zone and lower mantle, it will be trapped at some depths. If this is the case, a potential mechanism helps to interpret small-scale seismic wave anomaly at lower part of upper mantle (Vinnik and Farra, 2006; Li et al., 2016).

In addition, halogens are important volatiles, have been believed to strongly affect physical and chemical properties of melt (Edgar and Pizzolato, 1995). Single-crystal X-ray diffraction experiment has indicated that superfluorous B ($Mg_{10}Si_3O_{14}F_4$) has same orthorhombic structure with superhydrous phase B ($Mg_{10}Si_3O_{14}H_4$) in which F^- has similar ionic charge and radius as OH^- (Hazen et al., 1997). We may infer that Al^{3+}+F^- also readily substitute for Mg^{2+} and Si^{4+} as Al^{3+}+H^- in DHMSs. Therefore, water together with those halogens will be transported not only to transition zone, but also in deep lower mantle, playing remarkable role for global volatiles cycle, since a trace amount of volatiles hugely effects geodynamic process in earth's interior.

Tables in chapter 2

Table 1. Chemical composition (wt %) of starting materials

	ChN	ChM
MgO	34.1	36.1
Al_2O_3	13.3	18.4
SiO_2	34.0	32.5
FeO	2.8	0
H_2O	15.4*	13.0
Total	100	100

* deficit from EPMA weight total

Table 2. Experimental conditions and run products for ChN and ChM.

Run	Pressure	Temperature	Time	Results	
	(GPa)	(℃)	(min)	ChN	ChM
OS3052	14	800	300	PhE+PhD	Gt+PhE+PhD
OS3056	14	1050	120	Gt+PhE+L(n.a.)	Gt+PhE+SUB+L(n.a.)
OS3033	14	1200	180	Gt+PhE+L(n.a.)	Gt+PhE+SUB+L
OS3050	14	1250	330	Gt+PhE+L	Gt+PhE+SUB+L
OS3031	16	1100	180	Gt+PhE+PhD	Gt+PhE+PhD
	16	1200	120	Gt+PhE+L	Gt+PhE+L
OS3061	16	1500	20	Gt+L	Gt+L(n.a.)
	17	1300	20	Gt+L	Gt+L
OS3048	18	950	1200	PhE+SUB(T)+PhD +Br(T)	PhE+SUB(T)+PhD + Br(T)
OS3042	18	1100	300	Gt+PhE+SUB+PhD	Gt+PhE+SUB+PhD
OS3021	18	1200	180	Gt+PhE+SUB+L	Gt+L
OS3060	18	1520	20	Gt+SUB+L(n.a.)	Gt+L(n.a.)
	19	1300	20	Gt+SUB+L(n.a.)	Gt+L
	19.5	1100	180	SUB+PhD	SUB+PhD
OS3046	21	950	660	PhE+PhD+Br(T)	PhE+PhD+Br(T)
OS3025	21	1200	180	SUB+PhD	SUB+PhD
OS3035	21	1300	180	SUB+PhD	SUB+PhD
OS3059	21	1560	20	Gt+L(n.a.)	Gt+SUB+L
OS3044	23	950	450	PhE+PhD+Br(T)	PhE+PhD+Br(T)
OS3043	23	1100	360	SUB+PhD+Br(T)	SUB+PhD+Br(T)

OS3040	23	1300	240	SUB+PhD	SUB+PhD
OS3058	23	1600	20	Gt+Brg+L(n.a.)	Gt+L(n.a.)
OS3055	25	900	300	PhE+PhD+Br(T)	PhE+PhD+Br(T)
OS3053	25	1150	210	PhE(T)+PhD	PhD
OS3051	25	1300	180	SUB+PhD	SUB+PhD
	25	1400	20	SUB+PhD+L(n.a.)	SUB+PhD+L(n.a.)
OS3057	25	1600	30	Gt+Brg+L	Gt+L

ChN: natural clinochlore, ChM: chemical mixture with the composition similar to natural clinochlore. PhE: Al-bearing phase E, SUB: Al-bearing superhydrous phase B, PhD: Al-bearing phase D. Gt: garnet, Br: brucite, Brg: bridgmanite, L: melts. na: not analysed, T: trace

Table 3. Compositions of various phases in ChN and ChM

ChN	P (GPa)	T (℃)	Phase	MgO	Al_2O_3	SiO_2	Fe_2O_3	Total
	14	800	PhE	35.20(22)	11.34(21)	34.00(17)	2.85(22)	83.40(34)
			PhD	25.01(36)	20.44(75)	37.22(64)	1.89(33)	84.57(21)
		1050	Gt	29.85(6)	20.34(31)	44.97(15)	2.98(10)	98.15(38)
			PhE	36.47(63)	11.75(53)	30.75(36)	2.81(13)	81.78(65)
		1200	Gt	31.77(31)	22.45(16)	47.32(46)	2.44(47)	103.98(16)
			PhE	44.67(86)	6.98(35)	31.10(65)	3.62(15)	86.4(41)
		1250	Gt	30.09(41)	21.50(138)	44.86(42)	2.39(42)	98.85(142)
			PhE	39.57(200)	11.65(237)	32.28(174)	2.88(46)	86.37(170)
			M	26.98	2.17	9.99	2.78	41.92
	16	1100	Gt	30.45(41)	21.07(73)	46.34(86)	2.63(29)	100.49(101)
			PhE	40.49(131)	8.36(63)	32.10(37)	2.77(19)	83.72(54)

		PhD	23.57(81)	19.64(140)	41.34(147)	1.88(20)	86.43(85)
	1200	Gt	30.95(57)	19.66(112)	46.54(55)	2.37(32)	99.52(69)
		PhE	41.19(112)	8.44(27)	17.88(42)	5.68(22)	73.18(151)
	1500	Gt	30.51(32)	22.81(35)	45.15(45)	1.06(13)	99.54(60)
		M	31.62	9.41	25.84	3.32	70.19
17.5	1300	Gt	30.97(72)	21.43(145)	46.54(100)	2.16(21)	101.10(137)
		M	30.36	3.21	12.62	4.28	50.48
18	950	PhE	43.91(88)	8.84(52)	32.05(45)	3.03(15)	87.84(72)
		PhD	23.37(77)	17.62(124)	40.38(115)	2.15(17)	83.52(84)
	1100	Gt	29.68(20)	19.23(115)	44.66(68)	1.89(26)	95.46(56)
		PhE	38.59(75)	6.24(26)	28.75(84)	2.60(29)	76.17(136)
		SUB	55.43(33)	3.26(54)	27.13(45)	2.40(15)	88.22(22)
		PhD	21.00(54)	18.63(51)	40.07(41)	1.85(17)	81.55(17)
	1200	Gt	31.21(61)	19.87(42)	46.44(95)	1.69(32)	99.22(81)
		PhE	41.17(21)	5.04(23)	24.56(74)	4.86(24)	75.64(74)
		SUB	57.00(54)	3.75(34)	25.92(28)	3.7(23)	90.38(83)
		M	32.33	3.14	14.55	3.95	53.97
	1520	Gt	30.73(38)	21.76(82)	45.55(55)	1.62(68)	99.66(59)
		SUB	56.93(32)	4.67(24)	25.41(27)	4.16(21)	91.17(38)
19	1300	Gt	32.29(10)	19.56(86)	48.15(18)	2.12(29)	102.12(60)
		SUB	59.27(22)	4.67(37)	26.60(25)	3.59(24)	94.13(45)
19.5	1100	SUB	58.93(129)	2.65(38)	28.04(37)	2.58(14)	92.21(85)
		PhD	22.31(43)	19.67(55)	41.20(20)	1.91(17)	85.09(91)
21	950	PhE	33.21(45)	13.25(81)	34.16(45)	2.83(21)	83.45(68)
		PhD	26.91(86)	16.72(72)	37.83(93)	2.53(18)	83.99(99)

	1200	SUB	60.38(78)	2.46(13)	27.47(47)	2.66(16)	92.97(114)
		PhD	22.01(42)	18.04(36)	41.97(40)	2.16(18)	84.18(71)
	1300	SUB	58.79(45)	2.82(25)	27.01(30)	2.87(37)	91.50(64)
		PhD	22.67(117)	18.53(53)	40.81(80)	2.15(20)	84.16(69)
	1560	Gt	30.00(24)	22.91(26)	43.85(31)	1.12(6)	96.76(53)
23	950	PhE	36.33(45)	12.42(160)	33.95(113)	2.57(13)	85.27(90)
		PhD	25.61(60)	17.27(45)	38.22(44)	2.44(21)	83.53(33)
	1100	SUB	58.42(174)	3.45(80)	28.07(69)	3.63(16)	93.57(74)
		PhD	23.80(88)	19.31(95)	40.02(80)	2.89(13)	86.03(102)
	1300	SUB	54.79(97)	2.83(37)	24.91(36)	1.86(14)	84.40(35)
		PhD	20.65(24)	17.65(29)	35.89(15)	1.79(18)	75.98(44)
	1600	Gt	30.51(28)	20.70(54)	45.18(24)	0.79(17)	97.18(56)
		Brg	31.60(108)	8.18(68)	46.96(36)	9.34(100)	96.08(129)
25	1150	PhD	25.95(93)	16.06(84)	39.57(43)	1.80(17)	83.38(49)
	1300	SUB	59.84(57)	2.98(12)	26.78(34)	2.67(13)	92.28(51)
		PhD	23.12(34)	19.07(38)	40.95(47)	2.29(7)	85.43(45)
	1400	SUB	57.98(35)	4.84(20)	25.67(32)	3.14(12)	91.62(58)
		PhD	22.01(73)	19.10(66)	42.42(63)	2.15(22)	85.68(68)
	1600	Gt	30.57(40)	21.86(54)	45.13(68)	0.69(5)	98.25(152)
		Brg	32.51(74)	8.11(46)	48.09(12)	8.86(34)	97.58(120)
		M	36.64	6.52	18.50	3.98	65.64

ChM	P (GPa)	T (℃)	Phase	MgO	Al_2O_3	SiO_2	Total
	14	800	Gt	30.97(40)	23.10(22)	45.98(59)	100.05(95)
			PhE	32.44(210)	16.43(45)	32.08(15)	80.95(98)
			PhD	23.06(127)	22.27(72)	37.24(113)	82.58(70)
		1050	Gt	31.11(41)	22.82(35)	45.87(60)	99.80(101)
			PhE	42.45(83)	8.39(22)	28.07(41)	78.90(117)
			SUB	38.57(134)	10.67(42)	17.35(52)	66.58(212)
		1200	Gt	30.85(57)	23.05(71)	45.14(52)	99.04(82)
			PhE	44.04(38)	8.55(13)	27.56(17)	80.15(59)
			SUB	41.48(95)	10.35(81)	18.94(55)	70.76(68)
			M	29.88	3.33	7.72	40.93
		1250	Gt	30.82(15)	24.43(8)	45.03(24)	100.28(31)
			PhE	43.38(77)	8.90(43)	26.65(50)	78.94(169)
			SUB	59.00(116)	8.02(24)	24.54(22)	91.56(151)
			M	29.17	3.93	6.63	39.73
	16	1100	Gt	31.69(43)	23.00(38)	46.56(65)	101.25(120)
			PhE	44.69(39)	13.95(26)	27.64(39)	86.29(76)
			PhD	22.98(27)	23.79(70)	39.41(92)	86.18(86)
		1200	Gt	30.55(33)	23.57(42)	45.09(45)	99.21(86)
			PhE	37.02(93)	11.63(49)	17.69(61)	66.34(203)
		1500	Gt	31.47(29)	22.97(49)	44.60(27)	99.04(65)
	17	1300	Gt	31.00(19)	24.34(34)	45.30(20)	100.64(62)
			M	34.82	5.31	9.11	49.24
	18	950	PhE	34.17(134)	17.84(120)	35.19(98)	87.19(111)
			PhD	24.24(77)	22.41(103)	38.11(72)	84.76(112)
		1100	Gt	29.64(37)	21.00(59)	43.98(61)	94.63(87)
			PhE	40.53(59)	12.89(29)	25.48(20)	78.91(95)
			SUB	59.59(58)	2.29(11)	27.01(34)	88.89(89)
			PhD	21.56(20)	21.91(40)	38.19(39)	81.66(69)
		1200	Gt	30.57(24)	23.67(41)	44.89(34)	99.13(67)
			M	31.07	4.95	8.88	44.90
		1520	Gt	30.74(16)	24.13(18)	44.93(43)	99.79(51)
	19	1300	Gt	31.50(24)	24.18(49)	46.08(50)	101.76(70)
			M	38.16	6.55	11.47	56.17
	19.5	1100	SUB	61.08(99)	3.74(48)	28.14(35)	92.97(59)

		PhD	22.45(23)	24.22(39)	39.14(31)	85.81(59)
21	950	PhE	32.34(27)	16.68(157)	34.31(137)	83.33(242)
		PhD	23.18(86)	21.27(77)	38.27(23)	82.72(58)
	1200	SUB	59.68(108)	5.29(47)	26.63(39)	91.60(65)
		PhD	22.47(99)	23.53(46)	39.22(74)	85.22(79)
	1300	SUB	60.07(79)	4.43(34)	26.92(47)	91.43(71)
		PhD	22.05(37)	23.18(61)	38.64(70)	83.87(77)
	1560	Gt	30.23(14)	20.62(41)	44.57(25)	96.54(77)
		SUB	55.29(35)	9.60(31)	23.27(18)	88.16(48)
		M	33.94	7.50	12.92	54.36
23	950	PhE	37.49(193)	15.51(143)	33.27(215)	86.27(283)
		PhD	24.05(103)	21.08(72)	38.67(75)	83.80(156)
	1100	SUB	62.08(59)	3.53(32)	28.01(61)	93.62(76)
		PhD	24.18(48)	23.25(107)	39.64(74)	87.07(72)
	1300	SUB	55.44(52)	5.27(30)	24.07(30)	84.78(57)
		PhD	20.31(21)	21.77(56)	34.70(58)	76.77(88)
	1600	Gt	30.04(24)	22.38(40)	44.01(26)	96.44(90)
25	1150	PhD	24.36(46)	20.77(38)	39.77(63)	84.90(110)
25	1300	SUB	61.74(19)	3.59(18)	27.23(30)	92.56(22)
		PhD	23.62(23)	21.93(49)	40.34(56)	85.89(44)
25	1400	SUB	59.15(51)	7.01(23)	25.40(39)	91.56(74)
		PhD	21.33(24)	23.65(83)	39.94(78)	84.93(51)
	1600	Gt	30.51(23)	22.81(27)	44.54(32)	97.85(50)
		M	36.71	9.18	15.55	61.44

Figures in chapter 2

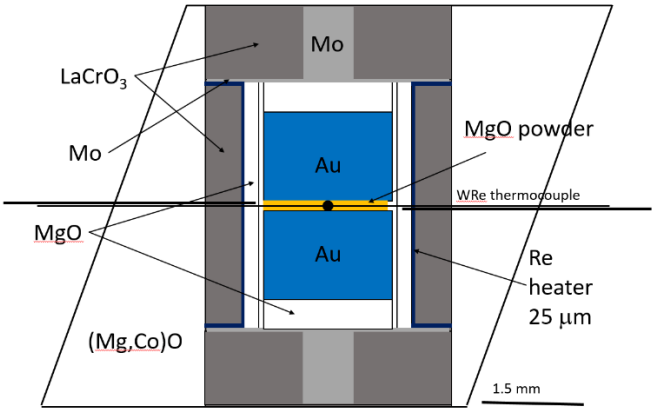

Figure 1. 10/4 cell assemblage for melting experiments.

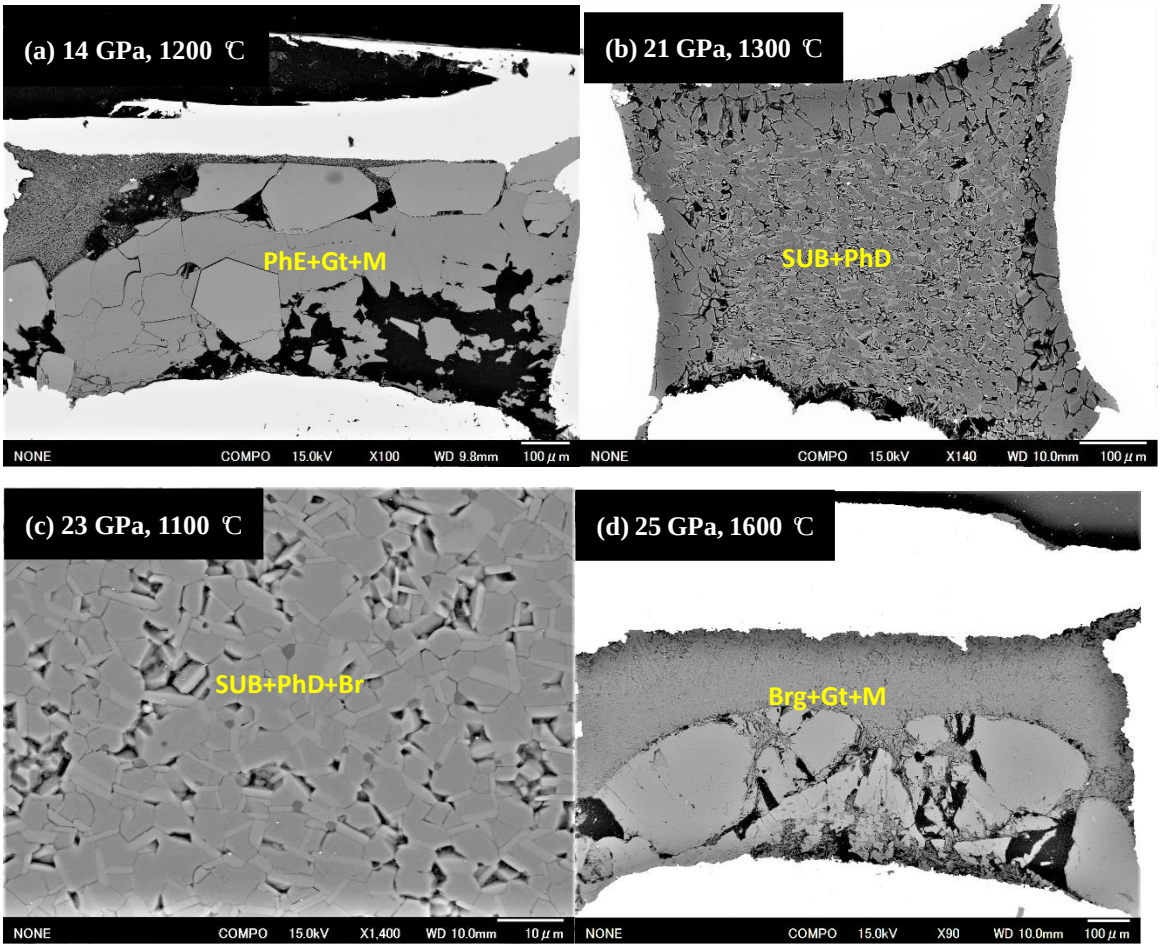

Figure 2. Backscattered electron images of representative run products at various pressure and temperature condition. (a) 14 GPa and 1250℃, crystal of PhE and Gt were big enough to be clarified. (b) 21 GPa and 1300℃, longer shaped SUB in bright color and PhD in relative dark color were identified. (c) 23 GPa and 1100℃, a trace of brucite in dark color was found coexisting with SUB+PhD. (d) 25 GPa and 1600℃,Brg and Gt were observed coexisting with Brg and melt whose phase assemblage transformed from SUB+PhD at high temperature.

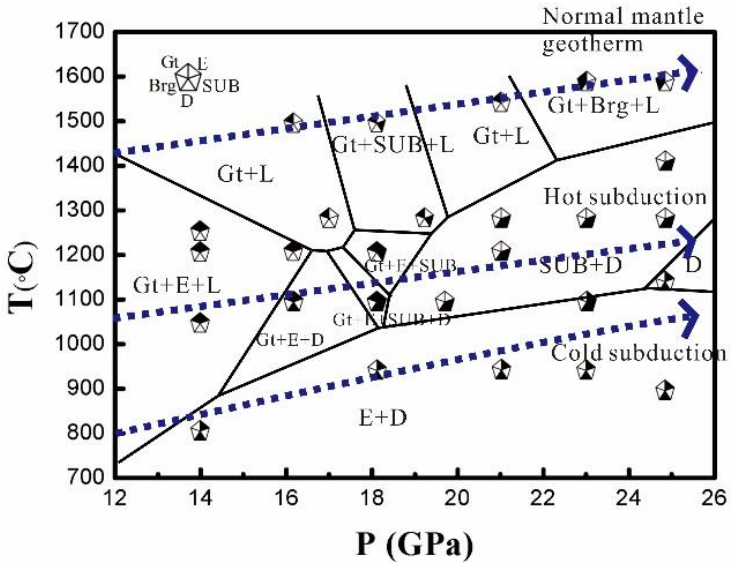

Figure 3. Phase relations in the natural clinochlore (ChN, $Mg_{4.8}Fe_{0.2}Al_2Si_3O_{18}H_8$) system up to 25 GPa and 1600 ℃. The Al-bearing hydrous PhE, SUB and PhD were observed at various *P-T* condition in present study.

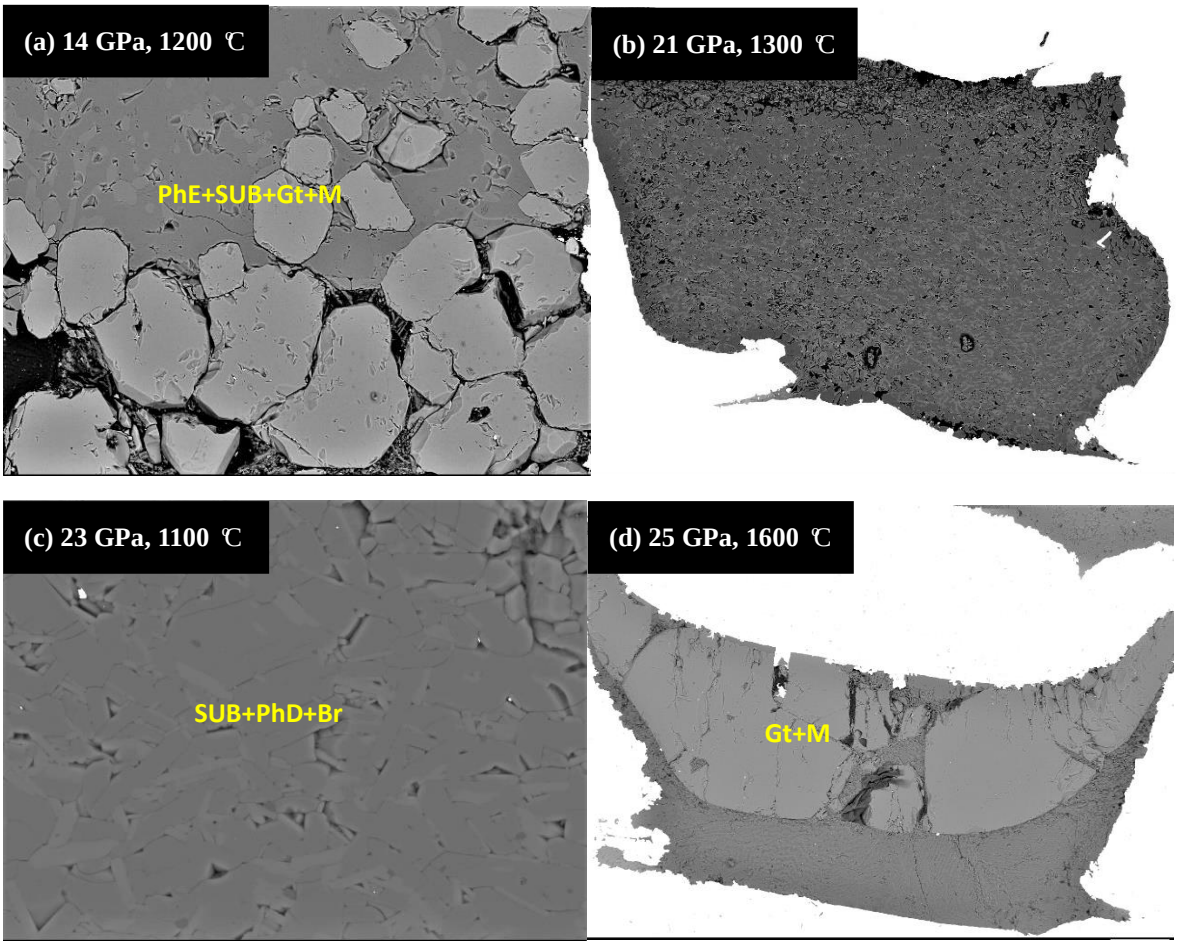

Figure 4. Backscattered electron images of representative run products at various pressure and temperature condition. (a) 14 GPa and 1200℃, crystal of PhE and Gt were big enough to be clarified. (b) 21 GPa and 1300℃, longer shaped SUB in bright color and PhD in relative dark color were identified. (c) 23 GPa and 1100℃, a trace of brucite in dark color was found coexisting with SUB+PhD. (d) 25 GPa and 1600℃, Gt was observed coexisting with melt whose phase assemblage transformed from SUB+PhD at high temperature.

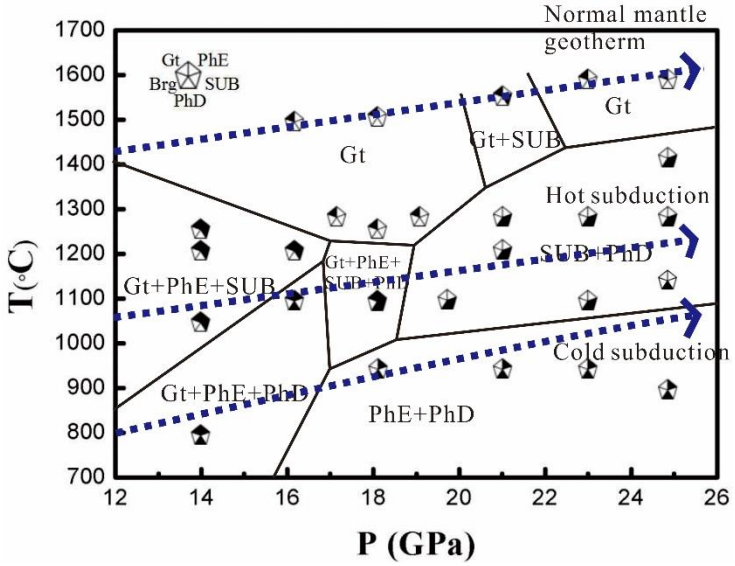

Figure 5. Phase relations in the natural clinochlore (ChN, $Mg_{4.8}Fe_{0.2}Al_2Si_3O_{18}H_8$) system up to 25 GPa and 1600 ℃. The Al-bearing hydrous PhE, SUB and PhD were observed at various *P-T* condition in present study.

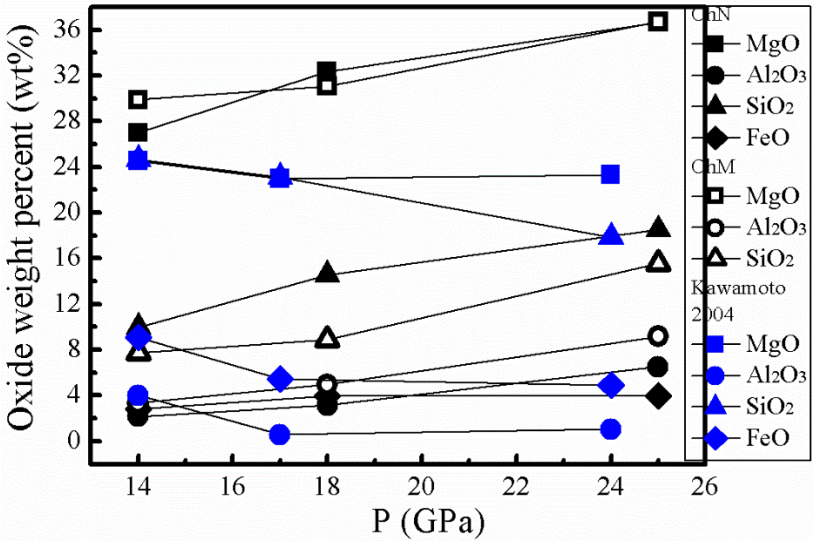

Figure 6. Relationship between composition and pressure in ChN and ChM compared with previous study.

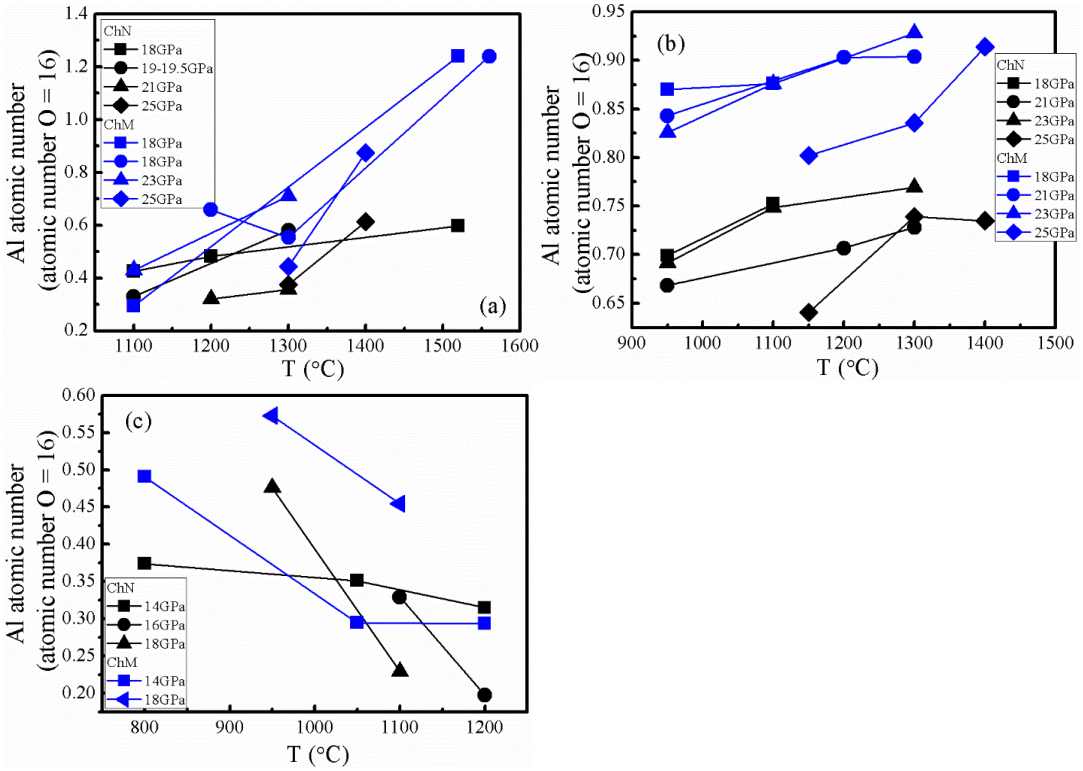

Figure 7. Relationship between temperature and Al content in (a) SUB, (b) PhD and (c) PhE at fixed pressures. The tendency for SUB and PhD was similar to each other, with temperature increased Al content also increasing. However, PhE has opposite trend.

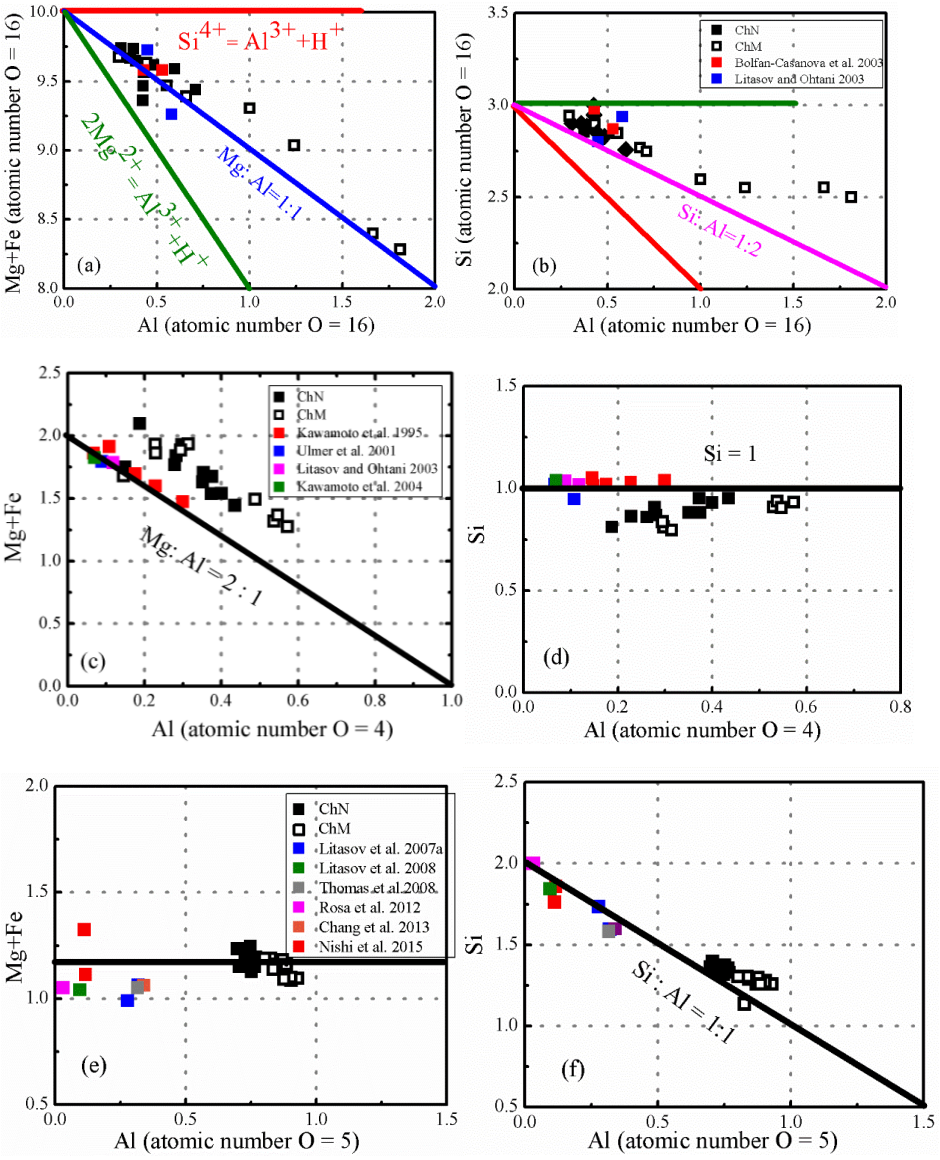

Figure 8. The Al substitution mechanism in DHMSs were analyzed by using cell check method, based on chemical composition of SUB, PhE, and PhD. Al substitution mechanism for SUB was shown in (a) and (b). We could easily recognized the Al substitution mechanism for Mg+Fe (Mg : Al = 1 : 1) and Si (Si : Al = 1 : 1), which can be written as $2Mg^{2+}+Si^{4+}\leftrightarrow 2Al^{3+}+ 2H^{+}$. The same method were used for analysis of PhE in (c) and (d), and PhD in (e) and (f).

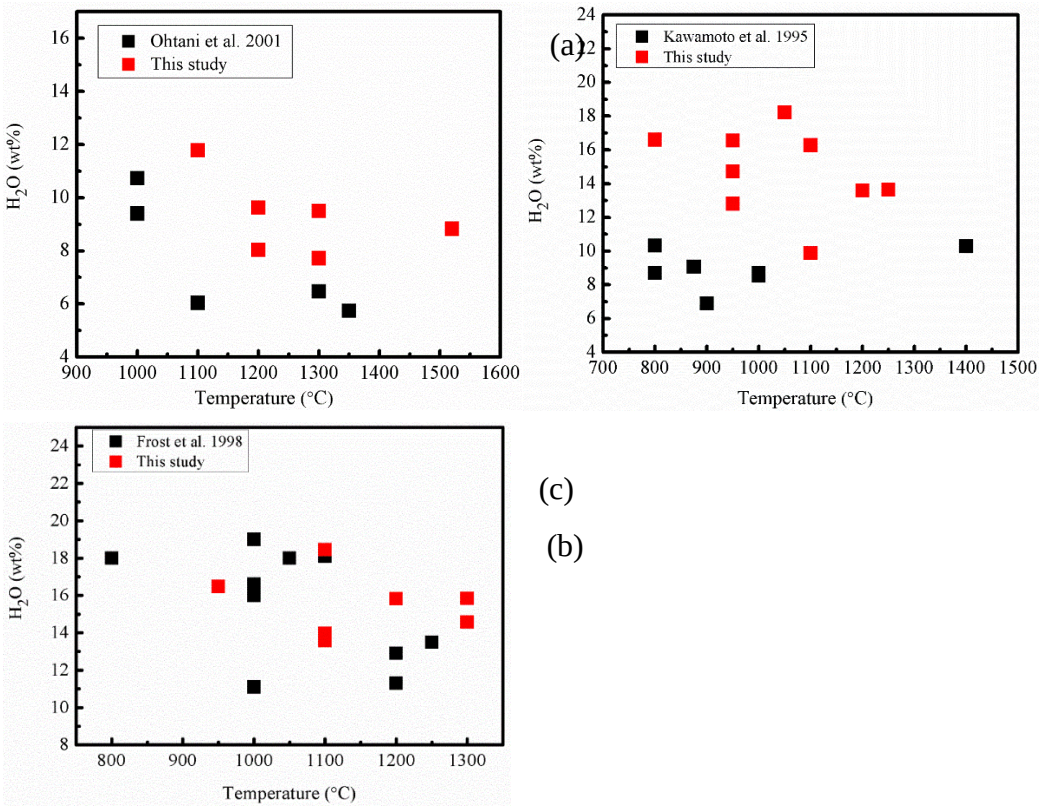

Figure 9. The water content in (a) SUB, (b) PhE and (c) PhD as a function of temperature obtained based on deficit of total weight percent. Water determined by SIM were shown in cycle.

Chapter 3

Melting of Al-rich phase D up to the uppermost lower mantle and transportation of H_2O to the deep Earth

(Accepted by Geochemistry, Geophysics, Geosystems)

Abstract

We investigated the stability of the Al-rich dense hydrous magnesium silicate phase D (PhD) in a MgO-Al_2O_3-SiO_2-H_2O (MASH) system between 14 and 25 GPa at 900–1500 ℃. Al-rich PhD has a very wide stability region from 900 ℃ and 14 GPa to at least 1500 ℃ and 25 GPa, showing strong temperature stability with increasing pressure. Al-rich PhD decomposes to phase Egg at pressure of the mantle transition zone, whereas it decomposes to δ-AlOOH phase with a temperature increase at pressure of the uppermost lower mantle. X-ray diffraction and Raman spectroscopy measurements of Al-rich PhD show that the unit-cell volume is slightly larger, but the Raman spectra resemble that of Al-free PhD.

The wide stability region of Al-bearing PhD would contribute an important storage site for water in the mantle transition zone, suggesting that it can deliver a certain amount of water into the lower mantle along hot subduction and even at the normal mantle geothermal P–T condition. Furthermore, the dehydration of Al-bearing PhD might be responsible for a series of observed seismic discontinuities from the transition zone to the uppermost lower mantle, and even for deep earthquakes in some typical locations.

1. Introduction

Many experiments and theoretical calculations have indicated that H_2O plays a key role in the geodynamics of the Earth's interior because it strongly affects the melting, phase transitions, and physical properties of minerals (Inoue, 1994; Irifune et al., 1998; Ohtani et al., 2000; Komabayashi and Omori, 2006; Ghosh and Schmidt, 2014; Myhill et al., 2016). A

series of dense hydrous magnesium silicate phases (DHMSs) such as phase A (PhA), phase E (PhE), superhydrous phase B (SUB), phase D (PhD), and phase H (PhH) have been suggested as potential water carriers to the mantle transition zone and even to the lower mantle under conditions presented in the cold subducting slabs (Kawamoto et al., 1996; Ohtani et al., 2001; Litasov and Ohtani, 2003; Komabayashi et al., 2005; Nishi et al., 2014). Because of their importance, DHMSs have been studied extensively in MgO-SiO_2-H_2O (MSH) systems. Among them, PhD is believed to be the main storage site for water in the uppermost lower mantle (Nishi et al., 2014). Actually, PhD is the decomposed product of serpentine in subducting slabs at mantle transition zone, with the ideal formula of $MgSi_2O_6H_2$. In the MSH system, it has been proposed that the maximum thermal stability of PhD is 1400 ℃ at 26 GPa (Frost and Fei, 1998). Reportedly, it can exist around 45 GPa along cold subduction (Frost and Fei, 1998; Shinmei et al., 2008; Tsuchiya, 2013; Nishi et al., 2014; Ohtani et al., 2014).

Experiments have been conducted to assess PhD stability in the MgO-Al_2O_3-SiO_2-H_2O (MASH) system at the transition zone and lower mantle conditions. Experiments of one type are aimed at ascertaining the melting phase relations of Al-bearing PhD at uppermost lower mantle condition (Ghosh and Schmidt, 2014). According to their experimentally obtained results, Al-bearing PhD containing 1 wt% Al_2O_3 was stable up to 1600 ℃ at 24 GPa. Experiments of the other type investigated stability limit of PhD in MASH system (Al_2O_3 content ranged from 2 to 10 wt%) in lower mantle condition by using laser-heated diamond anvil cell combined with synchrotron radiation, the results showed that Al-bearing PhD was stable up to a maximum temperature 1837 ℃ at 54 GPa (Walter et al., 2015). Furthermore,

Pamato et al. (2015) reported that end member Al-rich PhD was stable at temperatures up to 2000 ℃ at 26 GPa. Results of those studies indicate that Al can increase stability regions of DHMSs. Recently, Liu et al. (2019) checked the stability region of Al-rich PhD in a MORB bulk composition along a cold subducting slab, they found that Al-rich PhD could remain stable up to 23 GPa, which further transformed to Al-rich PhH, implying oceanic crust could be an important water reservoir in the lower mantle.

Reportedly, a new Al-rich form of PhD containing up to 50 wt% Al_2O_3 was synthesized with mid-ocean ridge basalt bulk compositions (MORB) at 1300 ℃ and 25 GPa (Ballaran et al., 2010). Unfortunately, the stability region was not reported. Therefore, the maximum thermal stability of PhD might have been underestimated in earlier studies because of the positive Clapeyron slope (dP/dT) of PhD and its ability to absorb large quantities of Al. In addition, at the mantle transition zone condition, we have observed Al-rich PhD in some of our previous quench experiments by using natural chlorite as starting material ($Mg_{4.8}Fe_{0.2}Al_2Si_3O_{18}H_8$). Therefore, in this study, we systematically ascertained the melting phase relations of PhD in MASH system with 20 wt% Al_2O_3. High-pressure and high-temperature experiments were conducted using a multi-anvil high pressure apparatus at pressures of 14–25 GPa and temperatures of 800–1600 ℃. Those P–T conditions cover cold, hot, and normal mantle geotherms. This study, which elucidates the stability region of DHMSs to Al-rich compositions, is useful to constrain the water distribution in the deep Earth.

2. Experimental

Experimental runs were conducted at pressures of 14–25 GPa and temperatures of 800–1600 ℃. To prepare compositionally homogeneous starting material of Al-rich PhD with composition approximating that of $MgAl_{0.7}Si_{1.3}O_6H_{2.7}$, the oxides and hydroxide reagents of $MgO + Mg(OH)_2 + SiO_2 + Al(OH)_3$ in appropriate stoichiometry were mixed carefully using an agate mortar. Table 1 presents the chemical composition.

We used a Kawai-type (MA-8-type) high-pressure apparatus (ORANGE-1000, ORANGE-2000) installed at the Geodynamics Research Center (GRC), Ehime University. At room temperature (25 ℃), the pressure in each multi-anvil experiment was estimated from pressure-load calibration curves based on diagnostic changes in the electrical resistances of ZnTe (9.6 and 12.0 GPa), ZnS (15.5 GPa), GaAs (18.3 GPa), and GaP (23.0 GPa) induced by semiconductor–metal phase transitions at high pressures. In some experiments (OS3081, OS3087, OS3091), we put forsterite in the center of cell assemblage to calibrate the pressures at high temperature. Results demonstrate that the pressures obtained at high temperatures are roughly consistent with calibration at room temperature (Morishima et al. 1994; Suzuki et al. 2000). Tungsten carbide cubes with a truncation edge length (TEL) of 4 mm were used in combination with Co-doped MgO-octahedra of 10 mm edge length (10/4 assemblage). Preformed pyrophyllite gaskets were used between the cubes. Rhenium was used as the heater. The gold sample capsule (1.5 mm outer diameter, 1.3 mm inner diameter and 1.3 mm length), was used in the cell assemblage. Subsequently, we welded both sides of the sample capsule (gold) to prevent water loss during the experiment. The temperature was monitored

using a $W_{97}Re_3$-$W_{75}Re_{25}$. The thermal gradients inside the cell should be less than 100 ℃ due to the small size of the capsule. The thermocouple electromotive force (EMF) was not corrected for the effects of pressure. The sample was first compressed to the desired pressure and then heated for 40 to 240 minutes depending on target temperature (e.g. heating longer time for low temperature). After heating at high pressure, the power was stopped by shutting off the electric power supply. The samples were recovered after releasing pressure slowly over 12 hr.

The recovered run products were mounted in epoxy resin and were polished to perform phase identification and composition analysis. The phase assemblages were identified using a micro-focus X-ray diffractometer (MicroMax-007HF; Rigaku Corp.), which is equipped with a rotative anode (Cu Ka_1 radiation), a two-dimensional imaging plate detector and ø100 μm collimator. The operating conditions were 40 kV, 30 mA, and exposure time for XRD analyses was 600 s. Lattice parameters of Al-bearing PhD were calculated using 6–8 peaks in a two-theta range from 15 ° to 80 °. We used polycrystalline Si as an external standard to calibrate the peak positions of the XRD patterns. The obtained data were processed by 2PD software, which can display and process two dimensional data, including smoothing, background correction and 2D to 1D conversion. Each 1D X-ray profile was analyzed using the PDIndexer software. The samples were coated with carbon for electron microscopic observation and compositional analysis. The microtextures and compositions were obtained using a field emission scanning electron microscope (FESEM, JSM7000F; JEOL) combined with an energy dispersive X-ray spectrometer (EDS, X-MaxN; Oxford Instruments plc.) with working parameters of 15 kV, 1 nA and collection times of 30–50 s.

The EDS data were processed by the software Aztec (version 2.4, Oxford Instruments Nanotechnology Tools Ltd) using the XPP method. In addition, the Raman spectra were obtained using a laser Raman spectrometer (NRS-5100gr, JASCO) to identify the recovered phases, with 532 nm laser excitation. Laser power applied to the sample was 10 mW. The Raman Spectra were obtained from a linear baseline, and peak characteristics were carried out using the commercial software package.

3. Results and discussion

3.1 Lattice Parameters

An X-ray diffraction pattern of single phase Al-rich PhD (OS3081) is presented in Figure 1. The diffraction pattern is very sharp and useful to ascertain crystal parameters precisely. Table 2 shows unit cell parameters of Al-rich PhD obtained from quenched run products using micro-focus X-ray diffractometer. Those of Al-free PhD are also used for comparison.

PhD has a trigonal structure with both Mg and Si in octahedral coordination (space group $P\bar{3}1m$). In the crystal structure, layers of MgO_6 and SiO_6 octahedra are stacked alternately along the c direction. The H-bond positions were inferred as located within the Mg octahedral layer and as bonded to oxygens of the Si octahedral in Mg-PhD (Yang et al., 1997; Xue et al., 2008). The structural refinements of single crystal Al-rich PhD revealed a more disordered cation distribution compared to Mg-PhD, especially a higher degree of Si/Al disorder deduced from cation-oxygen distances by Ballaran et al., (2010). Table 2 shows that

the volume of Al-rich PhD in both OS3081 and OS3091 are larger than Al-free PhD, mainly because of the incorporated $^{VI}Al^{3+}$ ion (0.535 Å), for which the radius is larger than $^{VI}Si^{4+}$ ion (0.4 Å). Compared with Al-free PhD, the a-axis is slightly larger. The c-axis is smaller in Al-rich PhD, as presented in Table 2, probably because the shape of the Al octahedral is distorted slightly compared with Si octahedral when Al substitution occurs in PhD. For the axial lengths of Al-free PhD themselves, the a-axis and c-axis are also mutually different, as shown in Table 2, probably because of the disordered Mg/Si ratios in the structure. Because of the higher Al_2O_3 content, the volume of PhD is larger than those reported by Bindi et al. (2015) (Table 2) in MASH system. However, although the Al_2O_3 content in the present study is smaller than those reported by Ballaran et al. (2010), the volume of PhD is larger than theirs. We have known that the ionic radius of $^{VI}Mg^{2+}$ (0.72 Å) is larger than $^{VI}Fe^{3+}$ (0.645 Å) and $^{VI}Al^{3+}$ (0.535 Å). Due to the much larger MgO content measured here in PhD, leading to a larger volume in the present study. This tendency was also observed for Al-PhD (Pamato et al., 2015).

3.2 Raman spectrum

Figure 2 shows Raman spectra of Al-rich PhD obtained from the quenched run product in OS3091. The Raman bands of Al-rich PhD were broad and weak. This phenomenon was also observed in Al-free and Al-rich PhD at ambient conditions (Liu et al., 1998; Xue et al., 2008; Ballaran et al., 2010). Although the X-ray diffraction pattern in Fig. 1 shows that the Al-rich PhD would be well crystallized, we can only slightly obtain the Raman spectrum of single-phase Al-free PhD in OS3081, no matter how high the applied power or how long we

collect the data. Reportedly, whether lower temperature and/or high hydrostatic pressure method was used to improve the Raman spectrum resolution it was not possible to obtain high quality (Liu et al., 1998). Nevertheless, the peaks portrayed in Fig. 2 are much sharper than those reported by Liu et al. (1998), Frost and Fei (1998), and Xue et al. (2008). This sharpening of peaks might derive from the difference between Mg-O distance and Si-O distance between Al-free and Al-bearing PhD, which disorders the structure. The Al substitution in Si site reduces this difference because of the larger ion radius of Al. This reduction is similar to the Al end member PhD, as described by Pamato et al. (2015).

In all, seven peaks were observed in low-frequency, which is similar to the numbers reported by Liu et al. (1998), except for one peak of 1095 cm^{-1}, which was missing from this study. In hydroxyl stretching regions, we observe only one OH stretching mode at 2834 cm^{-1}. This observation is the same as those for some earlier Raman measurements which showed only a single broad OH stretching peak near 2850 cm^{-1} in Al-free PhD (Frost and Fei, 1998), but were quite different from those reported by Shieh et al. (2009), who observed six OH stretching modes based on IR measurements (2102, 2240, 2461, 2850, 3160, and 3426 cm^{-1}) for Al-free PhD. Compared with Raman spectra of Al-rich PhD, we observed two more vibrational bands in low frequency region in this study (Ballaran et al., 2010). Generally, the shape and frequencies of Raman vibrational bands in this study look very similar with those reported for Al-rich PhD in both lattice vibrational modes region and hydroxyl stretching region although the band around 1095 cm^{-1} disappeared in our result (Ballaran et al., 2010, Pamato et al., 2015).

At low frequencies of the 200–1200 cm^{-1} region, Raman spectra of Al-rich PhD resemble those reported previously for Al-free PhD (Frost and Fei 1998; Liu et al. 1998; Xue et al., 2008). A highest sharp band is evident near 774 cm^{-1} with a right shoulder near 811 cm^{-1}. The other sharp band is near 687, with smaller broad bands near 236, 337, 485, 572, and 687 cm^{-1} (Fig. 2).

3.3 Phase relations

Figure 3 portrays microtextures of some typical quench samples. The experimental conditions are presented in Table 3 along with the results. The phase relations in Al-bearing PhD at pressures to 25 GPa are portrayed in Fig. 4. As portrayed in Fig. 4, the tendency of phase relations in our results is fundamentally consistent with that of Al-free serpentine and Mg_2SiO_4+ 20.5 wt% H_2O composition (Frost and Fei, 1998; Irifune et al., 1998). In Fig. 4, Al-bearing PhD might coexist with brucite at very low temperatures according to the phase relations in an Al-free system (Frost and Fei, 1998). Along the cold subduction, Al-bearing PhD was observed coexisting with a small amount of St at 14 GPa (Fig. 3a); PhD + Gt + St appeared with pressure and temperature increasing to 16 GPa. The stability region of DHMSs is sensitive to the bulk composition. PhE should be observed from 10 GPa up to 17 GPa in the low temperature region, and then transforms to SUB at elevated pressure if we adopted serpentine or hydrous pyrolite as starting composition (Irifune et al., 1998; Litasov et al., 2003). In order to systematically clarify the stability field of Al-rich PhD, the starting composition used here was once observed for PhD in our previous experiments by using natural chlorite ($Mg_{4.8}Fe_{0.2}Al_2Si_3O_{18}H_8$) at mantle transition zone pressure. Therefore, in the

present study, PhD instead of PhE or SUB was the only DHMS identified in broad pressure and temperature region. In addition, although Al-rich PhD was expected to be the only phase in a wide pressure range in low temperature region, we noticed that St and Gt appeared with pressure increases before entering the single-phase region of PhD in Fig. 4. It is probably because the solubilities of Al and Mg in Al-rich PhD were changed at different pressures, which leading to form St and Gt. Along the hot subduction, PhD + Gt + St transformed to Gt + Egg + St + melt (Fig. 3b) with increasing temperature at pressures below 18 GPa. Our result differs greatly from those presented in earlier reports. In this study, we observed aluminous hydrous silicate, phase Egg $AlSiO_3(OH)$ at high temperatures instead of Wd or Rw after Al-bearing PhD decomposed at the transition zone. Reportedly phase Egg was found as an inclusion in natural diamond, raising the possibility of transportation of water into the deep Earth (Wirth et al., 2007), suggesting that phase Egg is an important water storage site. However, all earlier results demonstrated that wadsleyite (Wd) or ringwoodite (Rw) would appear after DHMS decomposed at high temperatures (Frost and Fei, 1998; Irifune et al., 1998; Ohtani et al., 2000; Ohtani et al., 2001; Litasov et al., 2003). This is because the solubility of Al_2O_3 is very low in Wd and Rw. The phase Egg should be formed when the excess Al_2O_3 would react with the water released from Al-rich PhD, and suppressing the formation of Wd or Rw at the same time.

At pressures higher than 18 GPa, SUB + PhD + melt was stable between 18 GPa and 26 GPa at temperatures lower than 1200 ℃ with serpentine composition (Irifune et al., 1998), which further transformed to Wd, Rw, and bridgmanite (Brg) with increasing pressure. SUB + PhD + melt was identified above the solidus in a very wide pressure range of 16 GPa and

26 GPa at temperatures lower than 1400 ℃ with Mg_2SiO_4+ 20.5 wt% H_2O composition in Fig. 4 (Frost and Fei, 1998). Moreover, in most of earlier studies, PhD only appeared at pressures higher than 18 GPa with hyrsous pyrolite composition (Ohtani et al., 2001; Kawamoto, 2004). In the MASH system, Al-bearing PhD (1 wt% Al_2O_3) is reportedly stable up to 1600 ℃ at 24 GPa, which transformed to Brg at higher temperatures. However, our result indicated that single phase Al-rich PhD (20 wt% Al_2O_3) was stable in pressures up to 25 GPa at temperatures around 1350 ℃ (Fig. 3c); also, PhD + Gt + δ + melt (Fig. 3d) were observed at 25 GPa and 1500 ℃. This observation suggested that Al-rich PhD transformed to δ phase instead of Brg at high temperatures. We also noticed that Al-rich PhD has positive Clapeyron slope (dP/dT) of the phase boundary in the present study, which means the decomposition temperature increases with increasing pressure. Therefore, Al-rich PhD may survive at elevated temperature in the lower mantle. Experiments have demonstrated that phase Egg decomposes to Al-PhD + δ + St under the mantle transition zone condition (Fukuyama et al., 2017). In Fig. 3, phase Egg appeared at low pressure; δ-AlOOH appeared at high pressure, which is consistent with their results. Reportedly, the phase H - δ-AlOOH solid solution might even exist at core mantle boundary (CMB), indicating that Al-bearing DHMSs are involved in lower mantle water cycling along typical geotherms (Panero and Caracas, 2017). Recently, Liu et al. (2019) reported the stability of Al-rich PhD with MORB bulk composition along cold subducting slab. They found that Al-rich PhD (7.5–22.6 wt% Al_2O_3) was only stable within 18–23 GPa and cold subducting environment (⩽1000 ℃), which further transformed to Al-rich PhH at elevated pressure. Unfortunately, they didn't check the stability limit of these two phases at higher temperatures. Combined their result

with the present study, at least we may infer that both in cold and hot subduction zones, the hydrous mafic oceanic crust would bring a certain amount of water into the mantle transition zone and the lower mantle. In addition, it is important to note that Al-rich PhH clarified by Liu et al. (2019) should better be called Al-rich δ phase, since the pressure where phase H appears should be at least higher than 35 GPa both from the result reported by Ohtani et al. (2014) and Nishi et al. (2014). On other hand, δAlOOH-εFeOOH-phase H has the isostructure ($CaCl_2$-type structure). Earlier results have also shown that phase H and δ-AlOOH form solid solution because of the isostructure (Ohira et al., 2014; Panero and Caracas, 2017). Thus, it is expected that δAlOOH-εFeOOH-phase H may form solid solution at broad pressure and temperature region.

4. Geophysical implications

Earlier reports have described that PhD is the most abundant DHMS in subducting slabs at the uppermost lower mantle. The PhD in MSH system will become unstable in conditions of higher temperature geotherms along subduction into the lower mantle (Frost and Fei, 1998; Irifune et al., 1998; Shieh et al., 1998; Kawamoto, 2004; Komabayashi and Omori, 2006). However, earlier research has shown that a trace of Al_2O_3 (1%) would increase the stability of PhD (Ghosh et al., 2014). The present study demonstrates that stability of such an Al-rich PhD shifts to higher temperatures and that water content increases drastically ($Si^{4+} = Al^{3+} + H^+$). Although we only used one starting composition in the present experiment, which may be insufficient to summarize the relationships between Al content and water content, study has shown that substitution mechanism of Al in Al-rich PhD can be expressed as $Al^{3+} + H^+$

$\leftrightarrow Si^{4+}$ (Liu et al., 2019), indicating that the H_2O content increases with increasing Al content. Furthermore, our previous results (paper in preparation) have shown that the Al content increases with temperature increasing. This tendency was consistent with those reported by Pamato et al. (2015). In a hydrous peridotite system, PhD was found to include a certain amount of Al_2O_3 (Kawamoto, 2004). It has been suggested that a large amount of Al would be transported into deep Earth in subducting slabs, which is more likely to incorporate into DHMSs, for example, PhD and its higher pressure hydrous phase PhH, than coexisting Rw or Brg (Ganskow and Langenhorst, 2014; Nishi et al., 2014). As proposed by Pamato et al. (2015), Al-rich PhD would form when migrating ultramafic compositional hydrous melt reacts with Al-rich mafic crustal rocks. More importantly, PhH, a higher pressure phase of PhD, was shown to coexist with bridgmanite along the slab geotherm (Ohira et al., 2014). If this is the case, then the stability region of Al bearing PhD is much broader than that reported in earlier studies, especially in subducting MORB composition.

Our results indicate that the maximum stability of Al-rich phase D occurs above 1500 ℃, which implies that it might still be stable within slabs that stagnate at the transition zone as they are warmed up by the mantle geotherm, which further transforms to δ-AlOOH at higher temperatures. Therefore, Al-rich δ phase is expected to be an important water carrier in mantle transition zone. Studies have suggested that δ-AlOOH, ε-FeOOH, and phase H can easily form solid solution in this ternary system, this solid solution was assumed to be stable at the base of the lower mantle (Ohira et al., 2014; Nishi et al., 2017). The breakdown of these hydrous minerals at the deep lower mantle would strongly affect the physical and chemical properties of surrounding materials.

Considering the points raised above, it is likely that the subducting oceanic crust can be an important long-term water reservoir in the convecting lower mantle because of the positive Clapeyron slope dP/dT of the phase boundary. This long-term dehydration might affect the melting and decarbonation of the overlying carbonated sediments (Ghosh et al., 2014). The released free water at lower mantle might contribute to the distinct seismic discontinuities between 660 and 780 km beneath northeastern China and 660 and 720 km discontinuities beneath southern California (Niu and Kawakatsu, 1996; Simmons and Gurrola, 2000), and might even trigger deep earthquakes beneath northeastern Japan (Omori et al., 2004).

Tables in chapter 3

Table 1. Chemical composition (wt %) of starting material

	PhD
MgO	22.5
Al_2O_3	20.1
SiO_2	43.8
H_2O	13.7
Total	100

Table 2. Electron probe microanalysis composition (wt %) of experimental run products

Run	**P (GPa)**	**T (℃)**	**Phase**	**MgO**	**Al_2O_3**	**SiO_2**	**Total**
OS3079	25	1500	Gt	31.16(8)	21.90(5)	46.12(4)	99.18(4)
			δ	1.85(7)	39.29(2)	50.68(8)	91.82(2)
			PhD	8.49(3)	44.46(3)	31.05(9)	84.00(1)
OS3081	25	1350	PhD	21.31(5)	20.24(4)	43.59(2)	85.14(2)
OS3086	25	1000	PhD	21.45(8)	20.35(0)	43.94(1)	85.73(7)
OD1854	20	1000	PhD	21.49(6)	20.17(4)	43.64(4)	85.34(4)
OS3088	19.5	1500	Gt	30.82(1)	23.13(3)	45.43(7)	99.38(9)
			St	0	1.50(8)	101.09(8)	102.69(8)
			δ	0.99(8)	37.72(1)	48.12(3)	86.83(1)
			Melt	19.23	4.67	13.97	37.87
OS3087	19.5	1300	PhD	21.16(5)	20.18(1)	43.97(6)	85.32(8)
OD1832	16	1200	Gt	31.26(1)	24.18(6)	46.19(8)	101.63(3)
			St	0	1.43(7)	100.65(6)	102.08(3)
			Egg	0.28(5)	40.82(7)	51.85(8)	92.95(1)
OD1857	16	1000	Gt	30.53(9)	23.30(2)	45.58(2)	99.41(1)
			St	0	0.89(5)	99.87(2)	100.76(9)
			PhD	21.03(4)	22.65(8)	40.53(9)	84.21(1)
			δ	3.68(4)	67.74(5)	7.61(8)	79.02(6)

OS3090	14	1300	Gt	30.79(5)	23.27(1)	45.41(9)	99.47(3)
			Egg	0.31(1)	42.65(1)	48.63(9)	91.60(0)
			δ	2.04(3)	72.74(7)	5.55(5)	80.33(6)
			St	0	1.31(8)	99.35(2)	100.66(5)
OS3091	14	900	PhD	21.16(5)	21.29(3)	41.27(6)	83.72(9)
			St	0	0.96(8)	100.01(8)	100.97(2)

Table 3. Unit Cell Parameters of PhD at ambient condition

Run No.	**Al_2O_3 (wt%)**	**a(Å)**	**c(Å)**	**V(Å^3)**
OS3081	21.31	4.810(1)	4.293(1)	86.03(7)
OS3091	21.16	4.820(1)	4.294(1)	86.41(8)
Y1997[a]	0	4.7453(4)	4.3450(5)	84.74(2)
F1998[b]	0	4.7702(13)	4.3405(21)	85.46(4)
F1999[c]	0	4.7749 (6)	4.3389 (7)	85.66 (3)
H2011[d]	0	4.754 (2)	4.327 (3)	84.70 (6)

[a] Y1997, Single-crystal X-ray diffraction measurement (Yang et al., 1997)

[b] F1998, Powder X-ray diffraction measurement (Frost and Fei, 1998)

[c] F1999, Powder X-ray diffraction measurement (Frost and Fei, 1999)

[d] H2011, Powder X-ray diffraction measurement (Hushur et al., 2011)

Table 4. Experimental conditions and results for Al-rich PhD

Run	P (GPa)	T (℃)	Time (min.)	Results
OS3079	25	1500	20	Gt + δ + PhD + M (n.a.)
OS3081	25	1350	60	PhD
OS3086	25	1000	330	PhD
OD1854	20	1000	60	PhD
OS3088	19.5	1500	60	Gt + Egg + St + M
OS3087	19.5	1300	120	PhD
OD1832	16	1200	60	Gt + St + Egg (T) + M (n.a.)

OD1857	16	1000	120	Gt + St + PhD
OS3090	14	1300	60	Gt + St + Egg + M (n.a.)
OS3091	14	900	120	PhD + St

PhD, Al-rich PhD; Egg, phase Egg; δ, δAlOOH; Gt, garnet; St, stishovite.

T, trace; M, melt; n.a., not analyze

Figures in chapter 3

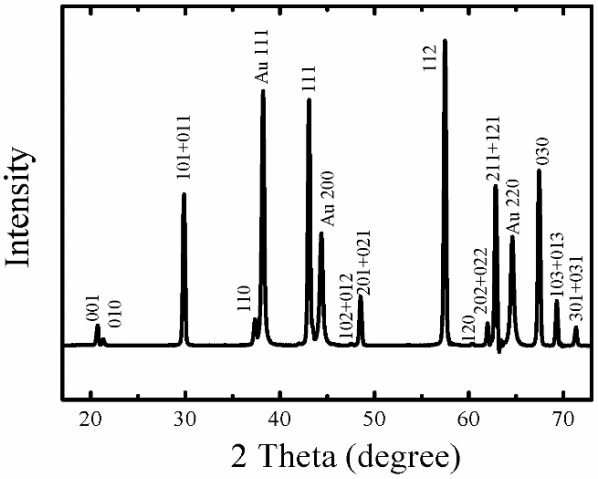

Fig. 1. XRD patterns of single phase Al-rich PhD in OS. Au capsule was involved in the XRD measurements, because of the small sample size.

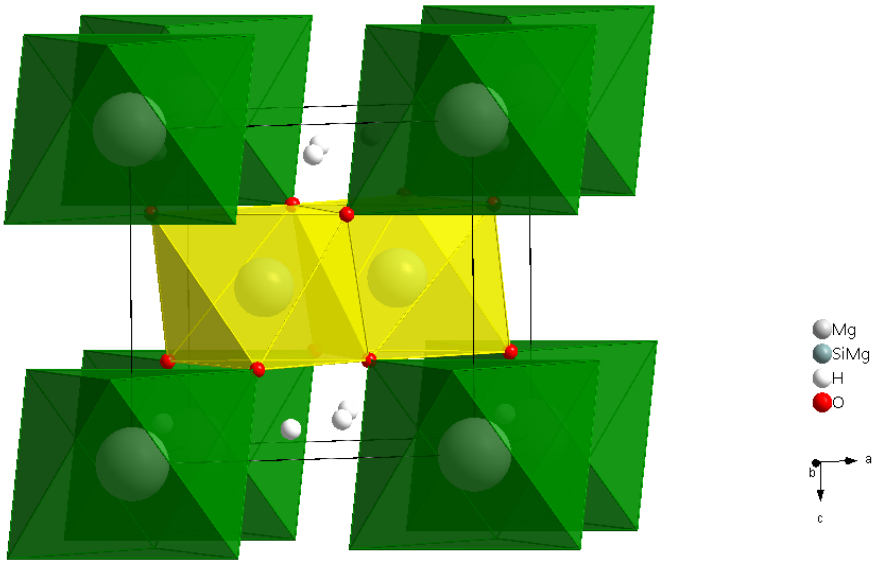

Fig. 2. PhD has trigonal structure with both Mg and Si in octahedral coordination (space group P-31m). In the crystal structure, layers of MgO6 and SiO6 octahedra alternatively stacked along the c direction.

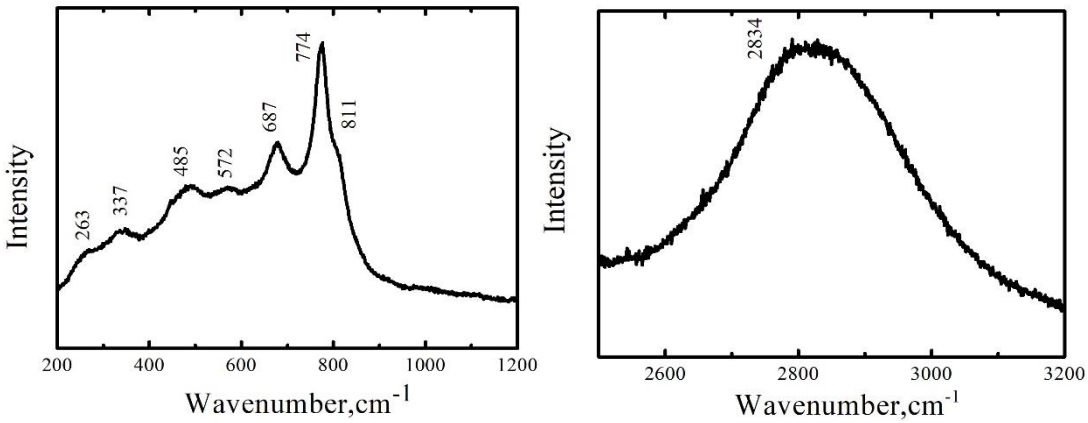

Fig. 3. Raman spectra of Al-rich PhD in low-frequency and hydroxyl stretching regions.

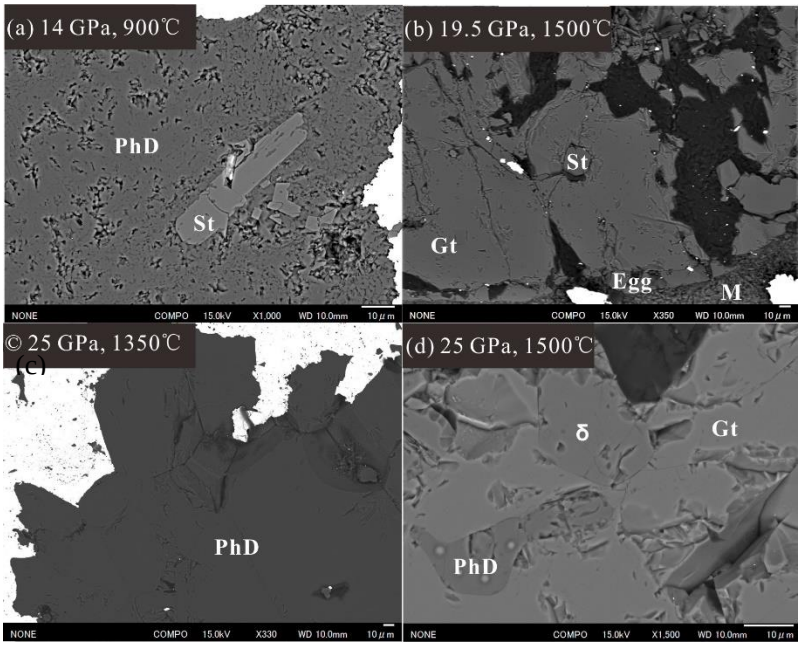

Fig. 4. Backscattered electron images of representative run products under various pressure and temperature conditions. The black color is epoxy. Symbols are defined as follows: *PhD*, Al-rich PhD; *St*, stishovite; *Gt*, garnet; *Egg*, phase Egg; *M*, melt; *δ*, δAlOOH.

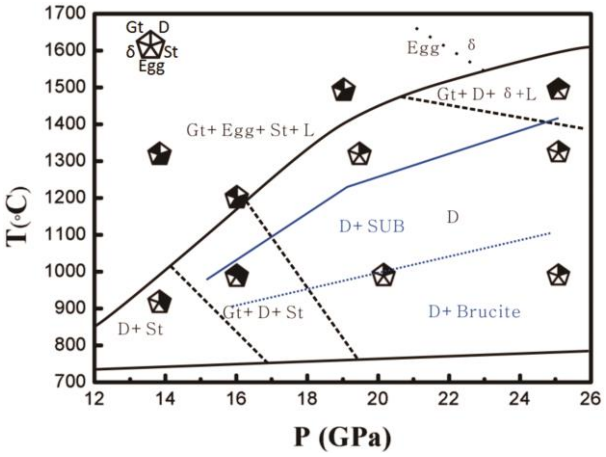

Fig. 5. The stability of Al-rich PhD between14 and 25 GPa at 900 ℃ to 1500 ℃. The solid black line show stability region of Al-rich PhD. The short-dashed black lines within stability region of Al-rich PhD show possible phase transition between adjacent regions. Two blue lines show the stability of Al-free PhD reported by Frost and Fei (1998). The dot black line shows the possible phase boundary between phase Egg and δ phase determined based on the study by Fukuyama et al. (2017).

Chapter 4

Melting phase relation of Fe-bearing PhD up to the uppermost lower mantle and transportation of H_2O to the deep Earth

(Will Submit to American Mineralogist)

Abstract

Dense hydrous magnesium silicates (DHMSs) are supposed to be one of the important water carriers to the deep Earth. We should think about the effect of Fe when considering the role of DHMSs in water cycle, because Fe is not only one of the most abundant elements in the Earth, but also in Fe-enriched planetary systems such as Mars. In spite of the importance, few experiment has been conducted so far to clarify the effect of Fe in DHMSs systematically. Therefore we investigated the stability of Fe-bearing phase D (PhD) in AlOOH-FeOOH-PhD system between18 and 25 GPa at 1000-1600 ℃.

Fe-bearing PhD was synthesized by using two different iron contents in FeOOH-PhD binary system, and the Al, Fe-bearing compositions were like analog materials of MORB and pyrolite in AlOOH-FeOOH-PhD ternary system. Compared with Mg-PhD, Fe slightly decreased the stability region of PhD in FeOOH-PhD system. We notice that iron substitution mechanism in PhD changed based on the cell volume parameter analysis.

Although Fe decreases the stability region of PhD, Al, Fe-bearing PhD drastically shift to higher temperatures in both MORB and pyrolite type compositions compared to pure Mg-PhD. Therefore, Al, Fe-bearing PhD could act as long water reservoir along subduction to the deep lower mantle. As on Mars, some evidences have shown that water once existed on Mars surface. Hydrous crust may tectonically embedded and subducted into the deep interior. Therefore, Al, Fe-bearing DHMSs are expected to transport hydrogen to the Earth's deep mantle and even to Fe-rich Martian core-mantle boundary in the cold subduction region, broadening our knowledge to model geodynamic process associate with deep water cycle in

the Earth and Mars.

1. Introduction

Water as one of the most important volatiles is playing a crucial role to understand the evolution of the Earth. Even a small amount of water will greatly change the physical and chemical properties of Earth's interior, for example, decreases melting temperature of minerals, changes seismic wave velocity and rheological behavior, which further influences thermodynamic of mantle. It is reported that a series of dense hydrous magnesium silicate phases (DHMSs) such as phase A (PhA), phase E (PhE), superhydrous phase B (SUB), phase D (PhD) and Phase H (PhH) act as potential water carriers to the deep Earth by subducting (Kawamoto et al., 1996; Ohtani et al., 2001a; Litasov and Ohtani, 2003; Komabayashi et al., 2005; Nishi et al., 2014). Therefore, it is important to investigate stability of DHMSs in the Earth's interior.

Phase D is potential stabilizing phase in hydrous peridotite among DHMSs at upper part lower mantle, playing key role in transportation and reserving water, which further transforms to PhH at 50 GPa (Nishi et al., 2014). The experimental results have shown that additional Al_2O_3 could increase stability region of Phase D (Ghosh and Schmidt, 2014), and Al-rich PhD could remain stable up to 2000 ℃ at 25 GPa (Pamato et al., 2015). However, there remain discrepancy in effect of Fe on Phase D. Ghosh and Schmidt (2014) argued that PhD almost had same stability region in both FeO-MgO-Al_2O_3-SiO_2-H_2O (FMASH) and MSH system, but lower than that of MASH system between 22-24 GP, while Ganskow and Langenhorst (2014) found that Fe increased stability of PhD in FMASH system compared

with MSH system between 18-23 GPa, which even stabilized up to 1450 ℃ at 20.5 GPa. We know that Fe is an abundant and important element in both pyrolite and MORB composition (Irifune and Ringwood, 1987), may greatly change stability and water solubility of PhD. On the other hand, stability of PhD contains Al and Fe content simultaneously closer to pyrolite or MORB composition is still unknown. Due to the limited data, we could not fully understand stability, water solubility and crystal chemistry of PhD.

The aluminum and iron oxide hydroxide AlOOH and FeOOH are common minerals in aquifers, sediments, and in the Earth's crust (Otte et al., 2009; Panero and Stixrude, 2004). At low pressure, AlOOH has two polymorphic structure, named diaspora (α-AlOOH, orthorhombic with space group Pbnm) and boehmite (γ -AlOOH, orthorhombic with space group Amam), and transforms to δ-AlOOH (orthorhombic with space group P21nm) around 17 GPa and 1000 ℃ (Ohtani et al., 2001b) and then to Pyrite-type structure at 170 GPa (cubic with space group Pa-3) (Tsuchiya and Tsuchiya, 2011). FeOOH has three polymorphic structure, Goethite (α-FeOOH iso-structure with α-AlOOH), akaganeite (β-FeOOH, tetragonal with space group I4/m) and lepidcrocite (γ −FeOOH, orthorhombic with space group *Cmcm*) which transforms to ε-FeOOH above 5 GPa and 200 ℃ (Gleason et al., 2008) and to pyrite-type FeOOH between 60-90 GPa, 1500 K (Nishi et al., 2017). The experimental results have shown that δ-AlOOH, ε-FeOOH and PhH could form solid solutions at deep lower mantle and stable up to core-mantle boundary (Sano et al. 2008; Ohira et al. 2014; Ohtani et al. 2014; Nishi et al., 2017). However, we poorly understand the stability of ε-FeOOH at transition zone condition, which might be an important water carrier in Fe-rich Martian.

In the present study, we investigated the effect of Fe on the stability of PhD in FeOOH-PhD system at pressures between 18-25 GPa and temperatures between 1000-1600 ℃. This help us better understand a more Fe-rich condition, such as the hydrous minerals on Fe-rich Mars. We also determined the stability of PhD in a moderate Al and Fe content similar to pyrolite and MORB in AlOOH-FeOOH-PhD system whose composition is close to natural system .We can clarify the Mg and Si effect on phase relation of AlOOH-FeOOH binary system at transition zone condition simultaneously, which have been suggested that Mg and Si change symmetry of δ-AlOOH (Komatsu et al., 2011), might influence stability of AlOOH-FeOOH binary system.

2. Experimental procedures

To prepare compositionally homogeneous starting material PhD with composition close to $Mg_{1.11}Si_{1.89}O_6H_{2.22}$, we used mixture of $Mg(OH)_2$ + SiO_2 in appropriate stoichiometry. To study the effect of Fe on PhD, 15.0 wt% and 8.0% wt% of α-FeOOH + PhD were adopted, respectively. Furthermore, 5.7 wt% of AlOOH (Al_2O_3 + $Al(OH)_3$ in appropriate stoichiometry) + 9.4 wt% of α-FeOOH + PhD and 16.0 wt% of AlOOH + 8.8 wt% of α-FeOOH + PhD were adopted, respectively, whose Al and Fe composition are close to pyrolite and MORB-type.

Experiments were conducted at pressures of 18-25 GPa and temperatures of 1000-1600 ℃. We used MA-8 type apparatus (ORANGE-1000) installed at Geodynamics Research Center (GRC), Ehime University. Pressures at room temperature were calibrated by the diagnostic changes in the electrical resistances of ZnTe (9.6 and 12.0 GPa), ZnS (15.5 GPa),

GaAs (18.3 GPa) and GaP (23.0 GPa) induced by the semiconductor-metal phase transitions at high pressures. Tungsten carbide cubes with a truncation edge length (TEL) of 4 mm in combination with Cr-doped MgO-octahedra of 10 mm edge length (10/4 assemblage). Preformed pyrophyllite gaskets were used between the anvils. Lanthanum chromate $LaCrO_3$ was used as the heater. The gold sample capsule were used in cell assemblage to prevent water loss during the experiment. The temperature was monitored by using a $W_{97}Re_3$-$W_{75}Re_{25}$. The thermocouple emf was not corrected for the effect of pressure. The samples were recovered after releasing pressure slowly in 720h.

The recovered run products were mounted in epoxy resin and polished to perform phase identification and composition analysis. The phase assemblages were identified by a micro-focus X-ray diffractometer (Rigaku MicroMax-007HF) using Cu Kα radiation. The micro-textures and composition were obtained by using a field emission scanning electron microscope (FESEM, JEOL JSM7000F) combined with an energy dispersive X-ray spectrometer (EDS, Oxford Instruments X-MaxN). The working parameters of 15 kV, 1 nA and collection times of 30-50 s were used. Compositions determined by EPMA are presented and we adopted Aztec (version 2.4, Oxford Instruments Nanotechnology Tools Ltd) software to process EDS data.

3. Results and discussion

3.1 Phase relations

In order to clarify the effect of Fe on PhD, we used two different FeOOH content in

FeOOH-PhD binary system. One is 15.0% wt% of α-FeOOH, the other is 8.0 wt% of α-FeOOH. The composition of PhD adopted in present research is $Mg_{1.11}Si_{1.89}O_6H_{2.22}$, which has been used as starting material by previous scientists (Yang et al., 1997; Shieh et al., 2009). We also used two different starting materials in AlOOH-FeOOH-PhD ternary system. One had the Al_2O_3 and Fe_2O_3 content similar to MORB-type, the other was same to pyrolite-type. Figure 1 showed some of the back scattered electron (BSE) imagings of some typical run products. A summary of phase assemblages in quench experiments were given in Table 1. The phase assemblages were simple, which included PhD, Fe_2O_3, bridgmanite, garnet, stishovite and melt. A trace of ringwoodite was also observed.

At 25 GPa and 1200, BSE image (Fig. 1(a)) showed the presence of two phases in bright and relative dark colors with higher Fe content in FeOOH-PhD system, which were identified as Fe_2O_3 and PhD, respectively (Table 1). The same phase assemblages were observed at same *P*-*T* condition with lower Fe content in FeOOH-PhD system (Fig. 1(b)). This suggested that solubility of Fe in PhD was quite low. At elevate temperature, phase assemblages in both higher and lower Fe content were looked same, except for that some amount of Fe_2O_3 was identified in higher Fe content system (Fig. 1(c) and (d)). In AlOOH-FeOOH-PhD ternary system, garnet, stishovite and melt were found in both MORB and pyrolite-type composition at 21 GPa and 1500 ℃, respectively. However, phase Egg was also observed in MORB-type composition.

The phase diagram of FeOOH-PhD system was shown in Figure 2. At 18 GPa and 1000 ℃, phase assemblages looked similar to each other in two starting composition. PhD was observed in both higher and low iron content. A trace amount of ringwoodite was observed

in both quenched samples. At 20 GPa and 1100 ℃, ringwoodite disappeared in higher iron content. We also noticed that Fe_2O_3 instead of ε-FeOOH was observed in some quenched samples from 18 GPa to 25 GPa. Studies have reported that dehydration of δ-AlOOH at 20 GPa was 1200 ℃, although ε-FeOOH has the similar $CaCl_2$-type crystal structure with δ-AlOOH (Ohtani et al., 2001b; Suzuki 2010), our data showed that Fe-rich ε-phase decomposed into Fe_2O_3 + H_2O at all *P-T* range in this study, indicating that ε-FeOOH had a lower dehydration temperature than that of δ-AlOOH and Fe-bearing PhD.

PhD was observed at 21 GPa and 1100 ℃ in both starting composition, but disappeared at elevated temperature. At 25 GPa and 1200 ℃, PhD coexisted with Fe_2O_3 in both results. With temperature increasing up to 1400 ℃, both phase assemblage transformed into bridgmanite + stishovite + melt whose reaction was same to thermodynamic calculation PhD = Brg (Pv) + St + H_2O reported by Komabayashi and Omori (2006).

The highest thermal stability of PhD at 18 GPa, 20 GPa, 21GPa and 25 GPa is around 1100 ℃, 1150 ℃, 1200 ℃ and 1350 ℃, respectively, which indicated that PhD had a positive Clapeyron slope in Fe-bearing system. The positive slope was also determined by Frost and Fei (1998) in Fe-free system and Ghosh and Schmidt (1998) in Al, Fe-bearing system, but different from Fe-bearing and Al, Fe-bearing system suggested by Ganskow and Langenhorst (2014).

The phase relation of AlOOH-FeOOH-PhD was shown in Figure 2. At 21 GPa and 1300 ℃, PhD + melt were obtained in both results, but some amount of Fe_2O_3 appeared in pyrolite-type composition. Apparently, Al_2O_3 enhanced solubility of Fe in PhD. In addition, the added Al_2O_3 in starting composition had great influence on the stability limit of PhD at 21 GPa,

whose stability limit moved to around1400 ℃. At 1500 ℃, PhD decomposed to Gt + St + Melt, however, hydrous Egg was observed in MORB-type starting composition at high temperature. The stability condition of Egg in this study is consistent with stability region of those previous reports (Sano et al., 2004; Fukuyama et al., 2017).

3.2 Mineral chemistry

Representative mineral compositions were summarized in Table 2. In FeOOH-PhD binary system, the range of MgO and Si_2O content in PhD were very narrow, from 20.44-22.91 wt% and 58.83-62.26 wt% in high Fe content, and from 20.27-21.79 wt% and 60.59-63.58 wt% in low Fe content between 18-25 GPa, respectively. H_2O content in PhD calculated from the deficit of total weight percent in the microprobe analysis for an average 12.19 wt% and 12.02 wt%, respectively. The relationship between pressure and Fe_2O_3 content in PhD was determined in Figure 3. It clearly showed that with pressure increasing, Fe content decreased below 21GPa, and then slightly increased up to 25GPa. This trend was almost consistent with previous result by Ganskow and Langenhorst (2014) as shown in Figure 3, although their starting composition contained very high FeO content (37.9 wt%). Compared with pressure, temperature seemed to have little effect on solubility of Fe in PhD. In AlOOH-FeOOH-PhD ternary system, both MgO and Si_2O decreased in PhD with pressure increasing, however, Fe content increased both in pyrolite and MORB-type composition compared with FeOOH-PhD binary system as shown in Fig. 3.

There was no garnet in FeOOH-PhD binary system may be due to the low temperature. Some amounts of garnet is found at 21 GPa and1500 ℃, containing 22.07 and 21.59 wt%

Al_2O_3 in MORB-type and pyrolite-type composition. The calculated Mg/Si ratio of ringwoodite appeared in FeOOH-PhD binary system is lower than 2, implying incorporation of H_2O. The H_2O content in ringwoodite estimated by EPMA total deficit is 1.5 wt% at 21GPa and 1300 ℃ in MORB-type composition and 1.3 wt% at 20 GPa and 1100 ℃ in pyrolite-type composition. Previous experiments have shown that H_2O solubility in ringwoodite was as high as 3.1 wt%, and mantle transition zone was suggested to be water-saturated (Inoue et al., 1995; Fei et al., 2017), which indicated that ringwoodite is potential water reservoir in transition zone.

3.3 Lattice parameters

Relationship between unit cell volume of PhD in FeOOH-PhD binary system and Mg/Si as shown in Figure 4. We noticed a distinctly different dependency of relstionship between 18-20 GPa and 25 GPa. The volume slightly decreased with increasing pressure from 18 to 20 GPa, and almost same Mg/Si were obtained in this pressure range. The change of volume consistent with changing of FeO content in PhD below 21 GPa as shown in Fig. 3. The decreased FeO content leading to decreasing volume because of larger ion size of Fe compared with Mg and Si. However, the volume increased even with low FeO content at 25 GPa, and we found Mg/Si also increased at same time. This phenomenon probably related to different substitution mechanism of Fe in PhD. The crystal structure of PhD was rather simple with all the Mg and Si occupying octahedral sites. Below 21 GPa, Tschermaks type substitution occurred in both Mg and Si sites ($Mg^{2+} + Si^{4+} = 2Fe^{3+}$), Thus, decreasing Fe content would lead to decrease of volume, however, Fe only occupied Si site at elevated

pressure ($Si^{4+} = 2Fe^{3+} + H^{+}$), leading to increase of volume even with low FeO content. PhD absorbed Fe^{3+} only in the Si-site may result in slightly increasing water content compared to the Mg-PhD.

3.4 The stability of Fe-bearing PhD in the mantle

PhD was analyzed in the MgO-SiO_2-H_2O (MSH) system between16 and 25 GPa at 900-1400 ℃ by Frost and Fei (1998)**.** Their results showed that PhD had a wide stability region from 1000 ℃ at 17 GPa and 1400 ℃ at 26 GPa. PhD was also investigated in MgO-Al_2O_3-SiO_2-H_2O (MASH) system, indicating that addition of Al_2O_3 increased its stability field (Ghosh and Schmidt, 2014). It was reported that Al-rich PhD could remain stable at temperature up to 2000 ℃ at 26 GPa (Pamato et al., 2015).

However, uncertainty still remains for effect of Fe, which has been known as abundant element not only on the Earth, but also on Fe-rich planet like Mars (Anderson 1972; Ringwood and Kesson, 1977; Morgan and Anders, 1980; Wänke et al., 1984; Sun 1982). Ghosh and Schmidt (2014) reported that Fe decreased stability of PhD by 200 ℃ when adding 4.3 wt% of FeO in MAFSH system compared with MASH system between 22-24 GPa. On the contrary, Ganskow and Langenhorst (2014) observed that Fe stabilized stability of PhD both in both MFSH and MAFSH system with 37.9 wt% and 17.9 wt% FeO, respectively. They showed that the highest thermal stability up to 1450 ℃ at 20.5 GPa, which was higher compared to the reported thermal stability of Mg-PhD (at 1400 ℃ and 25 GPa, Frost and Fei, 1998). According to our results, Fe slightly destabilized the stability region of PhD in both low (7.2 wt%) and high Fe_2O_3 (13.5 wt%) content. For example, in MSH system,

PhD was observed at 21.7 GPa and 1300 ℃ (Frost and Fei, 1998), whereas Fe-bearing PhD has already disappeared at same condition in our result.

This discrepancy seemed to attribute to the ferric and ferrous ions used in above studies. Previous research showed that even Fe^{2+} used in starting composition at very reducing redox conditions, a certain amount of Fe^{3+} would be found in synthesized samples (Frost et al., 2004; Saikia et al., 2009). Electron energy-loss spectroscopy showed $Fe^{3+}/\Sigma Fe$ = 60%, 74% was contained in Fe and Al, Fe-bearing PhD by Ganskow and Langenhorst (2014) even though FeO was adopted in starting material. On the other hand, studies have shown that Fe tended to partition into ringwoodite than PhD at transition zone condition (Saikia et al., 2009; Frost et al., 2004; Ganskow and Langenhorst, 2014). It may suggest that there was little difference to choose which valence state of Fe as starting composition in present pressure range. Therefore, Fe-bearing PhD possibly remain stable along hot subduction at least up to 25 GPa.

At 21 GPa, Fe-bearing PhD has decomposed below 1300 ℃, however, Al, Fe-bearing PhD remained stable above 1300 ℃ in both hydrous pyrolite and MORB-type composition as shown in Fig. 2. Meanwhile, previous investigations have clarified that Al preferred to partition into PhD than coexisting coexisting wadsleyite, ringwoodite, bridgmanite and phase H (Bolfan-Casanova et al., 2003; Litasov et al., 2005; Ghosh and Schmidt, 2014; Ohira et al., 2014; Bindi et al., 2015; Pamato et al., 2015). The main factor for this stabilization was attributed the effect of Al on stability of PhD. Our results indicated that Al could overcome the negative effect of Fe on stability of PhD and stabilize to higher temperatures. Consequently, taking into account of effect of Al, stability region of Al, Fe-bearing PhD

should drastically increase.

3.5 Long water reservoir

Stability region of DHMSs have been intensively reported by many workers in simple MSH or MAS composition (Kanzaki, 1991; Kawamoto et al., 1996; Frost and Fei, 1998; Ulmer and Trommsdorff, 1999; Ohtani et al., 2001, 2004; Litasov and Ohtani, 2002; Komabayashi et al., 2005; Komabayashi and Omori, 2006; Nishi et al., 2014). Among the DHMSs, PhD is an important water carrier from the transition zone to upper parts of the lower mantle, which expected to be stable along the hot subduction slabs in both hydrous pyrolite and MORB composition based on present result.

With pressure increasing, PhD transforms into high pressure polymorph phase H around 48 GPa, equivalent to 1,500 km depth (Nishi et al., 2014). Recently, experimental research showed that phase H could form solid solution with δ-AlOOH and coexist bridgmanite along the slab geotherm, which means water may be transported to the base of the lower mantle along subduction (Ohira et al., 2014).

As on Mars, some evidences have shown that there could be liquid water on early Mars (Baker 2001; Masson et al., 2001; Wade et al., 2017). Although it is not exactly clear where the water was, some parts of the hydrated crust of Mars may tectonically embed and subduct into the deep interior together with some hydrous materials (serpentinized composition) (Wade et al., 2017). In line with these arguments, we suggest that Al, Fe-bearing PhD may act as important water reservior on Fe-rich Mars, although we still didn't fully understand temperature profile of Mars' interior. Thus, Al, Fe-bearing PhD is expected to transport

hydrogen to upper parts of lower mantle on Earth and to Fe-rich Martian core, broadening our knowledge to model geodynamic process associate with deep water cycle in the Earth and Mars.

Tables in chapter 4

Table 1. Experimental run conditions and observed phase assemblages in αFeOOH-PhD and AlOOH-αFeOOH-PhD system.

Pressure (GPa)	Temperature (℃)	Results	
		15.0 wt% αFeOOH + PhD	8.0 wt% αFeOOH + PhD
25	1600	St+Melt	St+Melt
25	1400	Brg+fo+St+Melt	Brg+St+Melt
25	1200	PhD+fo	PhD+fo
21*	1500*	Gt+Egg+St+Melt	Gt+St+Melt
21*	1300*	PhD	PhD+fo+Melt
21	1300	rw+St+Melt	rw+St+Melt
21	1100	PhD+fo+Melt	rw+PhD+St+Melt
20	1100	PhD+fo+Melt	rw+PhD+St+Melt
18	1000	rw(T)+PhD+fo+Melt	rw(T)+PhD+Melt

*Staring composition were MORB and pyrolite-type as shown in starting composition

Table 2. Chemical compositions of typical coexisting phases (run a, 15.0 wt% αFeOOH + PhD; run b, 8.0 wt% αFeOOH + PhD; run c, pyrolite and MORB-type composition). Some of melt is not shown due to poor quality. Numbers in parentheses represent uncertainties.

Run	P (GPa)	T (℃)	Phase	MgO	SiO_2	Fe_2O_3	Total
a	25#	1600#	St	0	105.78(3)	0	105.78(3)
			Melt	31.43	27.40	20.99	79.82
		1400	Brg	36.89(2)	58.37(1)	7.32(8)	102.58(1)

			Fe_2O_3	11.27(6)	0.76(6)	88.01(2)	100.04(1)
			St	0	100.78(1)	0.23(1)	101.01(7)
		1200	PhD	21.63(7)	61.32(7)	5.27(5)	88.22(7)
			Fe_2O_3	6.89(2)	1.70(5)	90.46(7)	99.05(1)
		1300	Rw	44.00(8)	39.34(1)	16.86(5)	100.20(8)
			St	0	99.70(9)	0.52(7)	100.22(5)
		1100	PhD	22.91(1)	58.83(5)	4.93(4)	86.67(1)
			Fe_2O_3	2.32(3)	0	99.09(2)	101.41(9)
	20	1100	PhD	20.72(7)	62.26(3)	5.38(7)	88.36(2)
			Fe_2O_3	6.56(7)	0.25(8)	93.09(9)	99.90(1)
	18	1000	PhD	20.44(7)	61.70(4)	5.85(1)	87.99(7)
			Fe_2O_3	3.81(7)	0.79(2)	80.97(9)	94.57(6)
			Melt	15.9	51.41	6.66	73.97

Run	P (GPa)	T (°C)	Phase	MgO	SiO_2	Fe_2O_3	Total
b	25#	1600#	St	0	103.17(1)	0	103.17(1)
			Melt	36.15	27.75	13.12	77.01
		1400	Brg	38.04(6)	59.25(8)	4.58(2)	101.87(1)
			St	0	101.01(8)	0	101.01(8)
		1200	PhD	21.59(8)	60.59(9)	4.24(3)	86.42(7)
			Fe_2O_3	8.27(3)	0.27(4)	89.27(6)	97.81(9)
		1300	Rw	46.99(5)	40.30(5)	13.01(4)	100.30(8)
			St	0	100.16(1)	0	100.16(1)
		1100	Rw	48.18(3)	41.05(6)	13.2(8)	102.43(1)

		PhD	21.79(9)	63.58(9)	3.82(6)	89.19(6)
		St	0	100.94(6)	0.42(8)	101.36(1)
20	1100	Rw	42.28(2)	39.04(6)	19.32(4)	100.64(7)
		PhD	20.97(3)	62.69(3)	5.17(2)	88.83(4)
		St	0	98.89(6)	0	98.89(6)
18	1000	PhD	20.27(4)	62.04(1)	5.23(6)	87.54(6)
		Melt	16.40	52.86	5.63	74.89

#Sample thermal fracturing when putting in oven, the surface is not smooth

Run	P (GPa)	T (°C)	Phase	MgO	Al_2O_3	SiO_2	Fe_2O_3	Total
c								
MORB	21	1500	Gt	26.00(5)	22.07(9)	43.88(1)	8.49(4)	100.44(1)
			Egg	0.70(2)	39.70(8)	49.90(8)	0.57(5)	90.87(1)
			St	0	2.89(1)	96.08(9)	0	98.97(5)
			Melt	21.74	7.35	15.87	14.41	59.37
		1300	PhD	17.82(2)	16.18(4)	45.60(6)	7.13(1)	86.73(3)
Pyrolite	21	1500	Gt	29.50(8)	15.08(8)	48.03(8)	7.67(4)	100.27(8)
			St	0	0.68(6)	100.36(8)	0	101.04(3)
		1300*	PhD	20.19(1)	4.94(5)	56.83(1)	5.48(2)	87.44(4)
			Fe_2O_3	6.23(9)	0.36(8)	0.68(9)	92.36(3)	99.63(7)
			Melt	31.32	1.70	23.68	15.86	72.56

Figures in chapter 4

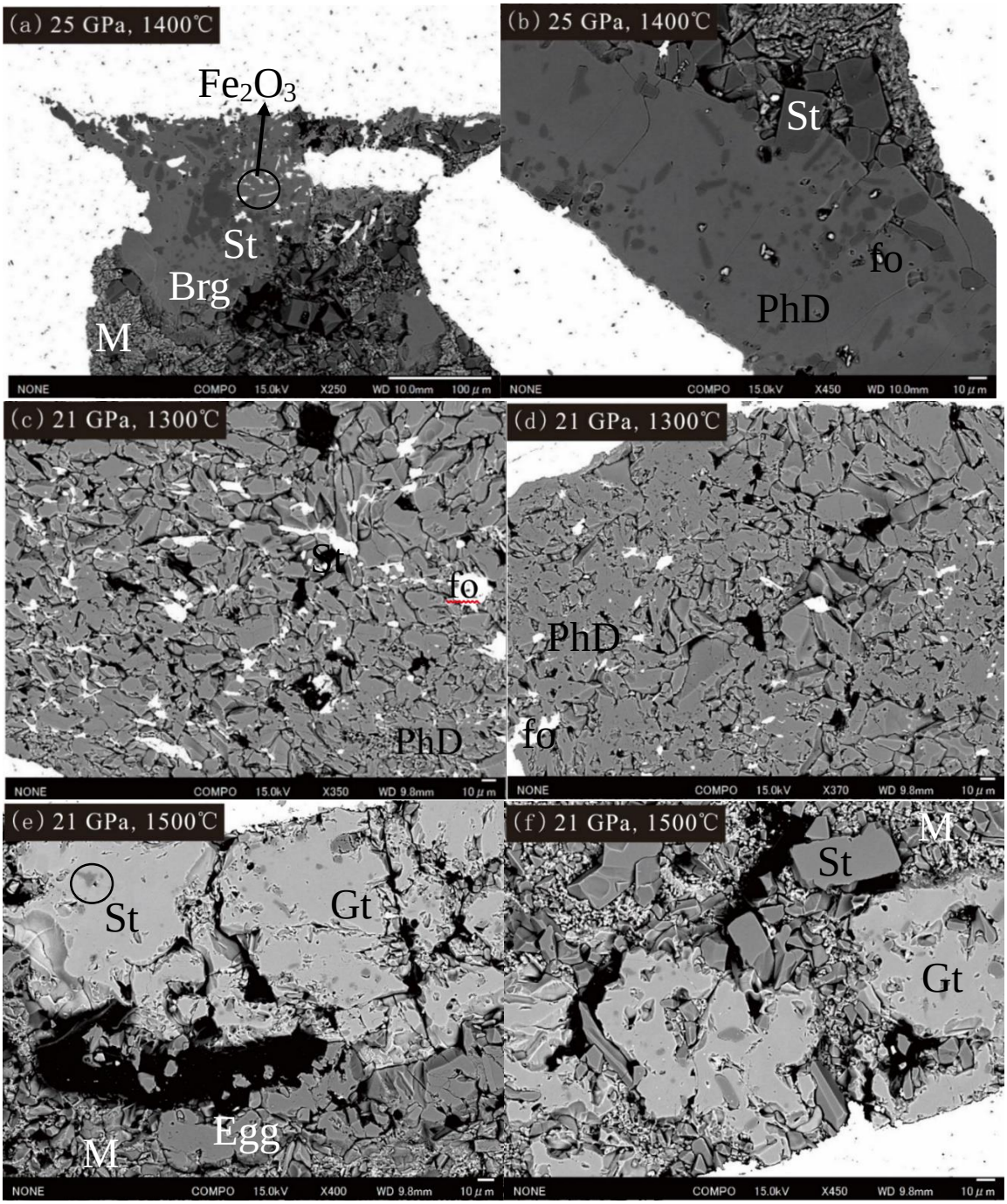

Figure 1. Backscattered electron images of representative run products. (a) and (b)samples synthesized at 25 GPa and 1400 ℃ in the 15.0 wt% and 8.0% wt% of αFeOOH + $Mg_{1.11}Si_{1.89}O_6H_{2.22}$, respectively. (c) and (d) 21 GPa and 1300 ℃. (e) and (f) 21 GPa and

1500 ℃ in MORB and pyrolite-type composition, respectively.

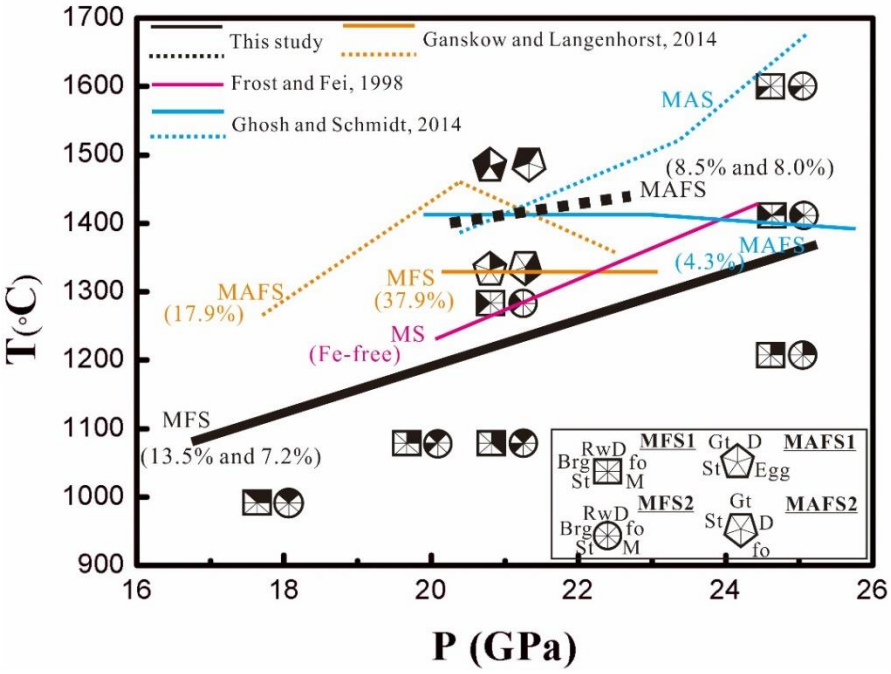

Figure 2. Phase diagram of PhD in present study. MAS, MgO-A_2O_3-SiO_2. MFS, MgO-FeO-SiO_2. MAFS, MgO-A_2O_3-FeO-SiO_2. The number1 and 2 mean different A_2O_3 and FeO content. Numbers in parentheses represent FeO content in starting composition. The black solid line showed stability limit of Fe-bearing PhD in both high and low Fe content, which slightly lower than that of Mg-PhD (pink solid line) (Frost and Fei, 1998), but much lower than that in Fe-rich staring composition (yellow solid line) (Ganskow and Langenhorst, 2014). The black dash line showed stability limit of Al, Fe-bearing PhD in both pyrolite and MORB-type composition, which was much higher than Fe-bearing PhD. The tendency of black dash line at high pressures was possibly located between blue dash line in MAS and blue solid line in MAFS (Ghosh and Schmidt, 1998). However, Ganskow and Langenhorst (2014) observed different behavior of PhD in MAFS (yellow dash line).

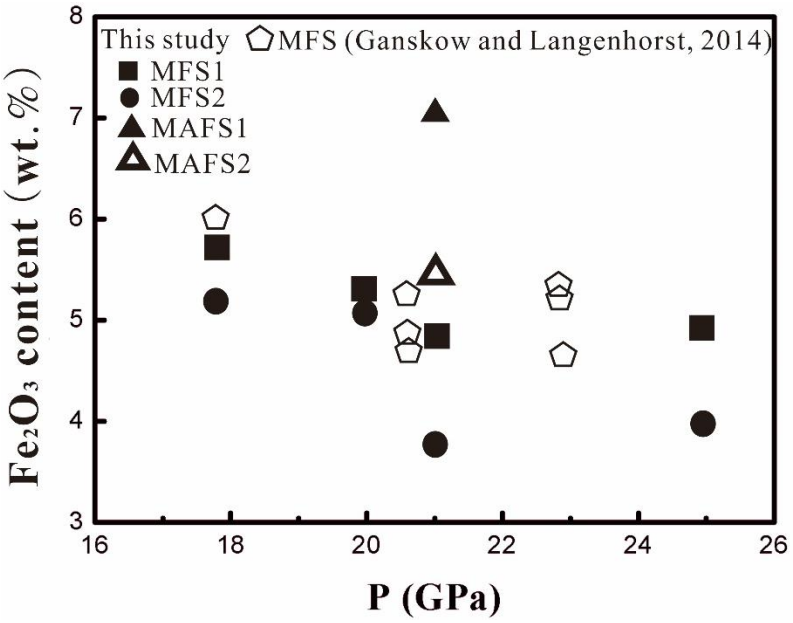

Figure 3. FeO content in PhD as a function of pressure. It was obvious that Fe content decreasing with pressure increased between 18 and and 21 GPa, whereas, slightly increasing between 21 and 25 GPa. This tendency almost consistent with reported result by (Ganskow and Langenhorst, 2014). We also found that FeO content increasing in PhD with Al_2O_3 content increased.

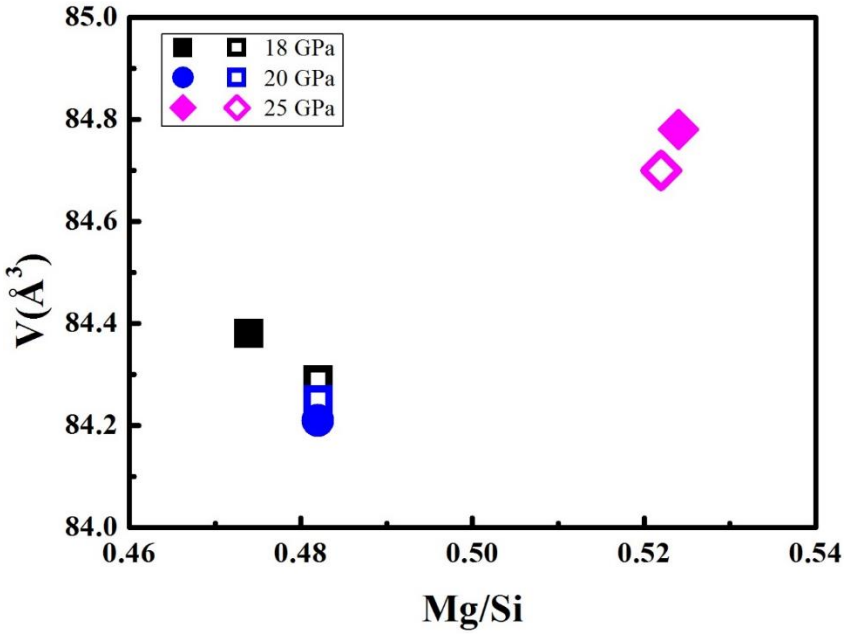

Figure 4. Relationship between volume and Mg/Si in PhD at different pressures. Solid and open symbol mean 15.0 wt% αFeOOH + PhD and 8.0 wt% αFeOOH + PhD, respectively. Obviously, different relationship of volume and Mg/Si were obtained between 18-20 and 25 GPa, respectively. This probably caused by different substitution mechanism of Fe in PhD. Between 18 and 20 GPa, Tschermaks type substitution occurred both in Mg and Si sites ($Mg^{2+} + Si^{4+} = 2Fe^{3+}$), Thus, decreasing Fe content would lead to decrease of volume, however, Fe only occupied Si site at elevated pressure ($Si^{4+} = 2Fe^{3+} + H^{+}$), leading to increase of volume even with low FeO content.

Chapter 5

Phase relations in MAFSH system up to 21 GPa: Implications for water cycles in Martian interior

(Submited to Minerals)

Abstract

In order to ascertain the possible water cycles in iron-rich Mars, we investigated the phase relation of a water-unsaturated (2 wt%) analog of Martian mantle in simplified MgO-Al_2O_3-FeO-SiO_2-H_2O (MAFSH) system between 15 and 21 GPa at 900–1500 ℃ using multi-anvil apparatus. We have found that Phase E coexisting with wadsleyite or ringwoodite is at least stable at 15–16.5 GPa and below 1050 ℃. Phase D coexisting with ringwoodite at pressure higher than 16.5 GPa and temperature below 1100 ℃. We also noticed that transition pressure of the loop in wadsleyite-ringwoodite boundary shifted towards lower pressure in iron-rich system compared with hydrous pyrolite model on Earth. As on Fe-rich Mars, some evidence has shown that water once existed on the Martian surface and existing possible plate tectonic activities on ancient Mars. The water present in hydrous crust might be tectonically embedded and subducted into the deep interior. Therefore, water may be transported to the deep Martian interior by hydrous minerals, such as phase E and phase D, in cold subduction plates, and further may be stored in wadsleyite or ringwoodite after those hydrous materials decompose when the plates equilibrate thermally with the surrounding Martian mantle.

1. Introduction

Water is one of the most important volatiles which affects physical and chemical properties of terrestrial planetary interior like Earth and Mars. Water transportation and storage are crucial component of water cycle which have great impact on geodynamic processes. On Earth, several studies suggested that some of hydrous minerals could hold and transport water to the deep Earth by cold subducting slabs (Gasparik 1993; Ohtani et al., 2001; Komabayashi and Omori, 2006).The so-called dense hydrous magnesium silicates (DHMSs) in MgO-SiO_2-H_2O (MSH) system, such as phase A ($Mg_7Si_2O_{14}H_6$), phase E ($Mg_{2.3}Si_{1.25}O_6H_{2.4}$), superhydrous phase B ($Mg_{10}Si_3O_{18}H_4$), phase D ($MgSi_2O_6H_2$) and phase

H ($MgSiO_4H_2$) are considered to be important carriers of subducted water from mantle transition zone even to the middle part of the lower mantle, have been widely investigated (Ohtani et al., 2001; Litasov et al., 2005; Gosh et al., 2014; Nishi et al., 2014; Pamato et al., 2015; Liu et al., 2019). On the other hand, the major minerals wadsleyite and ringwoodite in the Earth's mantle transition zone (MTZ) may act as large water reservoir, since they could hold several ocean's masses of H_2O (Inoue 1994).

The existence of water in Mars has long been controversial. According to the recent topographic features studies, for instance, northern plains, sedimentary deposits and valley networks (Cardenas et al., 2017; Chan et al., 2018; Ivanov et al., 2017), and to the finding of subsurface ice as well as various hydrous minerals in Lyot crater, suggesting existence of an ancient Martian ocean on surface (Byrne et al., 2009; Balme et al., 2015; Pan and Ehlmann, 2018). If there were tectonic activities on ancient Mars as proposed (Blasio and Martino, 2017; Dohm et al., 2018), some parts of the hydrated crust of Mars have been tectonically embedded and subducted into the deep interior together with some hydrous materials (serpentinized composition) (Wade et al. 2017). Therefore, as an Earth-like planet, there may exist some hydrous minerals in the subducting plate on iron-rich Mars, and wadsleyite and ringwoodite may also hold huge amount of water in Martian interior, as is argued on Earth today.

Several studies have identified phase relations in the MSH and MgO-Al_2O_3-SiO_2-H_2O (MASH) systems, and observed various hydrous minerals at *P*-*T* conditions related to the cold subduction slabs (Frost 1999; Litasov et al., 2005; Komabayashi and Omori, 2006; Ohira et al., 2014; Nishi et al., 2014; Pamato et al., 2015). However, few data available in hydrous iron-bearing system for the Earth, while data in iron-rich system like Mars is still remain unclear. A better understanding of the phase relations in MgO-Al_2O_3-FeO-SiO_2-H_2O (MAFSH) system may help to elucidate the geodynamic processes associated with the deep water cycles of Mars. Therefore, this study was conducted to determine phase relations in

iron-rich MAFSH system up to 21 GPa to estimate the possible water transportation into Martian interior by subducting processes.

2. Experimental procedures

High pressure and high temperature experiments were conducted at Geodynamics Research Center (GRC), Ehime University, using a Kawai-type 1000 ton multi-anvil apparatus. Tungsten carbide cubes with truncation edge length (TEL) of 4 mm were used in combination with Co-doped MgO-octahedra of 10 mm edge length (10/4 assemblage). Preformed pyrophyllite gaskets were used between the cubes, $LaCrO_3$ was used as the heater, and a gold sample capsule was used in the cell assemblage. Pressures were calibrated at room temperature by diagnostic changes in the electrical resistances of ZnTe (9.6 and 12.0 GPa), ZnS (15.5 GPa), GaAs (18.3 GPa), and GaP (23.0 GPa) induced by the semiconductor–metal phase transitions at high pressures. The temperature was monitored using a $W_{97}Re_3$-$W_{75}Re_{25}$ thermocouple and electromotive force (EMF) was not corrected for the effects of pressure. The sample was compressed to the desired pressure and then oil pressure was held constant. Subsequently, the AC power was supplied to the heater in the furnace assemblage. After heating at high pressure, then the power was stopped by shutting off the electric power supply. Samples were recovered after releasing pressure slowly for 12 hours. The recovered run products were mounted in epoxy resin and were polished for phase identification and chemical composition analysis.

The simplified Martian composition was adopted in this study was prepared by mixing oxide MgO, Al_2O_3, SiO2 and FeO in appropriate proportions, determined by Dreibus and Wänke (1985), which is analog of the primitive Martian mantle composition corresponding to mantle +crust. FeO was put in reduced furnace at 1000 °C for 24 hours before mixing in order to make sure the ferrous ion was used. We added 2wt% H_2O under the form of $Mg(OH)_2$

and adjusted the proportion of MgO. The chemical composition are shown in Table 1. In order to create reduced environment, we inserted some Mo foil in gold capsule before the starting material was encapsulated into. The recovered run products were mounted in epoxy resin and were polished to perform phase identification and composition analysis. The phase assemblages were identified using a micro-focus X-ray diffractometer (MicroMax-007HF; Rigaku Corp.) with Cu Kα radiation. The obtained data were processed by 2PD software, which can display and process two dimentional data, including smoothing, background correction and 2D to 1D conversion. The micro-textures and composition were obtained using a field emission scanning electron microscope (FESEM, JSM7000F; JEOL) combined with an energy-dispersive X-ray spectrometer (EDS, X-MaxN; Oxford Instruments plc.). Working parameters of 15 kV, 1 nA and collection times of 30–50 s were used. The chemical composition was analyzed using EDS. We used software (Aztec ver. 2.4; Oxford Instruments Nanotechnology Tools Ltd.) to process EDS data. The Raman spectrum were obtained by laser Raman spectrometer (NRS-5100gr) to identify some the recovered phases.

3. Results and discussion

3.1 Phase relations

Experimental conditions and the results are summarized in Table 2 and Fig. 1. Nominally anhydrous phase such as clinopyroxene, garnet, wadsleyite and ringwoodite are presented in quenched samples. Based on experimental conditions, different hydrous phases are observed with increased pressure. PhE is observed in the low-temperature region between 15-16.5 GPa to coexist with garnet and wadsleyite or ringwoodite. It became unstable at 16.5 GPa and temperature higher than 1100 ℃, however, thermal stability limite of PhE in this study is about 100 ℃ higher than that reported in iron-free hydrous peridotite system (Ohtani

et al., 2004). PhD remains as a major hydrous phase at present pressure range from18 GPa to 21 GPa below 1100 ℃. With increased temperature, PhD decomposed to ringwoodite, stishovite and garnet. It seems that PhD in MAFSH system has the same stability region as in MASH system (Ohtani et al., 2004). Therefore, it is expected that PhD has the positive pressure-temperature stability slope as shown in Fig. 1. The high iron content in MAFSH system may inhibit the SuB formation, leading to disappear of superhydrous phase B (SuB) in the whole pressure range.

Previous study has shown that the loop in the wadsleyite-ringwoodite boundary shifted towards higher pressure or higher iron content by the effect of H_2O (Inoue et al., 2010). In present study, wadsleyite was observed stable up to 16 GPa at 1200 ℃, and then transformed to ringwoodite. The formation of ringwoodite was also found shifting to low pressure, which was detected at 16 GPa and 1200 ℃. Therefore, this loop was more strongly influenced by higher iron content than by the effect of H_2O in the hydrous Martian mantle.

Clinopyroxene was observed at 16.5 GPa and 1300 ℃, which further transforms to garnet at elevated pressure. Sthishovite was found coexisting with ringwoodite at temperature higher than 1100 ℃. Some amount of ferrous oxide was detected at 21 GPa and 1050 ℃.

3.2 Mineral chemistry in DHMSs, wadsleyite and ringwoodite

The measured chemical compositions of the phases in the experiments are listed in Table 3. Several phases exhibit broad compositional variations. Phase E has the composition ranging from 4.5 at to 3.1 wt% for Al_2O_3 and from 12.8 to 8.5 wt% for FeO, respectively, at elevated pressure and temperature from 15 GPa and 900 ℃ to 16.5 GPa and 1100 ℃. With pressure increasing from 18 GPa to 21 GPa, Al_2O_3 decreases from 7.9 to 4.7 wt%, however, FeO almost remains stable around 4.3 wt%. The water content in Phase E and phase D is both estimated for 13 wt% on average, respectively, based on the deficit from EDS weight

total at above pressure and temperature conditions. Phase D in MAFSH system generally has low amounts of FeO < 4.4 wt%. The Al_2O_3 content range from 3.5 to 7.9 wt%, while the FeO content exhibits small variability from 3.9 to 4.8 wt% throughout the samples quenched at various pressure and temperature condition (Table 3).

The relationship between oxides content and temperature in garnet and ringwoodite are shown in Figure 2. The MgO and SiO_2 content decrease with increased temperature and then slightly increase in ringwoodite at 16 and 21 GPa (Fig. 2 (a)), however, the opposite trend is observed for FeO. At 18 GPa, the opposite trend are observed in MgO, SiO_2 FeO below 1250 ℃ compared with the pressures at 16 and 21 GPa. Both wadsleyite and ringwoodite have near-stoichiometric bulk composition. However, the (Mg+Fe)/Si ratio of wadsleyite and ringwoodite is lower than 2.0, indicating incorporation of H^+. The H_2O contents in ringwoodite is larger than that in wadsleyite based on deficit weight total estimation. Generally, Al_3O_2 content increases with increased pressure or temperature in garnet, which has opposite variation tendency compared with SiO_2 (Fig. 2 (b)). The FeO content basically unchanged in all of the quenched samples, except for the condtion at 15 GPa and 900 ℃ (Table 3)

3.3 The stability and water content of hydrous phases in iron-rich Martian mantle

Several petrological studies have reported that dense hydrous magnesium silicates (DHMSs) were reamin stable in the hydrous pyrolite mantle compositions along cold subducting slab (Gasparik 1993; Ohtani et al., 2004; Komabayashi and Omori, 2006). In this study, we observed that the stability regions of DHMSs in the hydrous iron-rich Martian mantle (2 wt% H_2O) are generally consistent with those obtained in CaO-MgO-Al_2O_3-SiO_2

(CMAS) pyrolite with 2 wt% of H_2O and water-saturated MSH system, however, some differences were noticed.

The stability region of PhE partially overlaps with wadsleyite or ringwoodite below 17 GPa in the low temperature field. Although wadsleyite can hold up to 3 wt% of H_2O in crystal structure (Inoue et al., 1995), it only accommodates ~0.8 wt% of H_2O in water undersaturated condition at 15 GPa and 900 ℃. The water content drastically increased to ~2.2 wt% after PhE decomposed at elevated temperature 1100 ℃ and 15 GPa, and then subsequently decreases to ~0.6 wt% with temperature increased to 1450 ℃. The water content in wadsleyite is consistent with those proposed in CMAS pyrolite with 2 wt% of H_2O at 15 GPa and 1450 ℃ (Litasov and ohtani, 2003), which indicating wadsleyite also has large water storage capacity within the stability field of Martian mantle.

SuB was reported to appear in CMAS or MHS system above 17 GPa (Litasov and ohtani, 2003), however, we observed PhD instead of SuB between 18 and 21 GPa, which means much water may be hold in low temperature region due to the higher water solubility in PhD. Although the size of Mars is still in debate, PhD may transport water to the deepest part of Martian interior, since PhD was reported to stable up to 44 GPa, which corresponds to depth of 1,250 km (Nishi et al., 2014).

Hydrous ringwoodite appears at pressure higher than 16.5 GPa, which exhibits a wide stability region than that in hydrous pyrolite. Obviously, water content in ringwoodite decreases with increased temperature as shown in Table 2. We observed trace amount of melt at 18 GPa and 1550 ℃, suggestting it is very close to the wet solidus in MAFS system under water-unsaturated condition. We also observed some amount of hydrous iron-rich metallic coexisting with ringwoodite and PhD at 21 GPa and 1050 ℃, implying it is a potential hydrous phase in low temperature region of hydrous iron-rich Martian mantle and, and may bring water to the Martian core if it has due to the larger density than surroudings.

4. Implications

The existence of water in Mars has long been controversial. Some evidence has shown that surface water disappeared from Mars surface after its formation (Baker 2001; Masson et al. 2001; Wade et al., 2017). Although the whereabouts of the water have long been debated, some parts of the hydrated crust of Mars have been tectonically embedded and subducted into the deep interior together with some hydrous materials (serpentinized composition) (e.g., Wade et al., 2017). We infer that DHMSs might act as an important water carrier during slab subduction on Fe-rich Mars, although the temperature profile of the Mars interior remains unclear. On ther other hand, several models have been proposed to constrain the structure of Martian interior based on geophysical observation and high pressure petrological studies, and they suggested the pressure of core-mantle boundary is 19-25 GPa (Bertka and Fei, 1997; Zharkovn and Gudkova, 2014; Raevskiy et al., 2015). Our results show that DHMSs can be expected to transport water even to the iron-rich Martian core in the cold subduction region.

Phase E and phase D potentially are relevant DHMSs in the Martain tranzition zone in simplified MAFSH model. The DHMSs will completely dehydrate if the temperature of surrounding Martian mantle is higher than their stability limit (Fig. 2). The released water will be stored in wadsleyite or ringwoodite. In the Martian mantle, where these two phases are stable, may act as large water reservoir like in the Earth's mantle. The results of present phase relation in iron-rich Martian are basically consistent with these data on hydrous pyrolite, except for SuB does not occur in the former. Also to be noted that much water could be hold in Martian mantle than that of Earth's mantle, because transition pressure of the loop in both olivine-wadsleyite and wadsleyite-ringwoodite boundary shifted towards lower pressure (Inoue et al., 2010).

Recently, the finding of stable body of liquid water on Mars suggested that large quantities of water may be hosted in the deeper region (Orosei et al., 2018). Present result

indicate that both DHMSs and nominally anhydrous minerals, wadsleyite and ringwoodite, have the potential to accommodate a certain amount of water, elucidating model geodynamic processes associated with the deep water cycles of Mars.

Tables in chapter 5

Table 1. Chemical composition (wt %) of starting materials

	MgO	Al_2O_3	FeO	SiO_2	H_2O	Total
MAFSH	30.2	3.5	19.9	44.4	2.0	100

Table 2. Experimental conditions and results.

Pressure (GPa)	Temperature (℃)	Time (min)	Phase
15	900	240	Gt, Wd, PhE
15	1100	240	Gt, Wd, Cpx
15	1250	120	Gt, Wd, Cpx
15	1450	90	Gt, Wd, Cpx
16	1200	120	Gt, Wd, Rw, Cpx
16.5	1100	120	Gt, Rw, PhE, St
16.5	1300	90	Gt, Rw, Cpx
18	1000	240	Rw, PhD
18	1200	120	Gt, Rw, St
18	1550	40	Gt, Rw, St, Melt
19.5	1400	40	Gt, Rw, St
21	900	240	Rw, PhD, St
21	1050	240	Rw, PhD, FeO
21	1250	120	Gt, Rw, St
21	1500	40	Gt, Rw, St

Gt garnet; Cpx Clinopyroxene; Wd wadsleyite; Rw ringwoodite; St sthishovite; PhE phase E; PhD phase D

Table 3. Representative mineral compositions

P (GPa)	T (℃)	Phase	MgO	Al_2O_3	SiO_2	FeO	Total
21	1500	Gt	26.48(54)	13.27(142)	48.63(84)	12.33(39)	100.71(23)
		Rw	36.20(29)	0	38.11(32)	25.42(45)	99.73(66)
		St	0	1.45(46)	100.68(81)	0.77(6)	102.90(52)
	1250	Gt	25.01(60)	15.21(142)	46.27(85)	12.34(37)	98.84(33)
		Rw	35.72(33)	0	37.49(23)	24.95(43)	98.15(58)
		St	38.20	0.55(38)	99.00(63)	0.78(33)	100.33(83)
	1050	Rw	41.60(98)	0	39.27(62)	15.99(27)	96.86(88)
		PhD	20.24(42)	4.71(71)	56.11(85)	4.79(34)	85.86(145)
		FeO	7.25(33)	0	0.87(60)	90.82(86)	98.95(70)
	900	Rw	43.57(86)	1.33(7)	40.54(73)	12.11(87)	96.22(143)

		PhD	29.36(78)	3.50(48)	52.95(90)	3.93(48)	89.74(81)
		St	1.53(71)	0	99.08(78)	1.15(27)	101.72(58)
19.5	1400	Gt	26.02(39)	12.76 (65)	47.78(60)	12.21(39)	98.78(92)
		Rw	35.26(13)	0	36.96(19)	25.55(34)	97.77(44)
		St	0	0.96(47)	98.42(58)	0.72(32)	100.10(81)
18	1550	Gt	27.78(29)	11.04(37)	49.70(30)	12.45(80)	100.45(37)
		Rw	34.88(37)	2.05(18)	37.77(30)	26.70(24)	99.35(58)
		St	0	1.54(58)	99.90(97)	0.62(36)	102.05(63)
		Melt	20.65	1.62	16.45	16.57	55.31
18	1200	Gt	25.88(90)	12.61(99)	47.96(67)	12.41(64)	98.86(76)
		Rw	35.55(35)	0	37.56(34)	25.61(47)	98.71(79)
		St	0	0.58(23)	99.49(71)	0.70(40)	100.77(82)
18	1000	Rw	32.89(61)	0	36.98(46)	27.86(81)	97.73(57)
		PhD	20.48(75)	7.86(59)	54.68(73)	4.57(46)	87.59(53)
16.5	1300	Gt	25.42(32)	11.23(48)	47.18(29)	12.76(57)	96.59(50)
		Rw	28.89(32)	0	34.88(27)	32.21(25)	95.98(64)
		Cpx	33.79(24)	19.19(60)	55.66(53)	6.98(47)	96.44(95)
16.5	1100	Gt	25.76(80)	12.81(36)	47.64(77)	14.74(57)	100.94(63)
		Rw	34.59(57)	0	37.72(17)	26.67(63)	98.97(37)
		PhE	38.42(75)	3.12(20)	37.82(18)	8.47(28)	87.82(57)
		St	1.38(67)	0.76(64)	96.75(75)	1.14(20)	100.03(27)
16	1200	Gt	24.28(47)	13.42(37)	46.67(33)	14.26(83)	98.63(44)
		Rw	28.36(42)	0	35.76(39)	33.43(59)	97.55(69)
		Wd*	-	-	-	-	-
		Cpx	34.99(51)	20.70(54)	56.73(58)	6.52(37)	98.25(37)
15	1450	Gt	26.61(71)	11.35(25)	49.48(61)	13.10(75)	100.54(82)
		Wd	34.43(35)	0	37.35(33)	27.61(46)	99.40(81)
		Cpx	34.68(74)	0	58.09(41)	7.56(70)	100.34(82)
15	1250	Gt	27.39(13)	11.00(54)	49.79(37)	13.06(34)	101.24(40)
		Wd	30.91(34)	0	36.54(18)	32.11(47)	99.55(46)
		Cpx	35.80(39)	0	58.17(57)	6.65(35)	100.61(67)
15	1100	Gt	25.19(57)	12.32(28)	47.52(64)	13.08(61)	98.11(81)
		Wd	31.03(96)	0	36.49(80)	30.23(94)	97.76(46)
		Cpx	35.32(70)	30.91(34)	56.57(72)	6.27(81)	98.16(13)
15	900	Gt	27.61 (31)	12.45(79)	44.08(83)	17.22(96)	101.35(74)
		Wd	27.91(46)	0	36.15(50)	35.08(27)	99.14(84)
		PhE	34.01(84)	4.54(26)	35.92(47)	12.79(54)	87.27(79)

* EDS is difficult to measure the chemical composition due to the small crystal size. This phase is identified by Raman spectrum. Gt garnet; Cpx Clinopyroxene; Wd wadsleyite; Rw ringwoodite; St sthishovite; PhE phase E; PhD phase D.

Figures in chapter 5

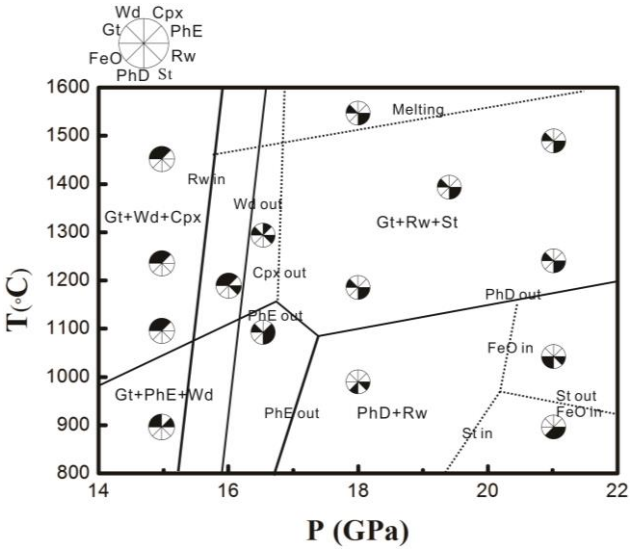

Figure 1. Phase relations in the system $MgO-Al_2O_3-FeO-SiO_2$ with 2% H_2O. Solidus lines are obtained according to the quenched samples combined with reported phase relation in $CaO-MgO-Al_2O_3-SiO_2$-pyrolite with 2% H_2O. Dash lines are proposed based on phase assemblages in recovered samples. Gt garnet; Cpx Clinopyroxene; Wd wadsleyite; Rw ringwoodite; St sthishovite; PhE phase E; PhD phase D.

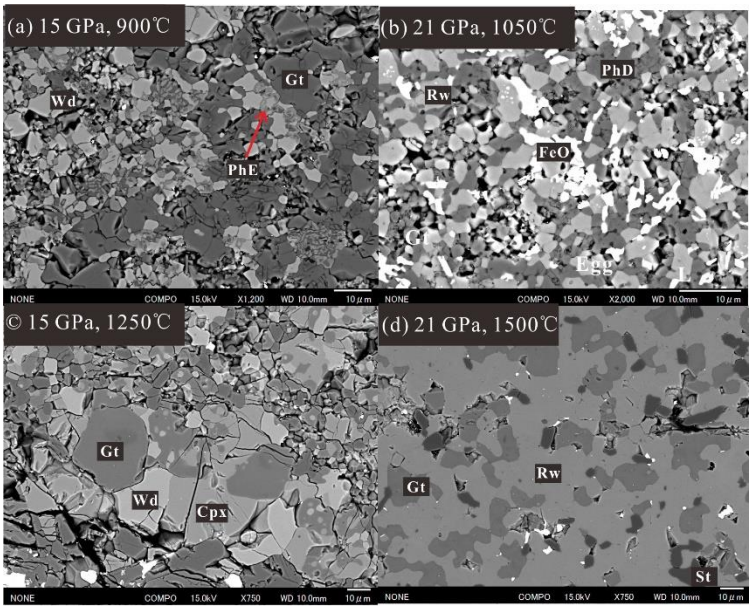

Figure 2. Backscattered electron images of representative run products under various pressure and temperature conditions: (**a**) 15 GPa and 900 ℃; (**b**) 21 GPa and 1050 ℃; (**c**) 15 GPa and 1250 ℃; (**d**) 21 GPa and 1500 ℃. Gt garnet; Cpx Clinopyroxene; Wd wadsleyite; Rw ringwoodite; St sthishovite; PhE phase E; PhD phase D.

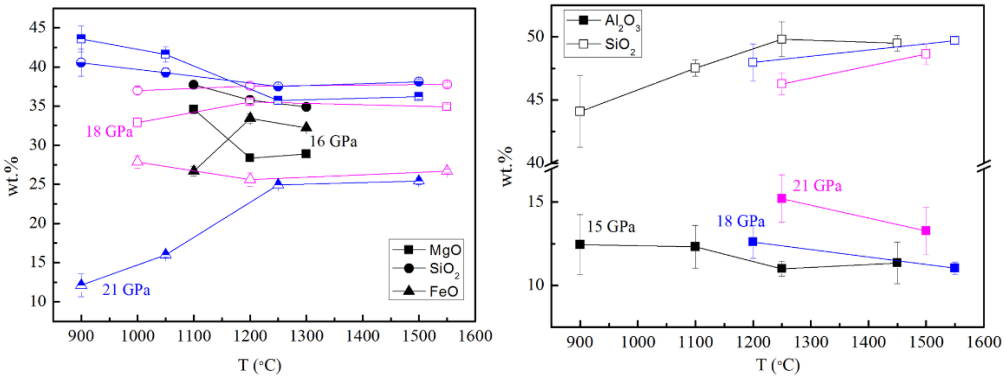

Figure 3. Ringwoodite and garnet compositions at different pressures and temperatures: (**a**) Oxides content in ringwoodite; (**b**) Oxides content in garnet.

Chapter 6

Al partitioning between phase D and bridgmanite up to 31 GPa: Implications for high electrical conductivity, velocity anomalies and deep earthquakes occur between 670 and 850 km

(Will submit to Geophysical Research Letters)

Abstract

Partitioning of Al between Brg and PhD was obtained at high pressures, because dense hydrous magnesium silicates (DHMSs) are supposed to be one of the important water carriers to the deep Earth. Phase D (PhD) is the dominant high pressure phase among DHMSs in hydrous pyrolite composition from the shallow parts of the lower mantle to at least middle region, has been shown to coexist with bridgmanite (Brg), which is widely viewed as the most abundant mineral assemblage in the Earth's interior. The experimental result indicated that Brg is the main host for Al_2O_3 in the lower mantle (e.g. Irifune, 1994), and the recent study reported that Al-rich PhD stabilized up to 2000 ℃ at 26 GPa in H_2O-bearing condition (Pamato et al., 2015). Therefore, partitioning of Al between Brg and PhD is particularly important to constrain water distribution in the deep mantle, especially because Al^{3+}+H^+ substitutes for Si^{4+} in PhD greatly enhances its water content. However, direct experimental results are limited.

To systematically illustrate this issue, we performed high pressure and high temperature experiments in MgO-Al_2O_3-SiO_2-H_2O system to investigate the partitioning of Al between pyrolite type Brg and PhD in volume ratio of 4:1 up to 31 GPa by MA8-type (Kawai-type) apparatus. Our result shows that Al is strongly partitioned into PhD than coexisting Brg, and partition coefficient of Al (K_D) between PhD and Brg slightly decreases with increasing temperature. Al-bearing PhD totally decomposes around 28 GPa and 1350 ℃, in which Brg is found to be coexisting with a large amount of melt. At 31 GPa and 1350 ℃, Brg coexists with trace amount of melt and Al-rich phase H, which means some amount of water might be transported into the lower mantle.

The decomposition of Al-bearing PhD around 28 GPa may be the second chock point for hydrous minerals and help to explain 770 km LVZ within Japan subduction zone in Western Pacific sand the discontinuity and the low-velocity zones (LVZ) around 800 km

beneath European Alp (Liu et al., 2016; 2018). The released water together with melts will migrate upward, and possibly causes high electrical conductivity between 670 Km and 830 Km in northeast Japan (Shimizu et al., 2010) and the trapped melt may also help to generate LVZ in some other typical regions, and even dehydration-linked deep earthquakes ~ 700 km (Frohlich, 1989).

1. Introduction

Water can be delivered into the deep Earth via subducting slabs. Several high pressure hydrous phases have been suggested as potential water carriers to Earth's interior, especially those dense hydrous magnesium silicate phases (DHMSs) (Frost and Fei, 1998; Litasov and Ohtani, 2002; Ohtani et al., 2001; Komabayashi and Omori, 2006; Nishi, 2015). These phases were demonstrated to remain stable along cold subducting environment only (Kanzaki, 1991; Irifune et al., 1998; Ohtani et al., 2004; Komabayashi et al., 2005). However, recent studies have found that trace amount of Al hugely increases thermal stability region of DHMSs (Ghosh and Schmidt, 2014). It was reported that Al-rich PhD stabilized up to 2000 ℃ at 26 GPa (Pamato et al., 2015).

PhD is the dominant high pressure phase among DHMSs in hydrous pyrolite from the shallow parts of the lower mantle to at least middle region, has been shown to coexist with Brg (Bolfan-Casanova et al., 2003; Litasov et al., 2005; Ghosh and Schmidt, 2014; Ohira et al., 2014; Nishi et al., 2014), which is widely viewed as the most abundant mineral assemblage in the Earth's interior (Irifune, 1994; Tschauner et al., 2014). The experimental result indicated that Brg is the main host mineral for Al_2O_3 in the lower mantle (Liu et al., 2016). Therefore, partitioning of Al between PhD and Brg is particularly needed to constrain water distribution in the deep mantle, since a trace amount of water may greatly influence geodynamic process of the Earth's interior, especially because Al^{3+}+H^+ substitutes for Si^{4+} in

PhD greatly enhances its water content, implying that water transported into the lower mantle along subducting may be underestimated by previously thought. However, direct experimental results are limited.

To systematically illustrate this issue, we performed multi-anvil experiments in the MgO-Al_2O_3-SiO_2-H_2O composition up to 31 GPa and 1350 ℃. This allow us to investigate the partitioning of Al between PhD and Brg simultaneously contribute to explain some important geophysical observations by analyzing phase relations.

2. Experimental procedures

In present work, the pyrolitic Al-bearing Brg with chemical formula $Mg_{0.95}Al_{0.1}Si_{0.95}O_3$ and PhD with chemical formula $Mg_{1.11}Si_{1.89}H_{2.22}O_6$ were used as starting materials in volume ration 4:1 base on modal compositions of mineral assemblages in hydrous peridotite (Ohtani et al., 2004), which were prepared by mixing the oxide mixtures of MgO, SiO_2, $Al(OH)_3$ and $Mg(OH)_2$ in appropriate proportions, respectively.

The starting materials were sealed into Au capsules, which were selected to prevent water loss during the experiments. Two kinds of tungsten carbide anvils BL150 and TF05 with truncation edge length of 3 mm were used to generate pressure up to 31 GPa. The Co-doped MgO-octahedra pressure medium were used. Preformed pyrophyllite gaskets were used between the anvils. $LaCrO_3$ was used as the heater. The temperature was monitored by using a $W_{97}Re_3$-$W_{75}Re_{25}$ the thermocouple emf was not corrected for the effect of pressure. The pressure has been well calibrated up to 25 GPa for BL150 (Kakizawa et al., 2015) and up to 31 GPa for TF05. The sample compressed to the target pressure first and then held constant, after that, the AC power was supplied to the $LaCrO_3$ heater and kept for 10-12 h depending on pressure. We conducted two groups of experiments. In first group, pressure was fixed at 25 GPa and temperature ranged from 1150 ℃ to 1500 ℃. On the contrary, in

second group, temperature was fixed at 1350 ℃ and pressure ranged from 25 GPa to 31 GPa.

The samples were recovered after releasing pressure slowly in 720 min. The recovered samples were mounted in epoxy resin and polished to perform phase identification and composition analysis. The micro-focused X-ray diffractometer (RIGAKU RAPIDII-V/DW) was used to identify the phases in the run products. The micro-textures were identified with a field emission scanning electron microscope (FE-SEM, JEOL JSM7000F), and the chemical compositions of those mineral phases were measured by an energy dispersive X-ray spectrometer (EDS, Oxford Instruments X-Max^N) combined with FE-SEM. More detailed information see Zhou et al. (2016). A synthetic $Mg_{0.95}Al_{0.1}Si_{0.95}O_3$ Brg was used to proofreading the composition of obtained Brg.

3. Results and Discussions

Experimental conditions and phase assemblages are summarized in Table 1 and the compostion was shown in Table 2. Fig. 1 shows partition coefficient of Al (K_D) between PhD and Brg compared with reported for representative pyrolite and MORB compositions as function of temperature. The K_D between PhD and Brg was calculated by using the formula $K_D = \frac{X_{Mg}^{Brg} \cdot X_{Al}^{PhD}}{X_{Al}^{Brg} \cdot X_{Mg}^{PhD}}$ modified from Frost (2003), with Mg = Mg^{2+}+ Fe^{2+} or Al = Al^{3+}+ Fe^{3+} in Fe-bearing system. It clearly shows that K_D decreases with increasing temperature. Compared with temperature, pressure seems to have little effect on K_D. We also calculated K_D when considering all Fe is assumed to be ferric or ferrous in both pyrolite and MORB bulk compositions shown in Fig. 1. We also found that K_D in MORB bulk compositions is much larger than that in pyrolite, may indicate that K_D increasing with Fe content increases.

Most of previous studies have indicated that PhD only survived below 1300 ℃ at mantle transition zone condition (Shieh et al. 1998; Frost 1999; Ohtani et al. 2000). However, recent

results shown that a trace amount of Al_2O_3 increases thermal stability of PhD up to 1600 ℃ at 24 GPa (Ghosh and Schmidt, 2014), and Al-rich PhD could stabilize up to 2000 ℃ at 26 GPa (Pamato et al., 2015). On the other hand, Nishi et al. (2014) has suggested that PhD could remain stable up to 48 GPa in Al-free system and further transformed to phase H. Therefore, considering K_D obtained in this study, Al-bearing PhD is supposed to possess a much broader stability region than previously thought. In line with these arguments, we noticed that PhD was observed coexisting with Brg from 1150 ℃ to 1500 ℃ at 25 GPa. However, PhD totally decomposes around 28 GPa and 1350 ℃, in which Brg is found to be coexisting with a large amount of melt. At 31 GPa and 1350 ℃, Brg coexists with a trace amount of δ-AlOOH phase and maybe a little amount of melt is found to be trapped in grain boundary.

The different phase relation obtained in this study probably attribute to starting composition. In previous studies, PhD was assumed to survive at least at pressures higher than 35 GPa by investigating stability of single phase superhydrous phase B or PhD in Al-free system, respectively (Ohtani et al., 2003; Nishi et al., 2014). Here, we use Fe-free pyrolite Brg ($Mg_{0.95}Al_{0.1}Si_{0.95}O_3$) and PhD mixture with volume ration 4:1(4.7:1, in wt.%) on the base of mineral fractions in hydrous peridotite bulk composition (Ohtani et al., 2004). Accordingly, the starting composition used in this study is considered to be more close to the condition along subduction in the uppermost lower mantle. Although we adopt Fe-free system, both K_D in Fig. 1 and those reported by Pamato et al. (2015) have indicated that with Fe content increases K_D also increasing, especially considering all Fe is assumed to be ferrous, which corresponding to reduced condition in the deep lower mantle. Previous study has shown that Fe slightly decreases stability region of PhD in Fe-bearing system, whereas, addition of Al increases its stability field in Al, Fe-bearing system (Ghosh and Schmidt, 2014). Therefore, Al-rich PhD obtained in this study in Fe-free system should have a much broader stability region. It is unexpected, however, Al-bearing PhD totally decomposes

around 28 GPa and 1350 ℃. Although the temperature 1350 ℃ applied at 28 GPa is slightly higher than slab geotherm, high content of Al absorbed in PhD could greatly increase its thermal stability at elevated pressure, for instance, observation of PhD at 25 GPa and 1500 ℃ in this study.

A plenty of studies have suggested that much of water would be lost at choke point (around 200 km depth), only a little water can be preserved in cold subducting slabs (Schmidt and Poli, 1998; Ohtani et al., 2001; Poli and Schmidt, 2002; Litasov and Ohtani, 2003; Fumagalli and Poli, 2005; Komabayashi and Omori, 2006). The totally decomposes of Al-bearing PhD around 28 GPa and 1350 ℃, implying that it is likely to be the second choke point for hydrous minerals, since large amount of melt is observed coexisting with Brg at this condition. At elevated pressure, only a trace amount of melt may be trapped in grain boundary and small amount of water is retained in δ-AlOOH coexisting with Brg. Since δ-AlOOH was shown to be stable up to 170 GPa (Sano et al., 2008; Ohtani et al., 2001; Tsuchiya 2013; Bindi et al., 2014; Nishi et al., 2014), this phase is supposed to play a remarkable role for water transportation, broadening our knowledge to model geodynamic process associate with the water cycle in the deepest part of the lower mantle.

4. Implications

As important water carrier, dehydration of PhD significantly effects physical properties of surrounding materials. The reaction PhD = Brg + St + H_2O obtained even above 35 GPa based on thermodynamic calculations in Fe, Al-free system, implying dehydration-linked deep seismic discontinuity (Komabayashi and Omori, 2006). However, as shown in this study, dehydration of PhD is only restricted to around 28 GPa by using appropriate starting composition similar to mineral fraction along subduction in hydrous pyrolite composition, corresponding to the maximum depth of ~900 km. On the other hand, for PhD itself, if

elasticity property comparable with superhydrous phase B (SUB), the parameters of longitudinal (V_p), shear wave (V_s) velocities are lower than those major mineral assemblages along cold subducting slab (Rosa et al., 2015; Li et al., 2016; Yang et al., 2017), displaying signature of lower velocities anomalies. Although SUB was investigated to explain local discontinuity and velocity anomalies (Rosa et al., 2015; Li et al., 2016; Yang et al., 2017), the single phase they used in Fe, Al-free system may be inappropriate to predict its thermal stability along subduction beneath transition zone, because both our result and previous study have shown Al prefers to distribute in DHMSs than coexisting wadsleyite, ringwoodite and bridgmanite (Bolfan-Casanova et al., 2003; Litasov et al., 2005; Ghosh and Schmidt, 2014; Ohira et al., 2014), which greatly influence stability of SUB in pyrolite composition. Until now, we still don't fully understand stability region of Al, Fe-bearing SUB in pyrolite composition at transition zone condition. Study has shown that PhD had broader stability limit than SUB in Fe-bearing system (Ganskow and Langenhorst, 2014). Since water trapped in Al-bearing PhD is two to three times higher than superhydrous phase B (estimate based on deficit of weight total), thus, dehydration of PhD instead of SUB may possibly generate more easily detectable low velocity zone and seismic discontinuity signals.

According to electrical conductivity and seismic analysis, down-going subducting oceanic slabs in Pacific plate possibly transports a certain amount of water to mantle transition zone (Karato, 2011; Liu et al., 2016) and some of Pacific slabs were indicated to penetrate into the lower mantle (Zhao and Ohtani, 2009). Therefore, Al-bearing PhD may be transported into the lower mantle along subduction. because Even if some of the short stagnant slab are heated by surrounding mantle, Al-bearing PhD can still survive at relative cold environment in ambient transition zone due to its high thermal stability. Furthermore, experimental studies have shown that nominally anhydrous wadsleyite and ringwoodite (Rw) could contain a certain amount of water (Inoue 1994; Inoue et al., 1995), which hints the mantle transition zone might be a large water reservoir. Due to the low water solubility in

Brg, much of water will be released when Rw transforming to Brg. The released water may react with surrounding bulk composition to form Al-bearing PhD and even Al-rich PhD as Pamato et al. (2015) argued, which also possibly be transported into lower mantle.

Previous result has observed the existence of high electrical conductivity region from 650 to 850 km instead of shallower depth at northern Japan beneath the north Pacific by inverting the observed cable and GDS responses (Shimizu et al., 2010). They ascribed this feature to temperature effect. Or more appropriate, this feature can be well explained by stability of Al-bearing PhD investigated in this study. Since a trace amount of melt is observed from 1150 ℃ to 1500 ℃ at 25 GPa, indicating dehydration may already begin from transition zone to second chock point (~ 900 km depth) along subduction, the released water or melt possibly produces a high electrical conductivity zone. Finally, the released water at second chock point will migrate upward and may also cause partial melting to generate velocity anomalies at shallower region.

Liu et al. (2016) observed low velocity zone (LVZ) at ~770 km depths within Japan slab. Recently, they also observed velocity reductions at ~800 km depths beneath the European Alps by seismic observation (Liu et al., 2018). They argued both of these two similar situation were possibly caused by melting of hydrous materials, which brought from hydrous mantle transition zone together with denser metallic Fe. Our laboratory studies here match their observations. Due to the low water solubility in brg and magnesiowustite, dehydration of Al-bearing PhD would easily cause partial melting of surroundings and further produce low-velocity anomalies locally. Therefore, the dehydration of Al-bearing PhD at 28 GPa (~ 800 km depth) in our experiment give a better explanation for these LVZ, which is much simple than explanation given by Liu et al. (2018). If this is the case, the observed low velocity zone and seismic discontinuity locally ~ 750 km in Western Pacific Subduction Zones, the observed intermittent low-velocity anomalies at ~730 km beneath North America and 770 km LVZ beneath North East China may also be well interpreted as dehydration of Al-bearing

PhD and the second chock point (Chen and Ai, 2009; Schmandt et al., 2014; Liu et al., 2016; Porritt and Yoshioka et al., 2016), which might even help to explain dehydration-linked deep earthquakes ~ 700 km (Frohlich, 1989), for example, the 30 May 2015 Chichi-jima M8 earthquake at depth of 682 km (Porritt and Yoshioka, 2016).

Tables in chapter 6

Table 1. Experimental conditions and run products

Pressure	Temperature	Time	Results
(GPa)	**(℃)**	**(min)**	**Phase assemblages**
25	1150	720	PhD+Brg
25	1350	600	PhD+Brg+Melt (T)
25	1500	600	PhD+Brg+Melt (T)
28	1350	720	Brg+Melt
31	1350	720	Brg+δ+Melt (T)

PhD: Al-bearing phase D, Brg: bridgmanite, δ: Al-rich δ phase
T: trace

Table 2. Chemical compositions of run product

P	T(℃	Phase	MgO	Al_2O_3	SiO_2	Total
25	1150	PhD	23.35(2)	15.65(8)	45.10(7)	84.10(3)
		Brg	39.80(3)	0.78(7)	60.72(1)	101.30(7)
25	1350	PhD	23.12(4)	19.07(1)	44.01(9)	86.20(3)
		Brg	39.19(9)	1.40(9)	59.91(3)	100.50(8)
25	1500	PhD	16.66(1)	27.34(5)	39.58(3)	83.58(4)
		Brg	39.25(6)	3.99(9)	60.97(4)	104.20(2)
28	1350	Brg	38.31(2)	4.96(1)	57.46(5)	100.73(2)
		Melt	19.52	2.97	11.99	34.48
31	1350	Brg	37.89(6)	2.39(6)	58.91(6)	99.19(3)
		δ	9.52(7)	47.13(3)	23.39(8)	80.04(2)

Figures in chapter 6

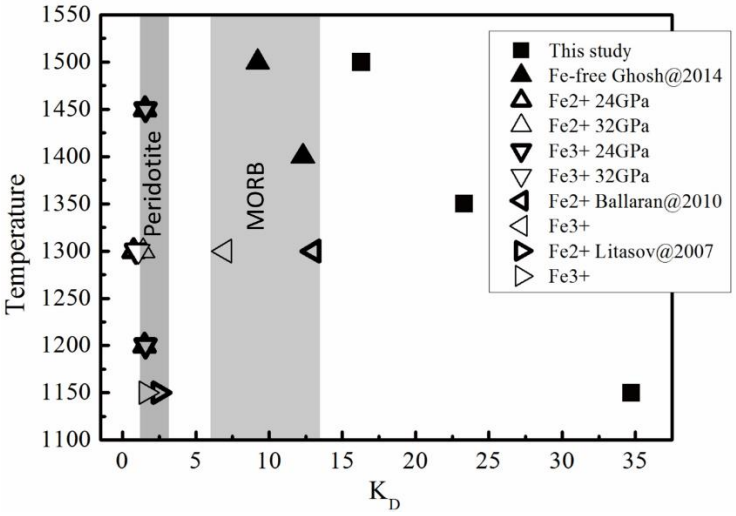

Figure 1. Partition coefficient of Al ($K_D = \frac{X_{Mg}^{Brg} \cdot X_{Al}^{PhD}}{X_{Al}^{Brg} \cdot X_{Mg}^{PhD}}$) between PhD and Brg as a function of temperature. Different symbols used here mean different pressure and temperature condition. Same symbol used in different thickness is to distinguish ferric or ferrous Fe adopted in K_D. Typical compositions in peridotite and mid ocean ridge basalt (MORB) are shown as grey bars. It is clear indicates that K_D increasing with temperature and Fe content increase compared with different bulk compositions, however, pressure seems to play a weak role on K_D.

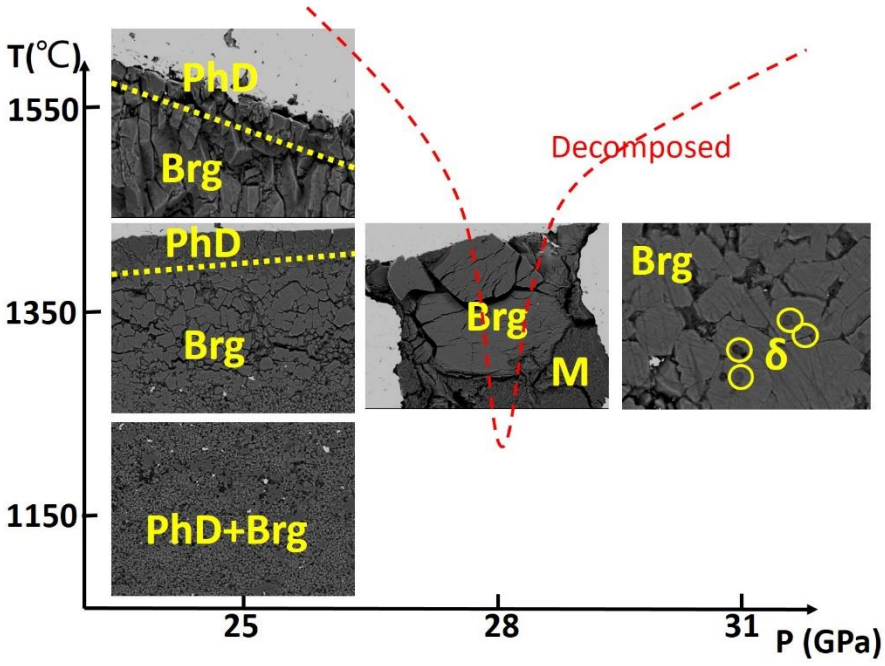

Figure 2. Backscattered electron images of representative run products under various pressure and temperature conditions. Red dot line means the possible stability limit of PhD and δ. Brg-bridgmanite，δ-δ Phase, M-melt.

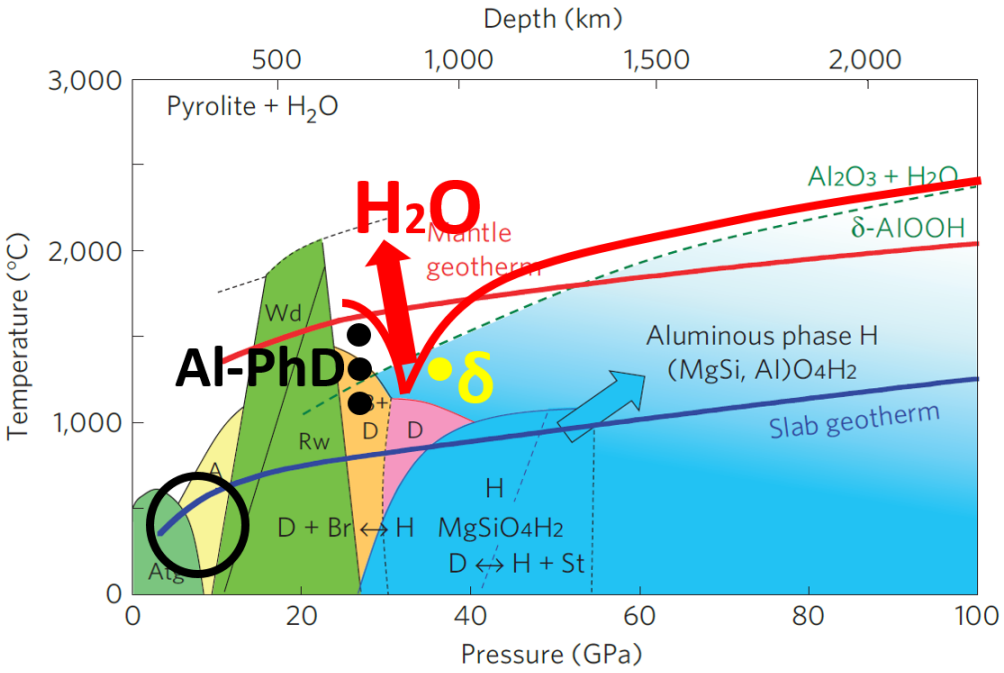

Figure 3. Second chock point for hydrous minerals modified from Nishi et al. (2015). Black circle means the chock point around 6 GPa reported by previous studies. Solid black and yellow circle means the observed Al-PhD and δ Phase. Much of the water may be released at the second chock point around 28 GPa.

Chapter 7

Solubility behavior of δ-AlOOH - ε-FeOOH at high pressures

(Accepted by American Mineralogist)

Abstract

Naturally occuring low-pressure polymorphs of AlOOH and FeOOH are common oxyhydroxides at the Earth's surface, which may transport hydrogen to the deep mantle as they are subducted. At elevated pressures, these low-pressure polymorphs transform into CaCl2-type δ-AlOOH and ε-FeOOH, which form a solid solution at high pressures. Nevertheless, few studies have examined the solubility behavior of this binary system in detail. In this study, we ascertain the phase relations in an AlOOH and FeOOH binary system at 15–25 GPa and 700–1200 ℃. Analysis of XRD patterns and unit cell volume of quenched samples show that δ-AlOOH and ε-FeOOH form partial solid solutions over wide pressure and temperature ranges. Our results demonstrated that a binary eutectic diagram is formed without dehydration or melting below 1200 ℃ at 20 GPa. We also observe that changes in Al and Fe contents in solid solution were more strongly influenced by temperature than by pressure. Our results suggest that $CaCl_2$-type hydroxides subducted in to the deep mantle form a solid solution over a wide composition ranges. As AlOOH and FeOOH are present in hydrous crust, these phases may be tectonically embedded and subducted into the deep interior, transporting a significant amount of hydrogen to deeper regions. Therefore, a greater understanding of the the solubility behavior of this binary system may help to elucidate the model geodynamic processes associated with the deep water cycles of the Earth.

1. Introduction

H_2O (present as H^+ or OH^- in the minerals) plays an important role in the Earth's interior, affecting the physical and chemical properties of its surroundings such as melting temperatures, melt composition, and phase relations (Inoue 1994; Chang et al. 2017; Hwang et al. 2017; Myhill et al. 2017). Water may be transported into the deep Earth via subducting

slabs within hydrous phase. Previous studies have been evaluated the stability regions of various hydrous phases, especially dense hydrous magnesium silicates (DHMSs), which have been suggested as potential water carriers to the transition zone and even to the lower mantle in cold subducting slabs (Frost and Fei 1998; Litasov and Ohtani 2003; Komabayashi et al. 2005).

The oxide hydroxides goethite (α-FeOOH) and AlOOH are common hydrous minerals in the sediments. δ-AlOOH is a high-pressure polymorph of diaspore (α-AlOOH) and boehmite (γ-AlOOH) (Suzuki et al. 2000; Xue and Kanzaki 2007) that has been shown to be stable up to 170 GPa (Sano et al. 2008; Tsuchiya and Tsuchiya 2011; Ohira et al. 2014). The other potential water carrier, ε-FeOOH, which is a high-pressure polymorph of goethite (α-FeOOH), akaganeite (β-FeOOH), and lepidocrocite (γ-FeOOH), has a $CaCl_2$-type crystal isostuctural with δ-AlOOH (Suzuki 2010). ε-FeOOH has been known to have a stability field in the lower mantle (Nishi et al. 2017). To investigate the physical properties of these $CaCl_2$-type structure hydrous phases, numerous experiments and calculations have been performed particularly addressing the stability, compressibility, and crystallography of endmember δ-AlOOH, ε-FeOOH, and phase H ($MgSiO_4H_2$) (Suzuki 2010; Tsuchiya et al. 2002; Panero and Stixrude 2004; Xue and Kanzaki 2007; Kuduvalli et al. 2008; Komatsu et al. 2011; Kuribayashi et al. 2013; Nishi et al. 2014; Bindi et al. 2014; Zhong et al. 2016; Thompson et al. 2017). Earlier results have also shown that phase H and δ-AlOOH form a solid solution because of their similar structures (Ohira et al. 2014; Panero and Caracas 2017). This AlOOH-$MgSiO_4H_2$ solid solution can coexist with bridgmanite above 40 GPa along slab geotherm (Nishi et al. 2014; Ohira et al. 2014; Nishi et al. 2015; Bindi et al. 2015; Walter et al. 2015; Panero and Caracas 2017).

The discovery of hydrous aluminum silicate phase Egg ($AlSiO_3OH$) as inclusions in diamond implies that the crustal hydrous material may be subducted to the transition zone, at least locally (Wirth et al. 2007). More recently, hydrous ringwoodite and ice-VII were also

found as inclusions in diamond, suggesting their presence in a partially hydrated mantle transition zone and the lower mantle (Pearson et al. 2014; Tschauner et al. 2018). Because AlOOH and FeOOH are common oxide hydroxides at Earth's surface, these solid solutions in the deep Earth play an important role for water transportation in subducted slabs (Nishi et al. 2017). Nevertheless, the solubility behavior of this binary system is not well constrained. A better understanding of this system will also help to elucidate the water cycle of iron-rich Martian mantle. Therefore, this study was conducted to determine the solubility behavior of AlOOH-FeOOH binary system at 15–25 GPa and 700–1200 ℃.

2. Materials and Methods

We conducted high-temperature and high-pressure experiments using a Kawai-type 1000-ton multi-anvil apparatus installed at the Geodynamics Research Center (GRC), Ehime University. Pressures were calibrated at room temperature by diagnostic changes in the electrical resistances of ZnTe (9.6 and 12.0 GPa), ZnS (15.5 GPa), GaAs (18.3 GPa), and GaP (23.0 GPa) induced by the semiconductor–metal phase transitions at high pressures. Tungsten carbide cubes with truncation edge length (TEL) of 4 mm were used in combination with Co-doped MgO-octahedra of 10 mm edge length (10/4 assemblage). Preformed pyrophyllite gaskets were used between the cubes, $LaCrO_3$ was used as the heater, and a gold sample capsule was used in the cell assemblage. The temperature was monitored using a $W_{97}Re_3$-$W_{75}Re_{25}$ thermocouple and electromotive force (EMF) was not corrected for the effects of pressure. The sample was compressed to the desired pressure and then oil pressure was held constant. Subsequently, the AC power was supplied to the heater in the furnace assemblage. After heating at high pressure, then the power was stopped by shutting off the electric power supply. Samples were recovered after releasing pressure slowly for 12 hours.

The recovered run products were mounted in epoxy resin and were polished for phase identification and chemical composition analysis.

The starting material, with a chemical composition of $(Al_{0.5}Fe_{0.5})OOH$, was prepared by mixing oxide $Al(OH)_3$, Al_2O_3 and Fe_2O_3 in appropriate proportions. The recovered run products were mounted in epoxy resin and were polished to perform phase identification and composition analysis. The phase assemblages were identified using a micro-focus X-ray diffractometer (MicroMax-007HF; Rigaku Corp.) with Cu Kα radiation. The obtained data were processed by 2PD software, which can display and process two dimentional data, including smoothing, background correction and 2D to 1D conversion. The micro-textures and composition were obtained using a field emission scanning electron microscope (FESEM, JSM7000F; JEOL) combined with an energy-dispersive X-ray spectrometer (EDS, X-MaxN; Oxford Instruments plc.). Working parameters of 15 kV, 1 nA and collection times of 30–50 s were used. The chemical composition was analyzed using EDS. We used software (Aztec ver. 2.4; Oxford Instruments Nanotechnology Tools Ltd.) to process EDS data. Stoichiometric composition of $(Fe_X,Al_{1-X})OOH$ was assumed, where X is found from the ratio of analyzing Fe and Al. The total weights of the $(Fe_X,Al_{1-X})OOH$ were approximately 85 wt.%.

3. Results and Discussion

Table 1 presents the experimental conditions and results, and the chemical compositions of the samples determined from EDS are presented in Table 2. In all runs, the back-scattered electron (BSE) images showed that recovered samples consist mainly of two phases except for the highest temperature likely above solidus (1200 °C) (Fig. 1). The X-ray diffraction (XRD) patterns of the samples clarified that these phases were ε-FeOOH and δ-AlOOH (Fig. 2), although the peak positions shifted from those of the ideal endmembers, as discussed later.

At 20 GPa and 900 ℃, a BSE image (Fig. 1(a)) shows the presence of two phases in bright and dark colors with respective chemical compositions of ε-$Fe_{0.78}Al_{0.22}OOH$ and δ-$Al_{0.91}Fe_{0.09}OOH$. These chemical compositions can be explained by forming solid solutions because of the similar crystal structures of the endmembers. The compositions and grain sizes of both phases changed at elevated temperatures up to 1100 ℃ (Fig. 1b). With increasing temperature, the Al/Fe ratio decreases in Al-rich δ-phase, it increases in Fe-rich ε-phase (Table 1). At 1200 ℃, Al-rich δ-phase was found coexisting with iron oxide (bright color) and melt (Fig. 1c), which means Fe-rich ε-phase totally decomposed at this condition. Some amount of H_2O escaped when the capsule was opened. At lower pressure of 15 GPa at 1000 ℃, the crystal shape of Al-rich δ-phase seems to transfer into elongated shape (Fig. 1(d)), which might occur because of the phase change as indicated by XRD profiles, as described later.

The selected room temperature XRD patterns of recovered samples are summarized in Figure 2. Al-rich δ-phase, Fe-rich ε-phase and low pressure Al-rich α-phase are observed in XRD patterns. Each peaks are consistent with earlier studies in δ-AlOOH and ε-FeOOH (Suzuki et al. 2000; Suzuki et al. 2010; Kuduvalli et al. 2008; Mashino et al. 2016). Our results suggest that the solid solutions are formed in δ-AlOOH - ε−FeOOH binary systems in large compositional ranges. The XRD peaks of Fe-rich ε-phase and Al-rich δ-phase were observed at higher and lower angle directions, respectively, at 1100 ℃ and 20 GPa compared to 900 ℃ and 20 GPa. These observations are consistent with SEM-EDS observations, which indicate that Al contents increase in Fe-rich ε-phase, whereas Fe contents increase in Al-rich δ-phase at higher temperature (Table 1). At 15 GPa and 1000 ℃, probably because of the low pressure, we observed a diffraction peak of α-AlOOH instead of δ-AlOOH, as presented in Fig. 2(c).

Figure 3 shows the unit cell volumes of solid solutions between δ-AlOOH and ε-FeOOH as a function of FeOOH content. Figure 3 shows that partial solid solutions were formed at

20-25 GPa and 700-1200 ℃. The volume of Fe-rich ε-phase increases with increasing Fe content likely because of the large size of $^{VI}Fe^{3+}$ ion (0.645 Å) relative to $^{VI}Al^{3+}$ ion (0.535 Å). This is consistent with previous experimental studies in a similar (Al, Fe)OOH bulk composition conducted at 21 and 40 GPa (Fig. 4; Kawazoe et al. 2017; Nishi et al. 2017).

The phase relations of the δ-AlOOH - ε−FeOOH binary system are presented in Figure 4. The dashed line in Figure 4 shows the dehydration temperature of δ-AlOOH (approximately 1200 °C) at 20 GPa (Ohtani et al. 2001). Similar thermal stability limit for δ-AlOOH was also reported in the previous study showing the decomposition of the phase Egg into δ-AlOOH + SiO_2 at around 1200 ℃ at transition-zone pressures (Sano et al. 2004; Fukuyama et al. 2017). In this study, a binary eutectic diagram is formed without dehydration or melting below the dashed line in Figure 4 from 700 ℃ to 1100 ℃ at 20 GPa, and at pressures of 15–25 GPa at 1000 ℃ (except for the stability field of α-AlOOH). AlOOH and FeOOH solid solutions are observed over wide temperatures and pressure ranges. Although a report of an earlier study described the dehydration of δ-AlOOH at 1200 ℃ (Ohtani et al. 2001), our data show that Al-rich δ-phase persists at 1200 ℃, whereas the Fe-rich ε-phase decomposed into Fe_2O_3 + H_2O (Fig. 2d) under the same *P*–*T* conditions. Al-rich δ-phase was observed at 1200 ℃ in contrast to previous studies (Ohtani et al. 2001). This indicates that a thermal gradient may exist in our cell but could not be conclusively identified, because we placed the thermocouple at the center of the heater, where the highest temperature should be expected. To the author's knowledge, no previous study has determined the melting temperature of ε-FeOOH in the transition zone pressure conditions. Our results suggest that ε-FeOOH has a lower dehydration temperature than that of δ-AlOOH. We also found that the Al-content in FeOOH is larger than the Fe-content of AlOOH. Because of the smaller ionic radius of Al^{3+} than Fe^{3+}, on the other hand, Al^{3+} is more compatible with octahedral site in ε-FeOOH than that of Fe^{3+} in δ-AlOOH, leading to the higher Al-content in ε-FeOOH than the Fe-content of δ-AlOOH. We should note that EDS is difficult to precisely measure chemical

compostion of recovered sample at 700 ℃ due to small crystal size. Therefore, chemical compositions of the two phases at 700 ℃ (dashed circles in Fig. 4) were estimated from the relation between unit cell volume and composition from Fig. 3.

The chemical compositions and their temperature dependences of δ-phase and ε-phase at 20 GPa of our study are consistent with those found at 40 GPa in an earlier study (Fig. 4; Nishi et a. 2017). Consequently, compared with pressure, temperature seems to play a more significant role in the partitioning of Al and Fe between δ-AlOOH and ε-FeOOH at pressures up to 40 GPa. For example, although the samples were recovered from different pressures, the similar Al/Fe ratios of hydroxides were observed at 1000 ℃. This means that temperature has a more profound influence on compositional stability than pressure in AlOOH-FeOOH binary system, so a series of intermediate compositions were identified in the whole temperature range 700–1250 ℃. On the other hand, the dehydration temperatures of both δ-phase and ε-phase are likely to increase concomitantly with increased pressures, because these phases were observed at 1240 ℃ and 40 GPa in an earlier study (Fig. 4). Therefore, AlOOH and FeOOH may form a complete solid solution near the solidus at higher pressures, although they do not at 20 GPa.

4. Implications

$CaCl_2$-type crystal structure has been observed to remain stable at 76 GPa and 2150 K with iron endmember (Hu et al. 2016). These endmembers form solid solutions at elevated temperatures and pressures in the subducting plate. As such, they are expected to transport water (H^+) into the deep lower mantle, even undergoing change in their respective chemical compositions depending on the temperature, as shown in this study. Moreover, δ-AlOOH reportedly forms a solid solution with phase H ($MgSiO_4H_2$), and coexists with bridgmanite along pressure and temperature path corresponding to the subduction (Nishi et al. 2014; Ohira

et al. 2014; Paneroa and Caracas 2017). Consequently, it is important to examine the influence of the addition of phase H ($MgSiO_4H_2$) to the stability of $CaCl_2$-type hydrous phases in δ-AlOOH ε-FeOOH - phase H ternary system, which are expected to form over a wide composition range, and may carry a significant amount of hydrogen deep to the lower mantle.

Tables in chapter 7

Table 1. Experiment run conditions and mineral compositions of recovered samples in AlOOH-FeOOH binary system.

P (GPa)	T (℃)	Duration time (min)	EDS analysis number	Phase	Al_2O_3	Fe_2O_3	Total
15	1000	60	27	α-$Al_{0.92}Fe_{0.08}OOH$	71.71 (200)	10.33 (98)	82.04 (178)
				ε- $Fe_{0.75}Al_{0.25}OOH$	14.39 (89)	67.83 (90)	82.22 (109)
20	700*	60	29	δ-$Al_{0.93}Fe_{0.07}OOH$	70.82 (169)	11.50 (62)	82.32 (136)
				ε-$Fe_{0.76}Al_{0.24}OOH$	14.29 (154)	69.20 (155)	83.49 (74)
20	900	60	32	δ-$Al_{0.90}Fe_{0.10}OOH$	72.21 (81)	12.06 (84)	84.27 (84)
				ε-$Fe_{0.78}Al_{0.22}OOH$	12.67 (113)	69.41 (97)	82.08 (43)
20	1000	60	35	δ-$Al_{0.81}Fe_{0.19}$ OOH	60.59 (107)	22.51 (73)	83.10 (180)
				ε-$Fe_{0.64}Al_{0.36}OOH$	22.27 (74)	62.00 (81)	84.27 (57)
20	1100	40	32	δ-$Al_{0.78}Fe_{0.22}$ OOH	58.89 (128)	26.36 (92)	85.25 (80)
				ε-$Fe_{0.55}Al_{0.45}OOH$	28.62 (125)	54.30 (126)	82.92 (56)
20	1200	40	25	δ-$Al_{0.72}Fe_{0.28}$ OOH	53.48 (158)	33.05 (140)	86.53 (50)
				Fe_2O_3	1.91 (17)	98.39 (48)	100.30 (52)
25	1000	90	30	δ-$Al_{0.86}Fe_{0.14}OOH$	65.13 (71)	17.27 (52)	82.40 (74)
				ε-$Fe_{0.70}Al_{0.30}OOH$	17.64 (64)	64.66 (63)	82.30 (45)

* Chemical composition of Fe-rich phase might have large uncertainty because of the small crystals.

Values in parentheses denote measurement uncertainties.

Figures in chapter 7

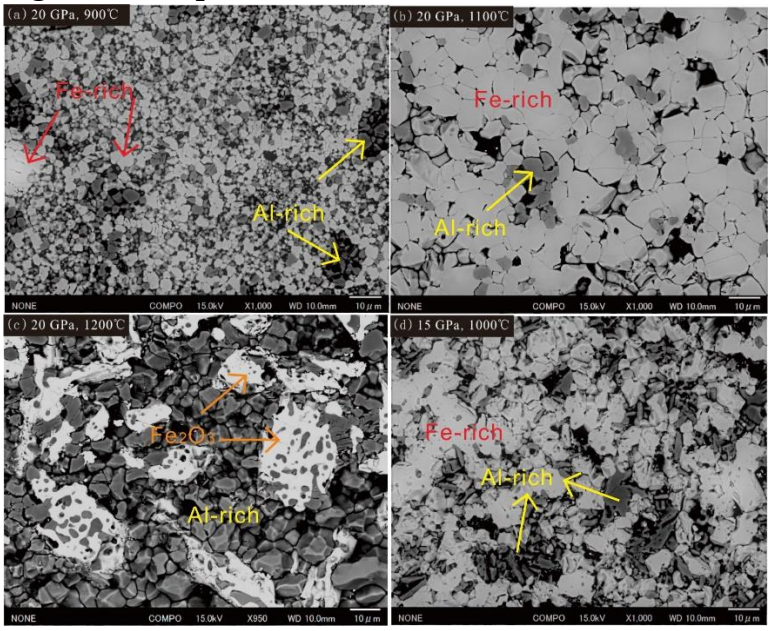

Figure 1. Backscattered electron images of representative run products under various pressure and temperature conditions. Al-rich: Al-rich phase, Fe-rich: Fe-rich phase. (a) 20 GPa, 900 ℃; (b) 20 GPa, 1100 ℃; (c) 20 GPa, 1200 ℃; and (d) 15 GPa, 1000 ℃. Some amount of H_2O escaped when the capsule was opened.

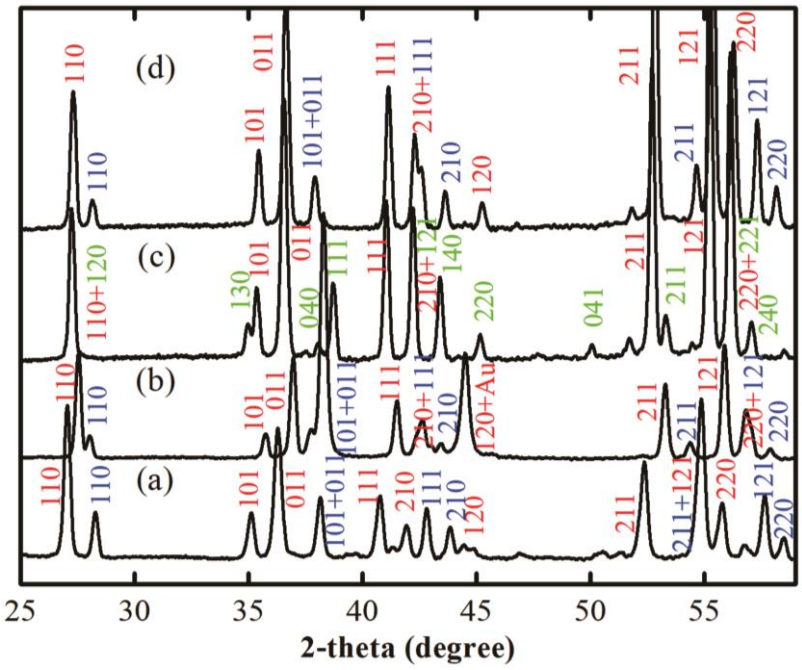

Figure 2. Selected XRD patterns of recovered run product: (a) 20 GPa, 900 ℃; (b) 20 GPa, 1100 ℃; (c) 15 GPa, 1000 ℃; and (d) 25 GPa, 1000 ℃. Index numbers in red and blue represent Fe-rich ε-FeOOH and Al-rich δ-AlOOH, respectively. At 15 GPa (c), α-AlOOH (green) appeared instead of δ-AlOOH.

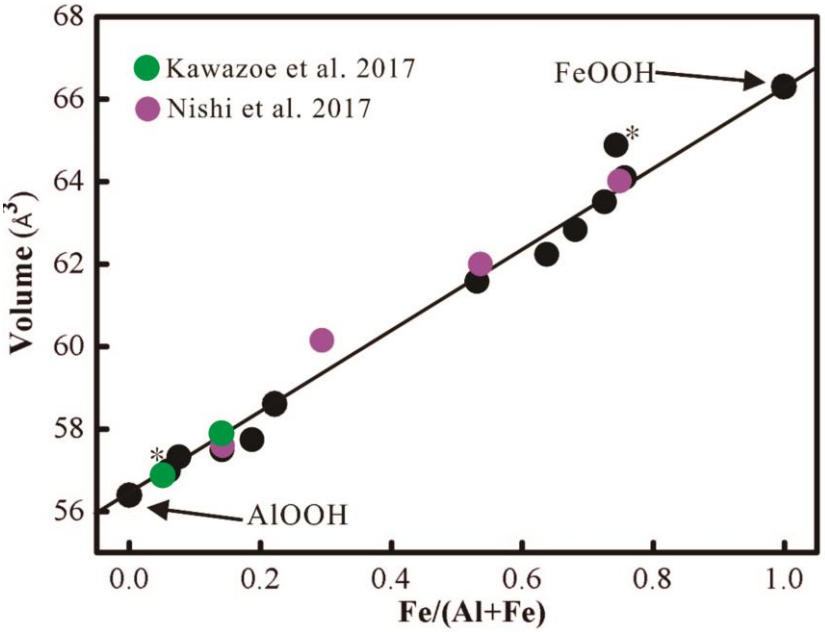

Figure 3. Cell volumes of intermediate compositions in δAlOOH-εFeOOH binary system at ambient conditions as a function of ε-FeOOH content. All chemical compositions (including literature data) were determined using EDS, and the volumes were determined from XRD. The trend of our data is consistent with those reported for solid solution in (Al, Fe)OOH bulk composition at 21 and 40 GPa (green and pink color), which suggests that solid solutions can be formed in a wide pressure range. An asterisk (*), denotes volume determined from the sample with large uncertainty due to small crystal size. The variation of volume was often so small that the error bars were smaller than the symbol size.

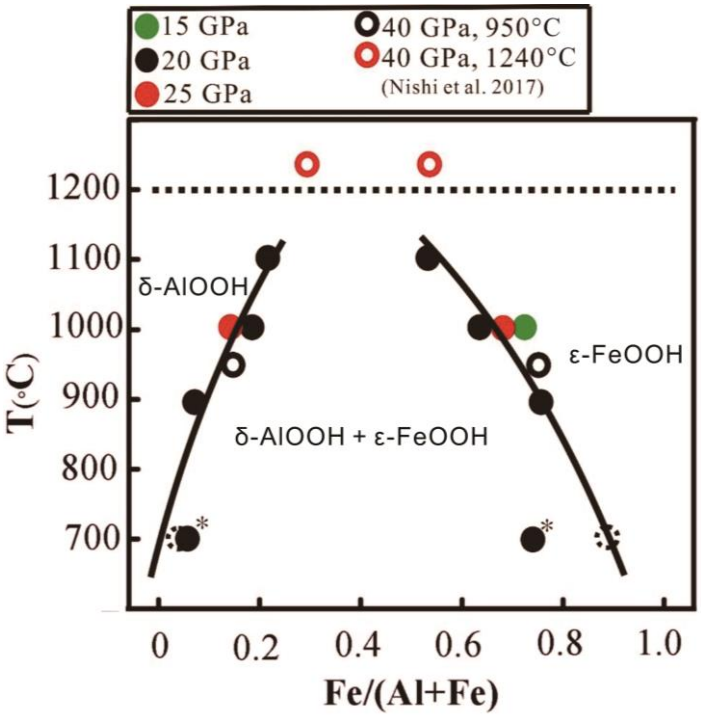

Figure 4. Phase relations in δAlOOH-εFeOOH binary system at various pressures and temperatures as a function of ε-FeOOH content. Dashed circles denote the composition at 700 ℃, as estimated from the relation between unit cell volume and composition from Fig. 3. The dashed line shows the dehydration temperature of δ-AlOOH (approx. 1200 ℃) at 20 GPa (e.g., Ohtani et al., 2001). A broad range of intermediate compositions in the FeOOH-AlOOH system were identified in the whole *P*–*T* range 15–25 GPa and 700–1200 ℃. Open circles show a solid solution between δ-AlOOH and ε-FeOOH synthesized at 40 GPa (e.g., Nishi et al., 2017), suggesting that pressure can increase the dehydration temperature.

Chapter 8

Sound velocities of Al-bearing phase D to 22 GPa and 1300 K

(Submited to Geophysical Research Letters)

Abstract

The sound velocities and density of Al-bearing phase D (PhD) was investigated up to 22 GPa and 1300 K by in situ synchrotron X-ray techniques combined with ultrasonic measurements. Modeled velocities of Al-bearing PhD in hydrous pyrolite along normal mantle geotherm shows that Al-bearing phase D generates high velocity anomalies compared with dry pyrolite in mantle transition zone, however, it is seismically invisible due to the small anisotropy. Once Al-bearing phase D is transported to the uppermost lower mantle, it shows a lower signature than dry pyrolite or higher velocities within the slab region. Thus the observed velocity anomalies at the uppermost lower mantle may be considered as the presence of water in subduction zone. Due to its high thermal stability region, Al-bearing phase D is expected to transport water to the Earth's lower mantle, elucidating model geodynamic processes associated with the deep water cycles.

1. Introduction

Water plays an important role in the Earth's interior, which affects the physical and chemical properties of the surrounding materials, for instance, elasticity, rheology, electrical conductivity, and melting behaviors (Inoue, 1994; Yoshino et al., 2009; Myhill et al., 2017). Nominally anhydrous minerals, wadsleyite and ringwoodite, which are the most abundant minerals in the Earth's mantle transition zone (MTZ), have been shown to have the potential to accommodate several ocean's masses of H_2O (Inoue et al., 1995). The recent discovery of diamonds with hydrous ringwoodite (1.4 wt % H_2O) and ice-VII inclusions, also revealed that some regions of the MTZ could be at least partially hydrated (Pearson et al., 2014; Tschauner et al., 2018), suggesting the existence of hydrous minerals in the MTZ, transported in cold inner parts of the subducting slabs (Gasparik, 1993; Komabayashi and Omori, 2006)

or as products of recrystallizing hydrous melts (Pamato et al., 2015). In this context, petrological studies have shown that dense hydrous magnesium silicates (DHMSs) in the MgO-SiO_2-H_2O system are the primary water carriers in the MTZ and could play an important role into delivering water down to the middle part of the lower mantle (Ohtani et al., 2001; Nishi et al., 2014; Litasov et al., 2005; Liu et al., 2019).

Among DHMSs, PhD is regarded as a potential carrier of water from the MTZ to the lower mantle due to this phase forming at 15 GPa while it is stable up to ~44 GPa, which corresponds to depths of 450 km and 1,250 km, respectively (Frost 1999; Nishi et al., 2014). The ideal chemical formula of the PhD endmember is $MgSi_2H_2O_6$, however, the PhD shows nonstoichiometry and the Mg/Si ratio varies from 0.55 to 0.71 and H content from 2 to 3.6 formula units (Frost and Fei, 1999), thus holding up to ~10 wt% water at high-pressure. The structure is trigonal symmetry ($P\bar{3}1m$) (Kudoh et al. 1997; Yang et al. 1997) with SiO_6 and MgO_6 octahedra alternatively stacking along the c-axis (Yang et al. 1997). A former study by Frost and Fei (1998) demonstrated that PhD is potentially stable under the pressure and temperature conditions of the lower mantle due to the postitive Clapeyron slope of the superhydrous phase B to PhD transformation. More recently, Al-rich PhD (56.6 wt% Al_2O_3) was shown to be stable at temperatures up to 2,000 °C and 26 GPa (Pamato et al., 2015), from what it was concluded that aluminous PhD, which is more likely to crystallize in a realistic slab composition, could be stable in a large P and T range.

The direct measurements of velocity-density data for hydrous phases is therefore particularly needed to interpret seismic anomalies related to the presence of hydrated regions at the bottom of the MTZ. Despite such importance, there are only few studies that investigated the effect of H_2O incorporation on the sound velocities of nominally anhydrous minerals (Inoue et al., 1998; Jacobsen et al., 2004; Mao et al., 2012), while those of hydrous minerals such as DHMSs remain poorly studied (Yang et al., 1997; Komabayashi and Omori, 2006; Ohira et al., 2014). The elasticity of PhD as well, is to this day poorly investigated,

because ultrasonic measurement requires well sintered samples with high purity, which is difficult to achieve for PhD as substantial amount of pores, chemical heterogeneities or accessory phases appear as a consequence of the high water content and therefore such sample were not available. The few existing studies (e.g. PVT studies) showed that hydrous phases generally have lower bulk moduli and densities than anhydrous mantle minerals and therefore could lower velocities compared to the surrounding dry mantle (Frost and Fei, 1998; Litasov et al., 2008; Hushur et al., 2011; Rosa et al., 2013). Presence of PhD at the lowermost part of the MTZ and in the uppermost part of the lower mantle could therefore be an alternative to partial melting or ancient basalts (Kaneshima 2009) to explain local seismic reflectors beneath 660 km depth.

In this work, we report the longitudinal (V_P) and shear (V_S) velocities, as well as the density of Al-bearing PhD up to 22 GPa and 1300 K by in situ synchrotron X-ray techniques combined with ultrasonic measurements of a polycrystalline sample in the multianvil apparatus at the BL04B1 beamline of SPring-8, Japan. Our results provide an understanding of the sound velocities of PhD under a wide pressure and temperature range in which elastic behavior of PhD can be modeled, therefore enhancing our knowledge of how water distribution in upper parts of lower mantle where melt generation may lead to be detected as local discontinuity and low-velocity zones in some typical region at top of the lower mantle.

2. Materials and Methods

A polycrystalline Al-bearing PhD sample was synthesized at 24 GPa and 1373 K for 1 h, from a mixture of MgO (15.8 wt %), SiO_2 (43.7 wt %), $Mg(OH)_2$ (9.8 wt %) and $Al(OH)_3$ (30.6 wt %) dried reagent-grade by using the 2000-ton Kawai-type apparatus installed at the Geodynamics Research Center (GRC), Ehime University. The recovered sample appeared well-sintered, in a cylindrical shape (1.8 mm in diameter) and exhibits an average grain's

size of less than 10 μm, which is accompanied by little porosity, chemical homogeneity, and is free of accessory phase (e.g. SiO_2 and $Mg(OH)_2$) as confirmed by FE-SEM-EDS and Micro-focus XRD analyses (Fig. 1). The EDS analysis of the sample yielded the composition: 20.7 wt% MgO, 44.5 wt% SiO_2 and 18.8 wt% Al_2O_3, which gives the calculated water content of 13.6 wt%, on the basis of the ideal chemical formula of PhD, which is within uncertainties well consistent with the total weight deficiency of measured oxides (16 wt%).The lattice parameters at ambient conditions are a = 4.8077(4) Å, c = 4.3218(6) Å, and V = 86.51(1) $Å^3$. We carefully polished the sample to 1.1 mm in length and to a ~0.5 μm mirror-surface using diamond-coated polishing disk at the GRC.

We used the Kawai-type multianvil apparatus equipped with eight cubic tungsten carbide (WC) anvils with an edge length of 26 mm and 5 mm truncation edge length for in situ ultrasonic experiments under high pressure and high temperature. An alumina rod was used as a buffer rod, providing a strong echo at the interface with the sample due to the impedance contrast of the two materials. Eight cubic anvils are compressed by high pressure apparatus combined with a synchrotron radiation source. The apparatus is equipped with an energy dispersive X-ray diffraction system with Ge solid state detector and a CCD camera for radiographic imaging of the sample. A polychromatic X-ray beam collimated to the dimensions of 0.05 mm horizontally and 0.2 mm vertically was directed to the sample through pyrophyllite gasket and pressure medium. A multichannel analyzer was used to acquire photons in a range of 30-150 keV, which was calibrated with characteristic fluorescence X-ray lines of several reference metals, including Cu, Mo, Ag, Ta, Pt, Au and Pb. The precision of the energy measurements was approximately ±30 eV per channel. The 2θ angle of SSD was set at ~6° with respect to the incident beam direction and accurately calibrated using known diffraction peaks from a standard material such as gold.

The W_3Re_{97}-$W_{25}Re_{75}$ thermocouple is used to monitor the temperature. The pressure is calibrated by using equation state of Au and NaCl (Tsuchiya 2003; Matsui et al., 2012). The

sample is first squeezed at room temperature and then heated to high temperature. Following this, the temperature is decreased to 300 K in step of 200 K. The press load is increased after the first data collection cycle, and then, the temperature is increased to high temperature to start another data collection cycle during cooling. A few data collection cycles were carried out in the same way. P- and S-wave velocities of PhD specimen was investigated up to 22 GPa and 1300 K and P-V-T relationship of PhD also can be obtained simultaneously. For more detailed experimental information, please refer to Gréaux et al. (2019).

3. Results and Discussion

3.1 Compressibility of Al-phase D

Totally 33 X-ray diffraction patterns were collected under various pressure-temperature conditions within the stability field of Al-PhD (Fig. 2). However, we observed a sudden broadening of diffraction peaks at 20 GPa and temperature higher than ~1400 K, suggesting that the sample partially dehydrated in the last heating cycle of this experiment, which was later confirmed by the analyses of the recovered sample (Fig. 3), and therefore only data obtained before those pressure and temperature conditions were used in the subsequent models. Fig. 4 shows a typical X-ray diffraction pattern collected at 21.9 GPa and 1300 K, before dehydration occurred. We can see clear and sharp diffraction peaks of the sample, which allowed for precisely determining the lattice parameters. The unit-cell volume of Al-bearing PhD was determined independently for each pressure and temperature conditions and plotted in Fig. 5a. The room temperature data of Al-bearing PhD collected up to 20.5 GPa were fitted to a third-order Birch-Murnaghan equation of state using a least-squares fitting with EosFit program (Angel 2001), which yielded V_0 = 86.71 Å^3 (fixed), K_{T0} = 143 (5) GPa, and K'_{T0}= 5.8 (7). The isothermal bulk modulus of our Al-bearing PhD is

much lower than K_{T0} = 166 (3) GPa Mg-PhD from Frost and Fei (1999) and K_{T0} = 168 (9) GPa from Hushur et al. (2011). The difference cannot be reconciled even if we fit our data by fixing K'_{T0} = 4.1 (3) as proposed by Frost and Fei (1999), which suggest a substantial effect of Al-incorporation on the bulk modulus of PhD. It is probably caused by the substitution $Al^{3+}+H^{+} = Si^{4+}$, since the increased water content makes the crystal structure softer, leading to the decrease of its bulk modulus. This result is well compatible with K_{T0}= 137 (3) GPa reported for (Fe, Al)-bearing PhD (Litasov et al., 2007) with their K'_{T0} = 6.3 (3) only slightly larger than our value.

The elastic parameters of Al-bearing PhD obtained in this study compared with some other DHMSs are plotted in Fig. 6 (Shieh et al., 2000; Crichton and Ross, 2002, 2002a; Inoue et al., 2006; Litasov et al., 2007, 2007a; Hushur et al., 2011; Rosa et al., 2013; Li et al., 2016). A wide range of isothermal bulk modulus and pressure derivative values are summarized from ~ 90 to 165 GPa for K_{T0} and from 4 to 7 for K'_{T0}. The bulk modulus of almost all DHMSs minerals from previous studies are smaller than those of nominal anhydrous minerals such as wadsleyite (K_{T0}= 172 GPa) from Li et al. (1998), ringwoodite (K_{T0}= 188 GPa) from Sinogeikin et al. (1998) and Mg-bridgmanite (K_{T0}= 253 GPa) from Fiquet et al. (2000), probably due to their large water content (e.g. low density). The thermoelastic parameters K_{T0}, K'_{T0}, $(\partial K_{T0}/\partial T)_P$, α_0. were determined by a least-square fitting of all the data up to 21.9 GPa and 1300 K to a high-temperature Birch-Murnaghan EoS, also using the EosFit program (Angel 2001). Due to limited data we chose to fix the zero-pressure value to V_0 = 86.71 Å^3, as given by the XRD pattern at room P, T conditions. The fitting yielded: K_{T0} = 143 (4) GPa, K'_{T0} = 5.8 (6), $(\partial K_{T0}/\partial T)_P$ = -0.027 (12) GPa/K^{-1}, and α_0 = 3.8 (4)$\times 10^{-5}$ K^{-1}, which are within uncertainties in very good agreement with the elastic parameters reported for Fe, Al-bearing PhD from Litasov et al. (2008) with K_{T0} = 140 (3) GPa, K'_{T0} = 6.6 (4),

$(\partial K_{T0}/\partial T)_P$ = -0.023 (8) GPa/K, and α_0 = 3.4 (2)$\times 10^{-5}$ K^{-1}, who used powder mixture as starting composition.

3.2 Sound velocity measurements

The compressional (V_P), shear (V_S) velocity and density of Al-phase D were measured up to ~21.88 GPa and 1300 K (Table 2). Both V_P and V_S increase with increasing pressure while they decrease with increasing temperature (Fig. 5 b and 5c). The shear and adiabatic bulk moduli of Al-bearing PhD were derived from the present velocities and the density data using the relations $G= \rho V_S^2$ and $K_S= \rho V_P^2$ -4G/3, respectively (Fig. 7). A 2D linear function of pressure and temperature was adopted to fit the longitudinal and shear moduli data and obtained the bulk and shear moduli K_{S0} and G_0 and their pressure and temperature derivatives (see results in Table 1). Because of the few datapoints at 1100 K and 1300 K, it is difficult to constrain the isotherm at these temperatures when fitting all the data simultaneously and therefore we chose to fit data up to 900 K. The results of fitting of all data at up to 900 K was then used to extrapolate values up to 1300 K, showing good consistency with our experimental data at 1100 K and 1300 K, for both K_S and G. It is worth noting that our adiabatic bulk modulus K_{S0} is only about 4 GPa larger than the isothermal bulk modulus K_{T0} derived from our density data, indicating a good consistency of the present measurements as $K_{T0} = K_{S0}/(1 + \alpha\gamma T)$, with the product of the thermal expansion α, the Grüneisen parameter γ and temperature T is ~zero at room temperature.

The elasticity of Al-bearing PhD was also investigated by fitting our velocity and density data to functions of the Eulerian finite-strain EOS, which is independent of any pressure scale (see Li and Liebermann, 2014). Because of limited data, the zero-pressure unit-cell volume was fixed to its experimental value V_0= 86.71 $Å^3$ while the thermal expansion α_0 = 3.8 (4)$\times 10^{-5}$ K^{-1} was fixed after the results of our high-T BM3 EoS fitting.

A least square fitting of all data simultaneously yielded the values of K_{S0},K'_S, $\partial K_S/\partial T$, G_0, G'_0 and $\partial G/\partial T$, which are summarized in Table 1. The values of K_{S0}, $\partial K_S/\partial T$ G_0 and $\partial G/\partial T$ from finite strain results are within uncertainties in good agreement with those derived from the 2D linear fitting while K'_S and G' are slightly smaller, which can be explained by the small pressure range (Δ P = 7 GPa) used when fitting the data by a 2D linear function.

4 Implications

Several studies have proposed that water can be transported into the MTZ by cold subduction slabs, and some of slabs even penetrate into the lower mantle (Fukao et al., 2001; Maruyama and Okamoto, 2007; Fukao and Obayashi, 2013; Liu et al., 2016). Hydrous phases are only stable at high pressure and low temperature conditions, and therefore it is generally considered that they decompose and release water in the MTZ, when the slab equilibrates thermally with the surrounding mantle. However, recent studies demonstrated that Al-bearing PhD could crystallize and remain stable in a hot slab environment, due to the incorporation of Al, which has been shown to significantly increase the pressure and temperature stability region of PhD (Ghosh and Schmidt, 2014; Pamato et al. 2015). It is also proposed that Al-bearing PhD could crystallize when hydrous melt formed upon dehydration of water saturated ultramafic rocks comes into contact with the Al-rich mafic crustal rocks (Pamato et al., 2015). Nevertheless, Al-bearing PhD is potentially an important hydrous mineral of the subducted slab at the bottom of the MTZ (Ohira et al., 2014).

Figure 8 shows estimates of V_P, V_S and density of Al-bearing PhD compared to those of other major phases in the MTZ and uppermost lower mantle at 300 K. Generally hydrous phases have lower density than those of nominally anhydrous minerals as shown in Fig. 8c. Our results show that V_P of Al-bearing PhD is about 0.7% lower than $MgSiO_4$ ringwoodite (Rw). However, former studies showed that velocities of Rw decrease when it incorporates

FeO and H_2O, leading to V_P of Al-bearing PhD ~2.8%-3.1% higher than iron-bearing Rw ($Mg_{1.82}Fe_{0.18}SiO_4$) and 4.1%-4.3% higher than that of hydrous iron-bearing Rw ($Mg_{1.633}Fe_{0.257}SiH_{0.179}O_4$ with 1.1wt % H_2O) (Higo et al., 2008; Mao et al., 2012). V_S of Al-bearing PhD is found ~2.1%-2.5% than pure Mg_2SiO_4 Rw, with the difference increasing with increasing FeO (6.8%-8.1% higher than iron-bearing Rw) and FeO and H_2O (8.6%-9.6% higher than hydrous iron-bearing Rw), respectively. In the lower mantle, our estimates show that V_P and V_S of Al-bearing PhD are 6.4%-7.5% and 6.6%-7.6% lower than those of bridgmanite (Brg), respectively, but 4.5%-4.6% and 2.2%-4.6% higher than those of ferropericlase (Fp), the two most abundant minerals in the lower mantle.

We used the elastic properties of Al-bearing PhD along with major minerals shown in Fig. 8 to further model velocities and density of dry pyrolite and hydrous pyrolite along a normal mantle geotherm, assuming phase D is the only hydrous phase and its fraction represents 5%, 10% and 20% of the hydrous pyrolite models (Fig. 9a and 9b), respectively. Velocities and density of 1D seismological models PREM and AK135 were also shown for comparison. One of the modal compositions of mineral assemblages (mol%) used to calculate the velocity and density was shown as example in Fig.9c. Here we adopted an average mantle geotherm instead of cold or hot slab geotherm as Al-rich PhD is one of the few hydrous phases who remains stable at mantle geotherm on top layer of the subducting slab, as argued by Pamato et al. (2015). In Fig.9a, we found that V_P and V_S of hydrous pyrolite models are generally higher than dry pyrolite in between depths of ~450 km and 660 km. Although those results suggest that partial hydration of the mantle through the formation of Al-bearing PhD could explain increase of velocities in the MTZ, it also show that accumulation of Al-bearing PhD, even with a large molar fraction of 20%, only slightly increases compressional (+0.3%) and shear velocities (+0.5%), which is insufficient to explain high-velocity scatterings (about +1% V_P, +2% V_S) observed in some regions such as Kuriles and Japan subduction zones (Hirahara 1980; Fumiko and Stephen, 1995; Li et al., 2010). These results therefore imply

that layers of hydrated pyrolite with a more realistic composition (~5-10 mol% Al-bearing PhD), which could form in between the slab and mantle (Pamato et al., 2015), are likely to be seismically invisible at the depths of the lowermost MTZ (~520-660 km).

Due to the stability of Al-bearing PhD at high P and T, it has been speculated that this phase could be transported to the uppermost lower mantle as the slab descend into the lower mantle (Frost 1999). In this scenario, V_P, V_S and density of hydrous pyrolite models are found substantially lower than those of dry pyrolite, suggesting that if such hydrated layers were to be delivered to the uppermost lower mantle by the subducted slab, they would contribute to the buoyancy of the slab and the low velocity profiles in between depths of 660 km to 800 km beneath subduction regions. The velocities of the hydrous models are however higher than those of MORB (Fig. 9a), although a velocity crosses over with MORB was obtained deeper than ~800 km depth. This is more likely to explain globally the magnitude of the shear velocity reduction in between depths of 660 km to 800 km, provided that the surrounding mantle has pyrolite composition (Gréaux et al., 2019). The presence of hydrated components in the subducted slab could therefore be characterized locally by higher velocities within the slab region or lower velocities in portions of the mantle surrounding the stagnating slab. Therefore, we estimated that the observed velocity anomalies at uppermost lower mantle may be considered as evidence for the presence water in subduction zone. Further works are expected to classify the mineral assemblages in hydrous pyrolite at uppermost lower mantle, which can offer quantitative analysis to the observed velocity anomalies.

This new hypothesis is however difficult to reconcile with the partial-melting model as the crystallization of Al-bearing PhD in the MTZ would inhibit release of water upon decomposition of hydrous ringwoodite and thus decrease the occurrences of dehydration melt beneath depth of 660 km. It should also be noted that superhydrous phase B (SuB), another important DHMS phase, which is stable at the MTZ and the uppermost lower mantle was also shown to have low velocities in these regions (Li et al., 2016; Yang et al., 2017) and

therefore if present, would also contribute to reduce the occurrences of partial melting in the uppermost lower mantle similarly to Al-bearing PhD.

Although the proportions of Al-bearing PhD are less compared with those of major minerals in the deep earth, it may act as important water carrier in the subducted oceanic crust. Because it has low density compared with other mineral phases of the MTZ and lower mantle (Fig. 9b), the existence of Al-bearing PhD would contribute to regime of positively buoyant slab if present in the slab. It also should be noted that PhD could contain a certain amount of Fe (Litasov et al., 2007), which would make PhD even denser and therefore able sink to deeper region of the uppermost lower mantle where it may further transforms to phase H ($MgSiH_2O_4$) at ~44 GPa (Nishi et al., 2014). Because of the high water content of Al-bearing PhD and the debatable ability of Al-bearing bridgmanite to accommodate H_2O, there is a possibility for free water to be released at these depths, which could in turn promote partial melting with some possible implications for the discontinuities recently observed at depths below 800 km (Liu et al., 2016)

Tables in chapter 8

Table 1. Thermoelastic parameters of Al-bearing PhD obtained by fitting different types of EoS

phase	*P/T conditions*	V_0 (Å^3)	K_{S0}/K_0 (GPa)	K'_S/K'_T	$\partial K_S/\partial T$ (GPa.K^{-1})	G_0 (GPa)	$\partial G/\partial P$	$\partial G/\partial T$ (GPa.K^{-1})	a_0 (10^{-5}.K^{-1})	b_0 (10^{-8}.K^{-2})
Birch-Murnaghan EoS (Gold P-scale, Tsuchiya 2003)										
Al-PhD	0-21 GPa/300 K	86.71*	143(4)	5.8(7)	-	-	-	-	-	-
Al-PhD	0-23 GPa/300-900 K	86.71*	143*	5.85(4)	-0.023(6)	-	-	-	3.5(3)	0.9(5)
Al-PhD	0-23 GPa/300-900 K	86.71*	142(3)	6.0(5)	-0.036(1)	-	-	-	3.6(4)	1.0(6)
2D linear (Gold P-scale, Tsuchiya 2003)										
Al-PhD	0-21 GPa/300 K	-	148(2)	4.7(1)	-	107(2)	2.0(1)	-	-	-
Al-PhD[a]	0-23 GPa/300-900 K	-	147(2)	4.7(1)	-0.023(1)	107(3)	2.1(2)	-0.031(1)	-	-
Finite strain EoS (P-scale free)										
Al-PhD	0-21 GPa/300 K	86.71*	144(5)	5.5(5)	-	106(3)	2.4(1)	-	-	-
Al-PhD	0-23 GPa/300-900 K	86.71*	144*	5.5*	-0.023(1)	106*	2.4*	-0.030(1)	3.5*	0.9*
Al-PhD	0-23 GPa/300-900 K	86.71*	144*	5.55(7)	-0.024(1)	106*	2.45(4)	-0.032(2)	3.5*	0.9*
Al-PhD	0-23 GPa/300-900 K	86.71*	134(7)	6.6(7)	-0.024(1)	109(4)	2.4(2)	-0.030(2)	3.5*	0.9*

*, the value was fixed when calculating

Table 2. Experimental pressure and temperature, longitudinal and shear velocities, and density of Al-phase D.

P* (GPa),** ***Au scale*	***e*(P)**	***P*(GPa),** ***Finite Strain***	***T*(K)**	V_P**(km/s)**	***e*(**V_P**)**	V_S**(km/s)**	***e*(Vs)**	ρ**(g/cm^3)***	***e*(**ρ**)**
0	0	-	300	-	-	-	-	3.217	0.001
14.2	0.0	14.3	300	10.67	0.04	6.25	0.03	3.484	0.001
15.4	0.0	15.1	300	10.76	0.03	6.30	0.03	3.497	0.001
16.9	0.1	16.6	300	10.88	0.03	6.35	0.03	3.521	0.001
18.0	0.1	17.8	300	10.94	0.03	6.37	0.03	3.538	0.001
19.1	0.1	19.0	300	11.01	0.04	6.40	0.03	3.556	0.001
20.5	0.0	20.3	300	11.11	0.05	6.44	0.05	3.576	0.001
14.9	0.1	14.7	500	10.59	0.04	6.17	0.04	3.473	0.001
16.8	0.0	16.5	500	10.72	0.03	6.24	0.02	3.502	0.001
18.0	0.1	17.7	500	10.81	0.03	6.29	0.03	3.520	0.001
18.5	0.1	18.2	500	10.84	0.04	6.29	0.03	3.527	0.001
19.7	0.0	19.4	500	10.94	0.04	6.33	0.03	3.546	0.001
20.8	0.1	20.3	500	11.03	0.05	6.36	0.05	3.558	0.001
15.4	0.0	14.9	700	10.46	0.04	6.04	0.04	3.459	0.001
16.6	0.0	16.3	700	10.64	0.03	6.14	0.02	3.481	0.001
17.8	0.1	17.5	700	10.71	0.03	6.18	0.03	3.500	0.001
19.2	0.1	18.5	700	10.79	0.03	6.21	0.03	3.517	0.001
20.4	0.0	19.9	700	10.85	0.03	6.23	0.03	3.537	0.001
21.3	0.1	20.8	700	10.96	0.05	6.28	0.05	3.551	0.001
16.1	0.1	15.4	900	10.34	0.04	5.90	0.04	3.451	0.001
17.6	0.0	17.0	900	10.50	0.03	5.99	0.02	3.477	0.001
18.8	0.1	18.0	900	10.60	0.03	6.04	0.03	3.492	0.001
20.0	0.1	19.2	900	10.68	0.03	6.08	0.03	3.511	0.001
21.0	0.1	20.2	900	10.75	0.04	6.11	0.03	3.526	0.001

22.2	0.0	21.4	900	10.85	0.05	6.15	0.05	3.544	0.001
22.7	0.1	21.4	1100	10.69	0.05	5.95	0.05	3.530	0.001
21.9	0.1	20.5	1300	10.42	0.05	5.80	0.04	3.503	0.001

*. Tsuchiya 2003

Figures in chapter 8

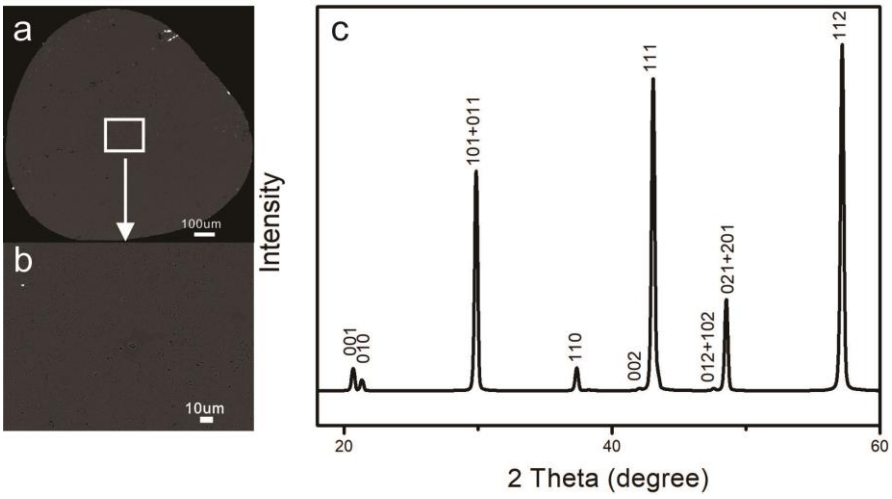

Figure 1. Back scattered electron image and x-ray diffraction pattern of synthesized sample. **a** and **b**, A well sintered Al-bearing PhD with small grain size, little porosity and free of accessory phase. **c**, XRD also shows we obtained a pure phase after 1 h of heating at 24 GPa and 1,373 K.

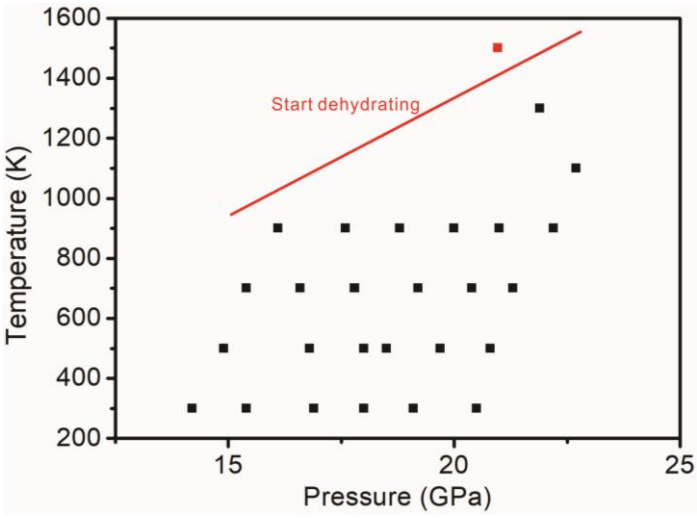

Figure 2. Pressure and temperature conditions of sound velocity measurement conducted within the stability field of Al-bearing PhD. Red line roughly shows stability limit of Al-bearing PhD based on present in-situ observation and melting experiment of Al-rich PhD by Liu et al. (2018). We observed dehydration of Al-bearing PhD at *P*-*T* condition where red square locates. Therefore, the data below the red line are used for current analysis.

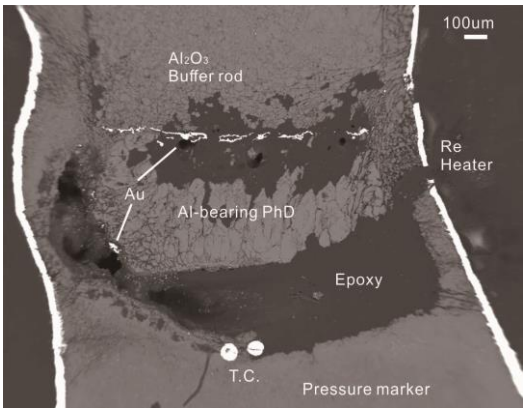

Figure 3. Backscattered-electron image of the experimental cell recovered after the ultrasonic experiment.

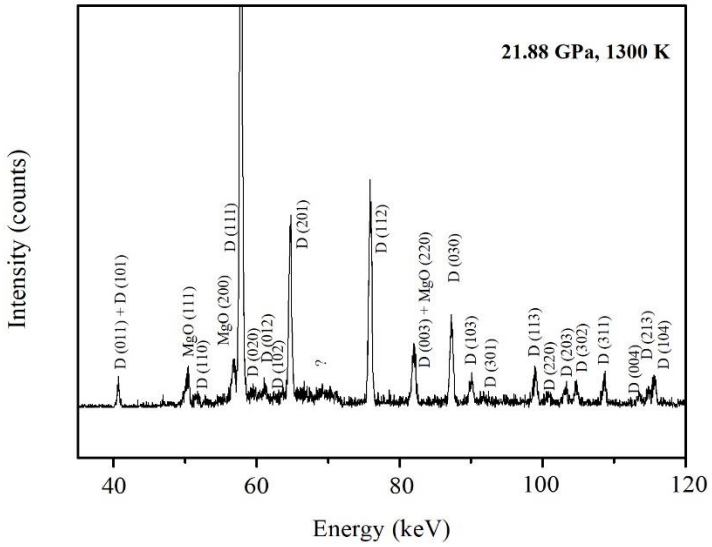

Figure 4. XRD obtained before the sample partially dehydrated in the last heating cycle of this experiment.

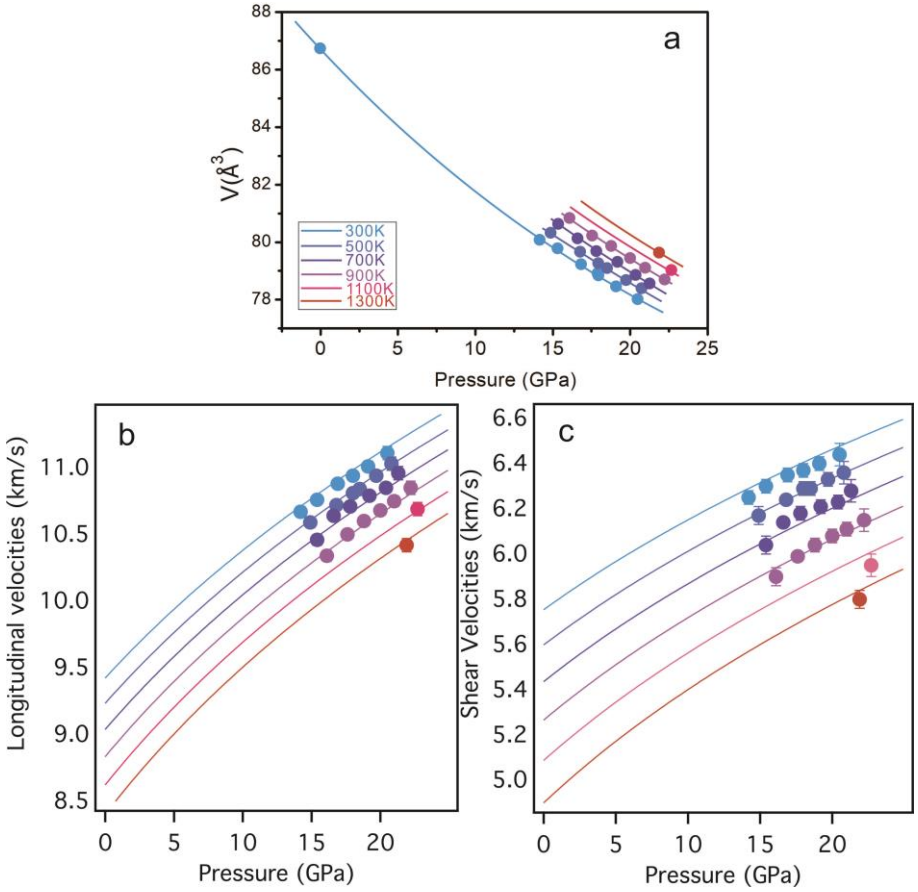

Figure 5. Volume, longitudinal and shear sound velocities of Al-bearing PhD changes with pressure and temperature.

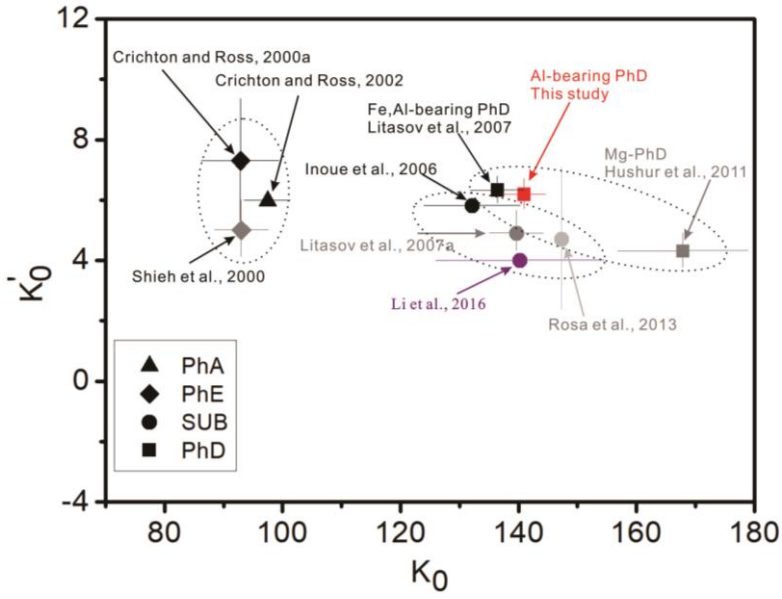

Figure 6. A comparison of isothermal bulk moduli and their pressure derivatives of different hydrous minerals in DHMSs.

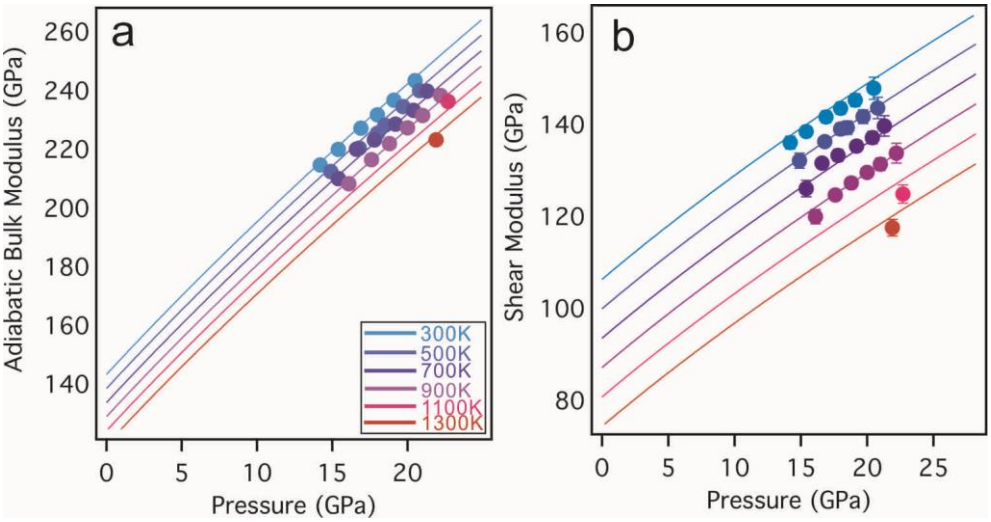

Figure 7. Bulk and shear moduli of Al-bearing PhD at various temperatures.

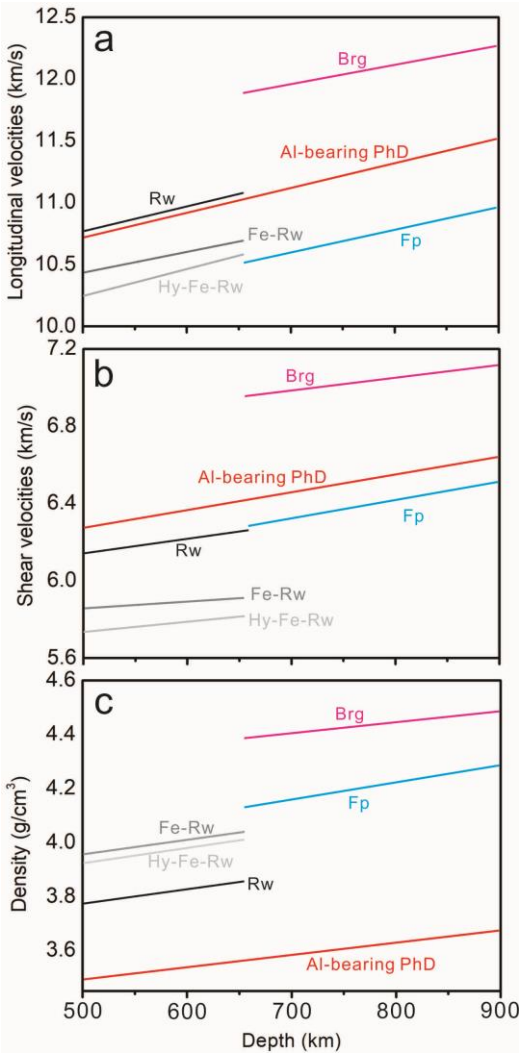

Figure 8. Longitudinal wave (*V*p), shear wave (*V*s), density and *V*p/*V*s of Al-bearing PhD compared to those of different models. The value in **a**, **b** and **c** are calculated at room temperature. Brg: (Fiquet et al., 1998); Fp: (Jackson et al., 2006); Rw: (Li 2003); Fe-bearing Rw: (Higo et al., 2008) and hydrous Fe-bearing Rw: (Mao et al., 2012).

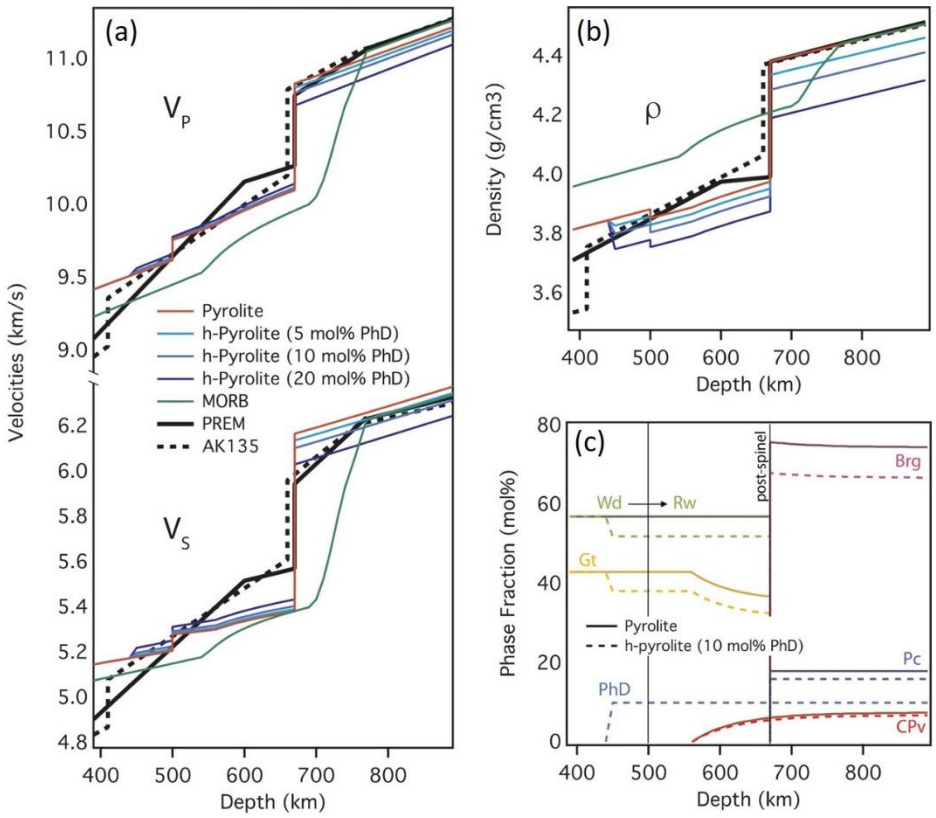

Figure 9. a and **b**, Comparison of sound velocities and densities of hydrous pyrolite with representative seismological models in and below the MTZ depth, calculated along a normal mantle geotherm, assuming phase D is the only hydrous phase in hydrous pyrolite model. **c**, The modal compositions of mineral assemblages (mol%) for dry pyrolite and hydrous pyrolite (with 10 mol% Al-bearing PhD) used to calculate the velocity and density were shown as examples. Black dashed line: AK135 (Kennettetal., 1995); black line: PREM (Dziewonski and Anderson, 1981); green line: MORB (Hirose and Fei, 2002).

Chapter 9

Discussion and conclusions

In current studies, we systematically investigate the effect of both Al and Fe on the stability region of DHMSs, and finally we measured the physical property of Al-bearing PhD.

1. Stability of DHMSs in Al-bearing system

A series of dense hydrous magnesium silicate phases (DHMSs) have been suggested as potential water carriers to transition zone and even to the lower mantle under the conditions present in the cold subducting slabs. However, these DHMSs seems to be stable in very cold subducting slabs only in MgO-SiO_2-H_2O (MSH) system. Recently, Al-bearing PhD was shown to remain stable up to 1600 ℃ at 24 GPa when only incorporating 1wt% Al_2O_3 (Ghosh and Schmidt, 2014) and end member Al-rich PhD was stable at temperatures up to 2000 ℃ at 26 GPa (Pamato et al., 2015). Both studies indicated Al increases stability regions of DHMSs.

First, we systematically investigate the effect of Al on the stability region of DHMSs, we conducted high-temperature and high-pressure experiments using natural chlorite. We found that Al-bearing PhE, SUB and PhD were observed with *P-T* increasing. Following the *P-T* path of cold subduction, the phase assemblage PhE + PhD was stable at 14-23 GPa, and even a trace of PhE was identified at 900 ℃ and 25 GPa coexisting with PhD. The phase SUB was stable between 16 and 22 GPa coexisting with PhE + PhD. Following the *P-T* path of hot subduction, the phase assemblage PhE + Gt was observed at 14-18 GPa coexisting with melt. The phase assemblage SUB + PhD was stable at 18-25 GPa, which was expected to survive at higher *P-T* condition. Some amount of SUB was even stable at normal mantle geotherm at transition zone pressure. Compared with Mg-DHMSs, the incorporated Al hugely increased the themal stability region of DHMSs, it is about 200 ℃ higher than the Mg-end member phases. It is obvious that Al enhanced the stability region of DHMSs. Those Al-bearing DHMS remained stable along hot subduction, and some of them even survived in

normal mantle geotherm condition.

The Al substitution mechanism in DHMSs were analyzed by using cell check method shown in chapter 2 based on chemical composition of SUB, PhE, and PhD. Studies have shown Al prefer to distribute in DHMSs than coexisting phases (Bolfan-Casanova et al., 2003; Litasov et al., 2005; Ghosh and Schmidt, 2014; Ohira et al., 2014). Therefore, Al-bearing PhD should have a large thermal stability region than previously thought due to its high Al content, which suggests much water can be transported into lower mantle in subducting slab.

PhD is believed to be the main storage site for water in uppermost lower mantle (Nishi et al., 2014), and could exist around 45 GPa along cold subduction (Nishi et al., 2014; Ohtani et al., 2014). Therefore, we further investigated the stability of the Al-rich dense hydrous magnesium silicate PhD in MgO-Al_2O_3-SiO_2-H_2O (MASH) system. Previous result has shown that a little trace of A_2O_3 (1%) would increase the stability of PhD (Ghosh et al., 2014). Here, we clearly see that stability of Al-rich PhD shifts to higher temperatures and water content drastically increases ($Si^{4+} = Al^{3+} + H^{+}$). We also noticed that Al-rich PhD has positive Clapeyron slope (dP/dT) of the phase boundary in the present study, which means the decomposition temperature increases with increasing pressure. Recently, Liu et al. (2019) reported the stability of Al-rich PhD with MORB bulk composition along cold subducting slab. They found that Al-rich PhD (7.5 – 22.6 wt% Al_2O_3) was only stable within 18 – 23 GPa and cold subducting environment ($\leqslant$1000 ℃), which further transformed to Al-rich PhH at elevated pressure. Unfortunately, they didn't check the stability limit of these two phases at higher temperatures. Combined their result with the present study, at least we may infer that both in cold and hot subduction zones, the hydrous mafic oceanic crust would bring a certain amount of water into the mantle transition zone and the lower mantle.

2. Stability of PhD in (Fe, Al)-bearing system

Fe is an abundant and important element in both pyrolite and MORB composition (Irifune and Ringwood, 1987), may greatly change stability and water solubility of PhD. Ghosh and Schmidt (2014) argued that PhD almost had same stability region in both FeO-MgO-Al_2O_3-SiO_2-H_2O (FMASH) and MSH system, but lower than that of MASH system between 22-24 GP, while Ganskow and Langenhorst (2014) found that Fe increased stability of PhD in FMASH system compared with MSH system between 18-23 GPa, which even stabilized up to 1450 ℃ at 20.5 GPa. We investigated the effect of Fe on the stability of PhD in both FeOOH-PhD binary and AlOOH-FeOOH-PhD ternary system at pressures between 18-25 GPa and temperatures between 1000-1600 ℃. We observed that iron slightly decreased the stability region of PhD in FeOOH-PhD system compared with Mg-PhD, however, (Fe, Al)-bearing PhD drastically shift to higher temperatures in both MORB and pyrolite type compositions compared to pure Mg-PhD. Therefore, (Fe, Al)-bearing PhD could act as long water reservoir along subduction to the deep lower mantle. Our results suggest that $CaCl_2$-type hydroxides subducted in to the deep mantle form a solid solution over a wide composition ranges.

At the same time, we ascertained the solubility behavior of δ-AlOOH - ε-FeOOH at high pressures. We observed solid solutions were formed in δ-AlOOH - ε−FeOOH binary systems in large compositional ranges based on XRD patterns. Our results demonstrated that a binary eutectic diagram is formed without dehydration or melting below 1200 ℃ at 20 GPa. We also observe that maximum solubilities of Al and Fe in the solid solutions were more strongly influenced by temperature than by pressure.

Furthermore, we also determined phase relations in iron-rich MAFSH system up to 21 GPa whose composition is analog of the primitive Martian mantle composition corresponding to mantle +crust. We noticed that PhD in MAFSH system has the same

stability region as in MASH system (Ohtani et al., 2004). PhE is observed in the low-temperature region between 15-16.5 GPa to coexist with garnet and wadsleyite or ringwoodite. PhD remains as a major hydrous phase at present pressure range from18 GPa to 21 GPa below 1100 ℃. With increased temperature, PhD decomposed to ringwoodite, stishovite and garnet. Thererfore, Phase E and phase D potentially are relevant DHMSs in the Martain tranzition zone in simplified MAFSH model. The DHMSs will completely dehydrate if the temperature of surrounding Martian mantle is higher than their stability limit. The released water will be stored in wadsleyite or ringwoodite.

3. Al partitioning between phase D and bridgmanite up to 31 GPa

Our result shows that Al is strongly partitioned into PhD than coexisting Brg, and partition coefficient of Al (K_D) between PhD and Brg slightly decreases with increasing temperature. Although Al increases the stability region of PhD as shown in chapter 3 and chapter 6. Recent results shown that a trace amount of Al_2O_3 increases thermal stability of PhD up to 1600 ℃ at 24 GPa (Ghosh and Schmidt, 2014), and Al-rich PhD could stabilize up to 2000 ℃ at 26 GPa (Pamato et al., 2015) However, we found Al-bearing PhD totally decomposes around 28 GPa and 1350 ℃, in which Brg is found to be coexisting with a large amount of melt. At 31 GPa and 1350°C, Brg coexists with a trace amount of δ-AlOOH phase. The decomposition of Al-bearing PhD around 28 GPa may be the second chock point for hydrous minerals and help to explain some observed velocity and high electrical conductivity anomalies at bottom of mantle transizition zone.

4. Elastic property of Al-bearing PhD

The isothermal bulk modulus of Al-bearing PhD obtained in this study are smaller than those of nominal anhydrous minerals such as wadsleyite, ringwoodite and and Mg-brg,

however, is within uncertainties in very good agreement with the elastic parameters reported for (Fe, Al)-bearing PhD from Litasov et al. (2008). The obtained elastic parameters of K_{S0}, $\partial K_S/\partial T$ G_0 and $\partial G/\partial T$ from finite strain results are within uncertainties in good agreement with those derived from the 2D linear fitting.

By using these parameters, we further modeled velocities of Al-bearing PhD at room temperature. We noticed that velocities of Al-bearing PhD are lower than bridgmanite, but similar or higher compared with other major minerals in transition zone and lower mantle. Modeled velocities of Al-bearing PhD along slab geotherms show it will generate positive velocity anomalies in transition zone, however, once Al-bearing PhD is transported to the lower mantle, it may become seismically invisible. Due to the lower density, the existence of Al-bearing PhD helps to generate a positively regime of buoyant slab if present in abundance in the subducting slab.

5. Futher work

In current studies, we systematically investigated the effect of Al of stability region of DHMSs only up to 25 GPa, however, the pressure higher than 25 GPa is particular need to ascertain the phase relations in hydrous system. Because of the phase assemblages are important to interpret seismic anomalies related to the presence of hydrated regions at the bottom of the MTZ.

SUB, as one of DHMSs, has been proposed to be main water carrier at bottom of mantle transition zone (MTZ) and uppermost lower mantle in the subduction slabs among the various hydrous minerals. Although the abundance of SuB in subdcuting slab is remain unknown, it may generate the observed low-velocity zone at uppermost lower mantle. Therefore, the velocity-density data for SuB is crucial to illustrate seismic discontinuities associated with the hydrated regions at the bottom of the MTZ. So far, the pressure and temperature

dependencies of acoustic velocities of SUB is unknown, because ultrasonic measurement needs well sintered samples with high purity, which is difficult to synthesize and therefore such data were not available.

References

Ai, Y., Zheng, T., Xu, W., He, Y., & Dong, D. (2003). A complex 660 km discontinuity beneath northeast china. *Earth and Planetary Science Letters, 212*(1–2), 0–71.

Anderson, D. L. (1975). On the composition of the lunar interior. *Journal of Geophysical Research, 80*.

Angel, R. J. (2001). Equations of State, *reviews in mineralogy and geochemistry, 41*, 35-59.

Baker, V.R. (2001). Water and the Martian landscape. *Nature, 412*, 228–236.

Ballaran, T. B., Frost, D. J., Miyajima, N., & Heidelbach, F. (2010). The structure of a super-aluminous version of the dense hydrous-magnesium silicate phase d. *American Mineralogist, 95*(7), 1113–1116.

Bertka, C. M., & Fei, Y. M. Mineralogy of Martian interior up to core-mantle boundary pressures. J. Geophys. Res. 1997, 102, 5251–5264.

Bindi, L., Nishi, M., & Irifune, T. (2015). Partition of al between phase D and phase H at high pressure: results from a simultaneous structure refinement of the two phases coexisting in a unique grain. *American Mineralogist, 100*(7), 1637–1640.

Bindi, L., Nishi, M., Tsuchiya, J., & Irifune, T. (2014) Crystal chemistry of dense hydrous magnesium silicates: The structure of phase H, $MgSiH_2O_4$, synthesized at 45 GPa and 1000 ℃. *American Mineralogist, 99*, 1802–1805.

Blasio, F., & Martino, S. (2017). The Acheron Dorsum on Mars: A novel interpretation of its linear depressions and a model for its evolution. *Earth and Planetary Science Letters, 465*, 92–102.

Bolfan-Casanova, N., Keppler, H., & Rubie, D. C. (2000). Partitioning of water between mantle phases in the system $MgO\text{-}SiO_2\text{-}H_2O$ up to 24 GPa: Implications for the

distribution of water in the Earth's mantle. *Earth and Planetary Science Letters*, *182(3–4)*, 209–221.

Bolfan-Casanova, N., Keppler, H., & Rubie, D. C. (2003). Water partitioning at 660 km depth and evidence for very low water solubility in magnesium silicate perovskite. *Geophysical Research Letters*, *30(17)*, 169–172.

Brown, J. M., & Shankland, T. J. (2007). Thermodynamic parameters in the Earth as determined from seismic profiles. *Geophysical Journal International*, *66*(3), 579–596.

Byrne, S., Dundas, C. & Kennedy, M. (2009). Distribution of mid-latitude ground ice on Mars from new impact craters, *Science, 325*, 1674–1676.

Cardenas et al. (2018). Fluvial stratigraphy of valley fills at Aeolis Dorsa, Mars: Evidence for base-level fluctuations controlled by a downstream water body. *Geological Society of America Bulletin, 130*, 484–498.

Cannat, M., Mevel, C., Maia, M., Deplus, C., Durand, C., Genre, P., Agriniet, P., Belarouchi, A., Dubuisson, G., Humlet, E., & Reynolds, J. (1995). Thin crust, ultramafic exposures, and rugged faulting patterns at the Mid-Atlantic Ridge (22^{o}-24^{o}N), *Geology*, *23*, 49-52.

Chan et al. (2018). New Evidence of an Ancient Martian Ocean From the Global Distribution of Valley Networks. *Journal of Geophysical Research: Planets, 123*, 2138–2150.

Chen, L., & Ai, Y. (2009). Discontinuity structure of the mantle transition zone beneath the north china craton from receiver function migration. *Journal of Geophysical Research: Solid Earth, 114*(B6).

Conway, S. J., Balme, M. R., Kreslavsky, M. A., Murray, J. B., & Towner, M. C. (2016). The comparison of topographic long profiles of gullies on Earth to gullies on Mars: a signal of water on Mars. *Icarus, 253*, 189–204.

Crichton, W. A., & Ross, N. L. (2002). Equation of state of dense hydrous magnesium silicate phase A, $Mg_7Si_2O_8(OH)_6$. *American Mineralogist, 87*(2), 333-338.

Crichton, W. A., & Ross, N. L. (2000a). Single-crystal equation of state measurements on Mg end members of the B-group minerals, *In Science and Technology of High Pressure*, edited by Manghnani, M. N., Nellis,W. J., & Nicol, M. F. *pp. 587-590*, Hyderabad, India.

Dohm, J. M., Maruyama, S., Kido, M., & Baker, V. R. (2015). A possible anorthositic continent of early mars and the role of planetary size for the inception of earth-like life. *Geoscice Frontier, 6*, 95–101.

Dreibus, G., & Wänke, H. (1987). Mars, a volatile-rich planet. *Icarus, 71*, 225–240.

Dziewonski, A. M., & Anderson, D. L. (1981). Preliminary reference Earth model, *Physics of the Earth and Planetary Interiors*, *25*, 297–356.

Fei, H., Yamazaki, D., Sakurai, M., Miyajima, N., & Yamamoto, T. (2017). A nearly water-saturated mantle transition zone inferred from mineral viscosity. *Science Advances, 3*(6).

Fiquet, G., Dewaele, A., Andrault, D., Kunz, M., & Bihan, T. L. (2000). Thermoelastic properties and crystal structure of $MgSiO_3$ perovskite at lower mantle pressure and temperature conditions. *Geophysical Research Letters, 27*, 21–24.

Frohlich, C. (2003). The nature of deep-focus earthquakes. *Annual Review of Earth and Planetary Sciences, 17*(1), 227–254.

Frost, D. J. (1999). The stability of dense hydrous magnesium silicates in Earth's transition zone and lower mantle. In Mantle Petrology: Field Observations and High Pressure Experimentation: A Tribute to Francis R. (Joe) Boyd. *The Geochemical Society*, pp. 283–296.

Frost, D. J., & Fei, Y. (1998). Stability of phase D at high pressure and high temperature. *Journal of Geophysical Research Solid Earth, 103*(B4), 7463–7474.

Frost, D. J., & Fei, Y. (1999). Static compression of the hydrous magnesium silicate phase d to 30 GPa at room temperature. *Physics and Chemistry of Minerals, 26*(5), 415–418.

Fukao, Y., & Obayashi, M. (2013). Subducted slabs stagnant above, penetrating through, and trapped below the 660 km discontinuity. *Journal of Geophysical Research: Solid Earth*, *118*(11), 5920–5938.

Fukao, Y., Widiyantoro, S., & Obayashi, M. (2001). Stagnant slabs in the upper and lower mantle transition region. *Reviews of Geophysics*, *39*(3), 291.

Fukuyama, K., Ohtani, E., Shibazaki, Y., Kagi, H., & Suzuki, A. (2017). Stability field of phase egg, $AlSiO_3OH$ at high pressure and high temperature: possible water reservoir in mantle transition zone. *Journal of Mineralogical and Petrological Sciences*, *112*(1), 31–35.

Fumagalli, P., Poli, S. (2005). Experimentally Determined Phase Relations in Hydrous Peridotites to 6.5 GPa and their Consequences on the Dynamics of Subduction Zones. *Journal of Petroleum Science and Engineering*, *46*, 555–578.

Ganskow, G., & Langenhorst, F. (2014). Stability and crystal chemistry of iron-bearing dense hydrous magnesium silicates. *Chemie der Erde - Geochemistry*, *74*(3), 489–496.

Gasparik, T. (1993). The role of volatiles in the transition zone. *Journal of Geophysical Research: Solid Earth*, *98*(B3).

Gréaux S., et al. (2019). Sound velocity of $CaSiO_3$ perovskite suggests the presence of basaltic crust in the Earth's lower mantle, *Nature*, *565*, 218–221.

Ghosh, S., & Schmidt, M. W. (2014). Melting of phase D in the lower mantle and implications for recycling and storage of H_2O in the deep mantle. *Geochimica et Cosmochimica Acta*, *145*, 72–88.

Hazen, R. M., Yang, H., Prewitt, C. T., & Gasparik, T. (1997). Crystal chemistry of superfluorous phase b ($Mg_{10}Si_3O_{14}F_4$): Implications for the role of fluorine in the mantle. *American Mineralogist*, *82*(5-6), 647–650.

Higo, Y., Inoue, T., Irifune, T., Funakoshi, K. I., & Li, B. (2008). Elastic wave velocities of $(Mg_{0.91}Fe_{0.09})_2SiO_4$ ringwoodite under *P-T* conditions of the mantle transition region. *Physics of the Earth and Planetary Interiors, 166*(3), 167–174.

Hu, Q., Kim, D., and Yang, W. et al. (2016). FeO_2 and FeOOH under deep lower-mantle conditions and Earth's oxygen-hydrogen cycles. *Nature, 534*, 241–244.

Hushur, A., Manghnani, M. H., Smyth, J. R., Williams, Q., Hellebrand, E., & Lonappan, D., et al. (2011). Hydrogen bond symmetrization and equation of state of phase d. *Journal of Geophysical Research Solid Earth, 116*(B6), 177–8.

Inoue, T. (1994). Effect of water on melting phase relations and melt composition in the system Mg_2SiO_4-$MgSiO_3$-H_2O up to 15 GPa. *Physics of the Earth & Planetary Interiors, 85*(3–4), 0–263.

Inoue, T., Ueda, T., Higo, Y., Yamada, A., Irifune, T., & Funakoshi, K. (2006). High pressure and high temperature stability and the equation of state of superhydrous phase B, *in Earth's Deep Water Cycle*, edited by S. D. Jacobsen, S. Lee, pp. 147-157, AGU, Washington, D. C.

Inoue, T., Ueda, T., Tanimoto, Y., Yamada, A., & Irifune, T. (2010). The effect of water on the high-pressure phase boundaries in the system Mg2SiO4-Fe2SiO4. International Conference on High Pressure Science and Technology,; Joint Airapt-22 and Hpcj-50. 215, 012101.

Inoue, T., Yurimoto, H., Kudoh, Y. (1995) Hydrous modified spinel, $Mg_{1.75}SiH_{0.5}O_4$: a new water reservoir in the mantle transition region. *Geophysical Research Letters,* 22, 117–120.

Inoue, T., Weidner, D. J., Northrup, P. A., & Parise, J. B. (1998). Elastic properties of hydrous ringwoodite (γ-phase) in Mg_2SiO_4. *Earth and Planetary Science Letters, 160*(1), 107–113.

Irifune, T. (1994). Absence of an aluminous phase in the upper part of the Earth's lower, mantle. *Nature, 370*(6485), 131–133.

Irifune, T., Kubo, N., Isshiki, M., & Yamasaki, Y. (1998). Phase transformations in serpentine and transportation of water into the lower mantle. *Geophysical Research Letters, 25*(2), 203–206.

Ivanov, M., Erkeling, G., Hiesinger, H., Bernhardt, H., & Reiss, D. (2017). Topography of the deuteronilus contact on mars: evidence for an ancient water/mud ocean and long-wavelength topographic readjustments. *Planetary and Space Science, 144*, 49–70.

Kakizawa, S., Inoue, T., Suenami, H., & Kikegawa, T. (2015). Decarbonation and melting in $MgCO_3$-SiO_2 system at high temperature and high pressure. *Journal of Mineralogical and Petrological Sciences, 110*(4), 179–188.

Kaneshima, S. (2009). Seismic scatterers at the shallowest lower mantle beneath subducted slabs. *Earth and Planetary Science Letters, 286*(1-2), 0–315.

Kanzaki, M. (1991). Stabillity of hydrous magnesium silicates in the mantle transition zone. *Physics of the Earth and Planetary Interiors, 66*(3–4), 307–312.

Karato, S. I. (2011). Water distribution across the mantle transition zone and its implications for global material circulation. *Earth and Planetary Science Letters, 301*(3–4), 0–423.

Kawamoto, T. (2004). Hydrous phase stability and partial melt chemistry in H_2O-saturated KLB-1 peridotite up to the uppermost lower mantle conditions. *Physics of the Earth and Planetary Interiors, 143–144*, 387–395.

Kawamoto, T., Hervig, R. L., & Holloway, J. R. (1996). Experimental evidence for a hydrous transition zone in the early earth's mantle. *Earth and Planetary Science Letters, 142*(3), 587–592.

Kawamoto, T., Leinenweber, K., Hervig, R. L., & Holloway, J. R. (1995). Stability of hydrous minerals in H_2O-saturated KLB-1 peridotite up to 15 GPa. *American Institute of Physics, 341*, 229–239.

Kawazoe, T., Ohira, I., and Ishii, T. et al. (2017). Single crystal synthesis of δ-(Al,Fe)OOH. *American Mineralogist, 102*, 1953-1956.

Kennett, B. L. N., Engdahl, E. R., & Buland, R. (1995), Constraints on seismic velocities in the Earth from travel-times, *Geophysical Journal International, 122*, 108–124.

Komabayashi, T., Hirose, K., Funakoshi, K. I., & Takafuji, N. (2005). Stability of phase A in antigorite (serpentine) composition determined by in situ x-ray pressure observations. *Physics of the Earth and Planetary Interiors, 151*(3), 276–289.

Komabayashi, T., & Omori, S. (2006). Internally consistent thermodynamic data set for dense hydrous magnesium silicates up to 35 GPa, 1600 ℃: Implications for water circulation in the Earth's deep mantle. *Physics of the Earth and Planetary Interiors, 156*(1), 89–107.

Inoue, T., Yurimoto, H., & Kudoh, Y. (2013). Hydrous modified spinel, $Mg_{1.75}SiH_{0.5}O_4$: a new water reservoir in the mantle transition region. *Geophysical Research Letters, 22*(2), 117–120.

Irifune, T., Kubo, N., Isshiki, M., & Yamasaki, Y. (1998). Phase transformations in serpentine and transportation of water into the lower mantle. *Geophysical Research Letters, 25*(2), 203–206.

Jackson, J. M., et al. (2006). Single-crystal elasticity and sound velocitites of $(Mg_{0.94}Fe_{0.06})O$ ferropericlase to 20 GPa, *Journal of Geophysical Research: Solid Earth, 111(B)*, B09203.

Jacobsen, S.D., Smyth, J. R., Spetzler, H., Holl, C. M. & Frost, D. J. (2004). Sound velocities and elastic constants of iron-bearing hydrous ringwoodite. *Physics of the Earth and Planetary Interiors, 143–144*, 47–56.

Li, X., Mao, Z., Sun, N., Liao, Y., Zhai, S., & Wang, Y., et al. (2016). Elasticity of single-crystal superhydrous phase B at simultaneous high pressure-temperature conditions. *Geophysical Research Letters, 43(16).*

Li, Z., Li, J., Lange, R., Liu, J., & Militzer, B. (2017). Determination of calcium carbonate and sodium carbonate melting curves up to Earth's transition zone pressures with implications for the deep carbon cycle. *Earth and Planetary Science Letters, 457*, 395–402.

Li, B., Liebermann, R. C., & Weidner, D. J. (1998). Elastic moduli of wadsleyite (β-Mg_2SiO_4) to 7 GPa and 873 K. *Science, 281*, 675–677.

Liu et al. (2019). Stability of the hydrous phases of Al-rich phase D and Al-rich phase H in deep subducted oceanic crust. *American Mineralogist*, 104, 64–72.

Li, J., Wang, X., Wang, X., & Yuen, D. A. (2013). P and SH velocity structure in the upper mantle beneath northeast china: evidence for a stagnant slab in hydrous mantle transition zone. *Earth and Planetary Science Letters, 367*, 71–81.

Li, X., & Yuan, X. (2003). Receiver functions in northeast China-Implications for slab penetration into the lower mantle in northwest Pacific subduction zone, *Earth and Planetary Science Letters, 216(4)*, 679–691.

Litasov, K., & Ohtani, E. (2002). Phase relations and melt compositions in CMAS-pyrolite-H_2O system up to 25 GPa. *Physics of the Earth and Planetary Interiors, 134*(1), 105–127.

Litasov, K., & Ohtani, E. (2003). Stability of various hydrous phases in CMAS pyrolite-H_2O system up to 25 GPa. *Physics and Chemistry of Minerals*, *30*(3), 147–156.

Litasov, K. D., & Ohtani, E. (2005). Phase relations in hydrous MORB at 18-28 GPa: implications for heterogeneity of the lower mantle. *Physics of the Earth & Planetary Interiors*, *150*(4), 239–263.

Litasov, K. D., & Ohtani, E. (2007). Effect of water on the phase relations in earth's mantle and deep water cycle. *Special Paper of the Geological Society of America, 421*, 115–156.

Litasov, K.D., et al. (2007a). Thermal equation of state of superhydrous phase B to 27 GPa and 1373 K, *Physics of the Earth and Planetary Interiors, 164(3)*, 142–160.

Litasov, K. D., et al. (2008). Thermal equation of state of Al- and Fe-bearing phase D, *Journal of Geophysical Research Solid Earth, 113(B8)*, B08205.

Litasov, K. D., Ohtani, E., Sano, A., Suzuki, A., & Funakoshi, K. (2005). Wet subduction versus cold subduction. *Geophysical Research Letters, 32(13)*, 370–370.

Liu, Z., Park, J., & Karato, S. I. (2016). Seismological detection of low-velocity anomalies surrounding the mantle transition zone in japan subduction zone. *Geophysical Research Letters, 43*(6), 2480–2487.

Liu, Z., Irifune, T., Nishi, M., Tange, Y., Arimoto, T., & Shinmei, T. (2016). Phase relations in the system $MgSiO_3$-Al_2O_3 up to 52 GPa and 2000 K. *Physics of the Earth and Planetary Interiors, 257*, 18–27.

Liu, L. G., Lin, C. C., Mernagh, T. P., & Irifune, T. (2002). Raman spectra of phase A at various pressures and temperatures. *Journal of Physics and Chemistry of Solids, 29*(3), 181–187.

Mao, Z. , Lin, J. F. , Jacobsen, S. D. , Duffy, T. S. , Chang, Y. Y. , & Smyth, J. R. , et al. (2012). Sound velocities of hydrous ringwoodite to 16 gpa and 673 k. *Earth and Planetary Science Letters, 331-332*, 0–119.

Maruyama, S., & Okamoto, K. (2007). Water transportation from the subducting slab into the mantle transition zone. *Gondwana Research, 11*(1-2), 148–165.

Mashino, I., Murakami, M., & Ohtani, E. (2016). Sound velocities of δ–AlOOHup to core–mantle boundary pressures with implications for the seismic anomalies in the deep

mantle. *Journal of Geophysical Research: Solid Earth, 121(2)*, https://doi.org/10.1002/2015JB012477.

Masson, P., Carr, M. H., Costard, F., Greeley, R., Hauber, E., & Jaumann, R. (2001). Geomorphologic evidence for liquid water. *Space Science Reviews, 96*, 333–364.

Morgan, J. W., & Anders, E. (1980). Chemical composition of earth, venus, and mercury. *Proceedings of the National Academy of Sciences, 77*(12), 6973–6977.

Nishi, M. (2014). Deep water cycle: mantle hydration. *Nature Geoscience*, *8*(1), 9–10.

Nishi, M., Irifune, T., Tsuchiya, J., Nishihara, Y., Fujino, K., & Higo, Y., et al. (2014). Stability of hydrous silicate at high pressures and water transport to the deep lower mantle. *Nature Geoscience, 7*(3), 224–227.

Nishi, M., Kuwayama, Y., Tsuchiya, J., & Tsuchiya, T. (2017). The pyrite-type high-pressure form of FeOOH. *Nature, 547*(7662), 205–208.

Niu, F., & Kawakatsu, H. (1996). Complex structure of mantle discontinuities at the tip of the subducting slab beneath northeast china: a preliminary investigation of broadband receiver functions. *Journal of Physics of the Earth, 44*(6), 701–711.

Ohira, I., Ohtani, E., Sakai, T., Miyahara, M., Hirao, N., Ohishi, Y., & Nishijima, M. (2014), Stability of a hydrous δ-phase, AlOOH-$MgSiO_2(OH)_2$, and a mechanism for water transport into the base of lower mantle. *Earth and Planetary Science Letters, 401*, 12–17.

Ohtani, E., Amaike, Y., Kamada, S., Sakamaki, T., & Hirao, N. (2015). Stability of hydrous phase H $MgSiO_4H_2$ under lower mantle conditions. *Geophysical Research Letters, 41*(23), 8283–8287.

Ohtani, E., Litasov, K., Hosoya, T., Kubo, T., Kondo, T. (2004). Water transport into the deep mantle and formation of a hydrous transition zone. *Physics of the Earth and Planetary Interiors, 143-144*, 255–269.

Ohtani, E., Litasov, K., Suzuki, A., & Kondo, T. (2001). Stability field of new hydrous phase, δ-AlOOH, with implications for water transport into the deep mantle. *Geophysical Research Letters, 28*(20), 3991–3994.

Ohtani, E., Mizobata, H., Kudoh, T., Nagase, T., Arashi, H., Yurimoto, H., Miyagi, I. (1997). A new hydrous silicate, a water reservoir, in the upper part of the lower mantle. *Geophysical Research Letters, 24*, 1047–1050.

Ohtani, E., Mizobata, H., Yurimoto, H. (2000). Stability of dense hydrous magnesium silicate phases in the systems Mg_2SiO_4-H_2O and $MgSiO_3$-H_2O at pressures up to 27 GPa. *Physics and Chemistry of Minerals, 27*, 533–544.

Ohtani E, Toma M, Kubo T, et al. (2003). In situ x-ray observation of decomposition of superhydrous phase B at high pressure and temperature. *Geophysical Research Letters, 30*(2), 1–1.

Ohtani, E., Litasov, K., Toma, M., Kubo, T., & Suzuki, A. (2001). Stability of dense hydrous magnesium silicate phases and water storage capacity in the transition zone and lower mantle. *Physics of the Earth and Planetary Interiors, 124*(1), 105–117.

Okuchi, T. (1997). Hydrogen partitioning into molten iron at high pressure: implications for Earth's core. *Science, 278*(5344), 1781–1784.

Omori, S., Komabayashi, & T., Maruyama S. (2004). Dehydration and earthquakes in the subducting slab; empirical link in intermediate and deep seismic zones. *Phys. Earth Planet. Inter., 146*. 297–311.

Orosei, R., Lauro S. E., Pettinelli, E., Cicchetti, A., Coradini, M., Cosciotti, B., Di Paolo, F., Flamini, E., Mattei, E., Pajola, M., Soldovieri, F., Cartacci, M., Cassenti, F., Frigeri, A., Giuppi, S., Martufi, R., Masdea, A., Mitri, G., Nenna, C., Noschese, R., Restano, M., & Seu, R. (2018). Radar evidence of subglacial liquid water on Mars. *Science, 361*, 490–493.

Pamato, M. G., Myhill, R., Boffa Ballaran, T., Frost, D. J., Heidelbach, F., & Miyajima, N. (2014). Lower-mantle water reservoir implied by the extreme stability of a hydrous aluminosilicate. *Nature Geoscience, 8*(1), 75–79.

Pan, L., & Ehlmann, B. (2017). Aqueous Processes From Diverse Hydrous Minerals in the Vicinity of Amazonian-Aged Lyot Crater. *Journal of Geophysical Research: Planets, 123*, 1618–1648.

Panero, W. R., & Caracas, R. (2017). Stability of phase H in the $MgSiO_4H_2$-AlOOH-SiO_2 system. *Earth and Planetary Science Letters, 463*, 171–177.

Pearson, D. G., Brenker, F. E., Nestola, F., Mcneill, J., Nasdala, L., Hutchison, M. T., Matveev, S., Mather, K., Silversmit, G., Schmitz, S., Vekemans, B., & Vincze, L. (2014). Hydrous mantle transition zone indicated by ringwoodite included within diamond. *Nature, 507*, 221–4.

Poli, S., Schmidt, & M.W. (2002). Petrology of Subducted Slabs. *Annual Review of Earth and Planetary Sciences, 30*, 207–235.

Porritt, R. W., & Yoshioka, S. (2016). Slab pileup in the mantle transition zone and the 30 May 2015 Chichi‐jima earthquake. *Geophysical Research Letters, 43(10)*, 4905-4912.

Raevskiy, S. N., Gudkova, T. V., & Zharkov, V. N. (2015). Diagnostic possibilities of body waves for studying the interior structure of Mars. *Izvestiya Physics of the Solid Earth, 51*, 143-155.

Ringwood, A. E., & Kesson, S. E. (1977). Basaltic magmatism and the bulk composition of the moon. *Moon, 16(4)*, 389–423.

Ringwood, A. E., & Major, A. (1967). High-pressure reconnaissance investigations in the system Mg_2SiO_4-MgO-H_2O. Earth and Planetary Science Letters, 2, 130-133.

Rosa, A. D., Mezouar, M., Garbarino, G., Bouvier, P., Ghosh, S., & Rohrbach, A., et al. (2013). Single-crystal equation of state of phase d to lower mantle pressures and the

effect of hydration on the buoyancy of deep subducted slabs. *Journal of Geophysical Research: Solid Earth, 118*(12), 6124–6133.

Rosa, A. D., Sanchez-Valle, C., Wang et al. (2015) Elasticity of superhydrous phase B, seismic anomalies in cold slabs and implications for deep water transport. *Physics of the Earth and Planetary Interiors, 243(1)*, 30–43.

Saikia, A., Ballaran, T. B., & Frost, D. J. (2009). The effect of fe and al substitution on the compressibility of $MgSiO_3$-perovskite determined through single-crystal x-ray diffraction. *Physics of the Earth and Planetary Interiors, 173*(1-2), 153–161.

Sano, A., Ohtani, E., Kubo et al. (2011). In situ X-ray observation of decomposition of hydrous aluminum silicate AlSiO. *International Journal of Radiation Oncology Biology Physics, 80(4)*, 1064–71.

Sano, A., Ohtani, E., Kubo, T., & Funakoshi, K. (2004). In situ X-ray observation of decomposition of hydrous aluminum silicate $AlSiO_3OH$ and aluminum oxide hydroxide δ-AlOOH at high pressure and temperature. *Journal of Physics and Chemistry of Solids, 65*, 1547–1554.

Schmandt, B., Jacobsen, S. D., Becker, T. W., Liu, Z., & Dueker, K. G. (2014). Earth's interior. Dehydration melting at the top of the lower mantle. *Science, 344*(6189), 1265.

Schmidt, M.W., Poli, S. (1998). Experimentally based water budgets for dehydrating slabs and consequences for arc magma generation. *Earth and Planetary Science Letters, 163*, 361–379.

Shieh, S. R., Mao, H. K., Hemley, R. J. & Ming, L. C. (1998). Decomposition of phase D in the lower mantle and the fate of dense hydrous silicates in subducting slabs. *Earth and Planetary Science Letters, 159*, 13–23.

Shieh, S. R., Mao, H., Hemley, R. J., & Ming, L. C. (2000). In situ x-ray diffraction studies of dense hydrous magnesium silicates at mantle conditions. *Earth & Planetary Science Letters,177*(1), 69–80.

Shieh, S. R., Duffy, T. S., Liu, Z., & Ohtani, E. (2009). High-pressure infrared spectroscopy of the dense hydrous magnesium silicates phase d and phase E. *Physics of the Earth and Planetary Interiors, 175(3),* 106–114.

Shimizu, H., Utada, H., Baba, K., Koyama, T., Obayashi, M., & Fukao, Y. (2010). Three-dimensional imaging of electrical conductivity in the mantle transition zone beneath the North Pacific Ocean by a semi-global induction study. *Physics of the Earth and Planetary Interiors, 183*(1-2), 252–269.

Shinmei, T., Irifune, T., Tsuchiya, J., & Funakoshi, K. I. (2008). Phase transition and compression behavior of phase d up to 46 GPa using multi-anvil apparatus with sintered diamond anvils. *High Pressure Research, 28*(3), 363–373.

Simmons, N. A., & Gurrola, H. (2000). Multiple seismic discontinuities near the base of the transition zone in the Earth's mantle. *Nature, 405(6786),* 559.

Sinogeikin, S. V., Katsura, T., & Bass, J. D. (1998). Sound velocities and elastic properties of Fe-bearing wadsleyite and ringwoodite. *Journal of Geophysical Research Atmospheres, 1032*(9), 20819–20826.

Sun, S. S. (1982). Chemical composition and origin of the Earth's primitive mantle. *Geochimica Et Cosmochimica Acta, 46*(2), 179–192.

Suzuki, A. (2010). High-pressure X-ray diffraction study of epsilon-FeOOH. *Physics and Chemistry of Minerals, 37(3),* 153–157.

Tonegawa, T., Hirahara, K., Shibutani, T., Iwamori, H., Kanamori, H., & Shiomi, K. (2008). Water flow to the mantle transition zone inferred from a receiver function image of the pacific slab. *Earth and Planetary Science Letters, 274*(3–4), 0–354.

Tschauner, O., Ma, C., Beckett, J. R., Prescher, C., Prakapenka, V. B., & Rossman, G. R. (2014). Discovery of bridgmanite, the most abundant mineral in Earth, in a shocked meteorite. *Science, 346*(6213), 1100–1102.

Tsuchiya, & Jun. (2013). First principles prediction of a new high-pressure phase of dense hydrous magnesium silicates in the lower mantle. *Geophysical Research Letters, 40*(17), 4570–4573.

Ulmer, P., Trommsdorff, V. (1999). Phase relations of hydrous mantle subducting to 300 km. *Mantle petrology: field observations and high pressure experimentation: a tribute to Francis R. (Joe) Boyd, 6*, 259–281.

Vinnik, L., & Farra, V. (2006). S velocity reversal in the mantle transition zone. *Geophysical Research Letters, 33*(18), L18316.

Wade, J., Dyck, B., Palin, R. M., Moore, J. D. P., & Smye, A. J. (2017). The divergent fates of primitive hydrospheric water on earth and mars. *Nature, 552*, 391–394.

Williams, Q., & Hemley, R. J. (2001). H ydrogen in the deep Earth. *Annual Review of Earth and Planetary Sciences, 29*(1), 365–418.

Wirth, R., Vollmer, C., Brenker, F., Matsyuk, S., & Kaminsky, F. (2007). Inclusions of nanocrystalline hydrous aluminium silicate "Phase Egg" in superdeep diamonds from Juina (Mato Grosso State, Brazil). *Earth and Planetary Science Letters, 259*(3–4), 0–399.

Xue, X., Kanzaki, M., & Shatskiy, A. (2008). Dense hydrous magnesium silicates, phase D, and superhydrous B: new structural constraints from one- and two-dimensional 29Si and 1H NMR. *American Mineralogist, 93*(7), 1099–1111.

Yang, D., Wang, W., Wu, Z. (2017). Elasticity of superhydrous phase B at the mantle temperatures and pressures: Implications for 800km discontinuity and water flow into the lower mantle. *Journal of Geophysical Research Solid Earth, 122(7).*

Zhao, D., & Ohtani, E. (2009). Deep slab subduction and dehydration and their geodynamic consequences: evidence from seismology and mineral physics. *Gondwana Research*, *16*(3–4), 401–413.

Zharkov, V. N., & Gudkova, T. V. (2014). Seismic model of Mars: Effects of hydration. *Planetary and Space Science*, *104*, 270–278.

Zhou, Y., Irifune, T., Ohfuji, H., Shinmei, T., & Du, W. (2016). Stability region of $K_{0.2}Na_{0.8}AlSi_3O_8$ hollandite at 22 GPa and 2273 K. *Physics and Chemistry of Minerals*, *44*(1), 1–10.

Acknowledgements

I would like to express my gratitude to my beloved supervisor Prof. Toru Inoue for his instructive advice and useful suggestions during my doctoral special course. I really appreciate his patience, encouragement, and professional instructions on my academic carrier. Without his patient assistance and friendly encouragement, it would not be possible for me to complete my studies in such a short period of time. He invited us to visit his family to enjoy the delicious Japanese traditional food, which broaden my knowledge about Japanese culture.

I also would like to express my heartfelt gratitude to Prof. Tetsuo Irifune, the director of Geodynamics Research Center for giving me precious chance to study at Geodynamics Research Center. He has a profound knowledge of high pressure geoscience and material science. I benefited greatly from his lectures.

I am also greatly indebted to all my teachers who have helped me directly and indirectly in my studies, and useful discussions on the seminars. Among them the following require mentioning: Prof. Hiroaki Ohfuji, Prof. Taku Tsuchiya, Prof. Masanori Kameyama, Prof. Jun Tsuchiya, Prof. Yu Nishihara, Prof. Yoshio Kono, lecturer Masayuki Nishi, lecturer Takeshi Sakai, lecturer Tomohiro Ohuchi and lecturer Haruhiko Dekura.

My sincere thanks should give to lab manager Dr. Toru Shinmei who supports me lot of experimental materials and gives me several advice to improve my high pressure technic. I appreciate Ms. Natsuko Miyamoto, Ms. Megumi Yashiro and Ms. Yukiko Mejima helped me a lot in the past three years. I also owe a special debt of gratitude to Miss Risa Onishi and Ms. Madoka Wada who helped me for preparing the documents for my research budget. High tribute shall be paid to Dr. Akira Yamada and Prof. Kiyoshi Fujino, who helped me a lot in

life and research. Special thanks should also give to the teachers who help my in-situ experiment in Spring-8 and in SIMS measurement in Hokkaido University.

Last my thanks would go to my beloved family for their supporting and great confidence in me during my study always. I also owe my sincere gratitude to my friends Dr. Youmo Zhou, Dr. Wei Sun, Dr. Steeve Gréaux, Dr. Hideharu Kuwahara, Dr. T Dr.akeshi Arimoto, Dr. Takehiro Kunimoto, Dr. Nadezda Chertkova, Dr. Sho Kakizawa and Dr. Hirokazu Kadobayashi, Masamichi Noda, Mana Tsuchida, Shunta Doi, Hokai Fujitani, Yoshie Takayama, Hideaki Kawamura, Chiaki Ueda, Omi Yokota who gave me their help and time in listening to me and helping me work out my problems in my study and my life.

I also would like to thank Y. Higo and T. Tange, the beamline scientists of BL04B1 at SPring-8 for conducting high-pressure in situ X-ray experiments. The synchrotron radiation experiments were performed at the BL04B1 of SPring-8 with the approval of the Japan Synchrotron Radiation Research Institute (JASRI) including our preliminary cell performance experiments (Proposal No. 2014B1435, 2015B1509, 2016B1497, 2017B1549 and 2018B1708). C.X. was supported by Research Fellowships of the Japan Society for the Promotion of Science (JSPS) for Young Scientists (DC2). Some works were supported by JSPS KAKENHI Grant Numbers 18J12511 for C.X. and 26247073, 15H05828 and 18H03740 for T.I..